Implantable microelectrode devices for chronic neuronal recordings in mice

(マウス慢性ニューロン計測に向けた埋め込みマイクロデバイス)

January 2022

Doctor of Philosophy(Engineering)

Koji Yamashita

山下　幸司

Toyohashi University of Technology

Abstract

Implantable microelectrode devices for chronic neuronal recordings in mice

To elucidate brain functions, it is important to record neuronal activity in the brain with great spatial and temporal resolution over a lengthy period. Several key human disorders, including Parkinson's disease, Alzheimer's disease, and major depressive disorders, require knowledge of the basic nervous system from mammal models.

Mice have frequently been utilized as a model organism for researching various human diseases. However, the traditional study employing mice provides data that is difficult to quantitatively evaluate from the behavioral test. Recent breakthroughs in microelectromechanical system technology allow us to fabricate multi-channel neural electrode devices and record electrical signals such as spikes and LFPs. However, these devices face some challenges with the failure mechanism of the neural electrode, which includes mechanical and biological origins.

In this study, I provide multiple neural electrodes and implant systems for chronic recording with excellent spatial and temporal resolution in mice. I developed surgical procedures using PEG dissolvable materials in the “solid phase” and “liquid phase” for less invasive device implantation.

I proposed the parylene-thread microelectrode as the first, and the tissue was penetrated by guiding the tungsten microneedle using the sewing mechanism. I was able to obtain EMG signals from a mouse's MG muscle as well as neuronal signals of LFP and spike from its visual cortex in vivo using the thread-bioprobe. The suggested thread-bioprobe device, which has device flexibility, electrodeposition controllability, and

implantation capability, will contribute to both acute and chronic in vivo electrophysiological recordings. To prevent physical stress on the tissue, a stitching method of the flexible thread device using a dissolvable material of PEG has been developed. These characteristics of the flexible thread device and the surgical procedure were previously unattainable using traditional methods and instruments.

Next, I proposed a chronic neuronal recording in mice in which a 5-μm-diameter microneedle electrode penetrates the brain tissue with dissolvable material-based detachment, and the device is placed on it without attaching the device to the cranium, achieving the floating electrode architecture. For device implantation, I presented a microelectrode penetration approach into brain tissue and device removal utilizing PEG dissolvable material. The approach demonstrated the advantage of reducing physical stress imposed on tissues during device implantation as well as removal from the manipulator. For six months, the electrode demonstrated stable recording with no substantial loss of signal-to-noise ratios, and minimal tissue damage was confirmed as compared to previous cranium-fixed electrodes with the same needle geometry. Although the electrode device requires additional development, such as downsizing and a wireless recording system, the proposed recording technology demonstrated substantial advantages in terms of high SNR during implantation and less tissue damage.

Finally, we proposed a microneedle-electrode-assembled flexible-film device for persistent in vivo recording with high spatiotemporal resolution multi-signal and low invasive implantation. The manufactured microneedle-electrode-assembled flexible-film device allowed us to record LFP and spike signals in an acute in vivo experiment. Furthermore, the fabricated device was put on brain tissue using PEG, and the device was implanted for persistent in vivo recording. For four months, the implanted device displayed LFP and spike signals. In addition, the SNR during the implantation was investigated. As a result, the SNRs for four months showed no significant difference. Based on these findings, the proposed microneedle-electrode-assembled flexible-film device provides signals with excellent spatial and temporal resolution and minimal invasive chronic implantation.

These investigations established persistent in vivo recordings with microelectrodes that allow for high spatial and temporal resolution signal recording in mice. Furthermore, the PEG implantation method allows for recording without

inflammation caused by factors such as tissue damage during device penetration, an elastic mismatch between neural electrodes and neural tissue in the context of relative micromotion, and chronic breach of the blood-brain barrier in mice brains. I hope that the findings of this study will be used as a potent tool in the future to speed the understanding of brain functions.

マウス慢性ニューロン計測に向けた
埋め込みマイクロデバイス

論文要旨

脳機能の解明のためには、神経細胞からの電気信号を高い時空間分解能で長期的に測定を行うことが必要不可欠となる。特に、パーキンソン病やアルツハイマー病、大うつ病性障害などの脳神経系に起因する重大な病を解決するためには、哺乳類のモデルを用いた基礎的な知見が要求されている。これらの重大な病の機序を解明するために、遺伝子組み換えによるモデル作製が容易でかつ短いサイクルで用意が可能なマウスがしばしば用いられる。しかし、従来の研究では行動実験等の定量評価が困難な情報を扱うことが主流となっているため、電気計測を用いた定量評価が期待されている。近年の MEMS 技術の発展により、脳組織からのスパイク信号や局所電場電位などの高解像度の信号を多点同時的に計測可能な神経電極が数多く提案されてきたが、マウス等の小さな動物に対する埋め込みに対応した技術は未だ不十分である。本研究では、マウスに対する長期埋め込み可能ないくつかの低侵襲デバイスおよび PEG を用いた埋め込み技術を提案した。

まず初めに、生体組織内で柔軟性を有する構造が実現可能な糸状パリレン電極とその埋め込み手法を提案した。糸状パリレンの先端部に針を接続することで裁縫の要領で生体組織への刺入を可能とした。特に、脳組織等の柔らかい組織に対しては、溶解性材料である PEG とマニピュレータを用いた針の持ち替え操作により機械的な振動を最小限に抑えたデバイス刺入及び電極配置を可能とした。生体組織へと埋め込まれたデバイスは、急性実験においてマウス後足の筋肉からの EMG を取得し、慢性実験においてマウス脳組織からのスパイク信号を取得可能であることが示された。

次に、シリコン基板上に直径 5 μm の針状電極を成長させたデバイスを脳組織への炎症を抑えた状態で埋め込む手法を提案した。埋め込み手法としては、デバイス留置の際に PEG を用いることにより、デバイス基板を機械的振動なしに脳組織へ配置することを可能とし、デバイスを頭蓋骨に固定することなく埋め込む手法を提案した。マウスの脳組織へと埋め込まれたデバイスは、6 ヶ月の期間にわたってスパイク信号を取得し続けた。また損傷評価の結果より、従来の埋め込み手法と比較して提案した埋め込み手法が優位に炎症を低減することを示した。

最後に、フレキシブルなフィルム基板上に低侵襲な針状電極アレイを形成したデバイスおよび埋め込み手技を提案した。シリコン基板を有するデバイスと同様に、PEG を用いたデバイス留置方法を用いることで、フレキシブルな基板を有するデバイスに対しても針状電極アレイを損なうことなく脳組織内へと刺入と留置が可能であることを示した。マウスの脳組織に埋め込まれたデバイスからは、数ヶ月にわたって安定したスパイク信号が取得された。

本論文においては、マウスに対して慢性埋め込みが可能ないくつかの低侵襲デバイスおよび長期安定的計測を可能とするための炎症を抑えるための埋め込み技術を提案した。これらの計測技術は、将来的に脳機能の解明へと貢献することを期待する。

Contents

Chapter 1

Introduction

1.1 General introduction

Large numbers of neurons in the nervous system constantly generate and send electrophysiological signals to communicate between neurons and brain areas[1]. Understanding information transport and processing within the mammalian nervous system is one of the biomedical community's most pressing concerns. Neurological, neurodegenerative, psychiatric, and neuromuscular diseases, such as Parkinson's disease, Alzheimer's disease, major depressive disorder, and multiple sclerosis, impact a growing proportion of our aging population[2]–[4]. Mice have frequently been utilized as a model organism for researching various human diseases due to their experimental tractability and genetic parallels with humans[5].

To understand brain function, neuronal activity in the brain must be measured. Methods for measuring the brain are essentially grouped into three types: magnetic resonance, optical, and electrical. They are also classed as either noninvasive or invasive. The properties of each measurement method[6] is demonstrated in Figure 1.1. Noninvasive measurements cause no harm to the measurement target; yet, invasive measurements provide finer temporal and spatial resolution than noninvasive measurements. Functional magnetic resonance imaging (fMRI) and

magnetoencephalography are two magnetic resonance-based approaches (MEG)[7]. fMRI is a noninvasive method that assesses cerebral blood flow in the brain by utilizing the various magnetization features of blood. Although the spatial resolution of fMRI is higher (a few millimeters) than that of other noninvasive measurement techniques, the temporal resolution (a few seconds) is poor since the measurement is based on hemodynamic changes. MEG employs a highly sensitive device known as a superconducting quantum interference device, which monitors the magnetic field of brain activity noninvasively. MEG has an excellent temporal resolution (~1 millisecond) but a low spatial resolution (~10 millimeters) because the magnetic field is driven by the current generated from synchronized brain activity. Large equipment and a shielded room are also required for these testing procedures.

Near-infrared spectroscopy (NIRS) and fluorescence imaging are two optical measurement methods. In the near-infrared region of the electromagnetic spectrum, NIRS noninvasively detects cerebral blood flow. Although this method is easier to execute than others, the spatial and temporal resolutions are both low. The former is degraded by scattering from the skull, while the latter is constrained by the method's reliance on hemodynamic changes. Fluorescent imaging uses microscopy techniques such as confocal microscopy and two-photon microscopy to acquire fluorescent signals. Because the sample is scanned by a Galvano scanner, these approaches have a great spatial resolution (a few hundred nanometers) but poor temporal resolution. Also, Ca2+ imaging in the cytoplasm can potentially reveal brain activity. These procedures, however, necessitate bulky equipment that is difficult to use in an ambulatory setting. A transparency approach can be used to observe deep areas in vitro[8], [9].

Electroencephalograms (EEGs), electrocardiograms (ECoGs), extracellular recordings (including local field potentials and action potentials), and intracellular recordings are all examples of electrical measurements. The electrical signals of brain activity are detected noninvasively by electrodes placed on the scalp during EEG tests. EEG has a relatively good temporal resolution (a few milliseconds) but a low spatial resolution (a few millimeters). The electrical signals of brain activity are measured by electrodes implanted behind the dura mater in ECoG. In comparison to insertion-type brain electrodes, this approach is less invasive and provides great spatial and temporal resolution (a few millimeters and ~1 millisecond, respectively). Some of the neuronal electrical probes are described in more detail in Section 1.2.

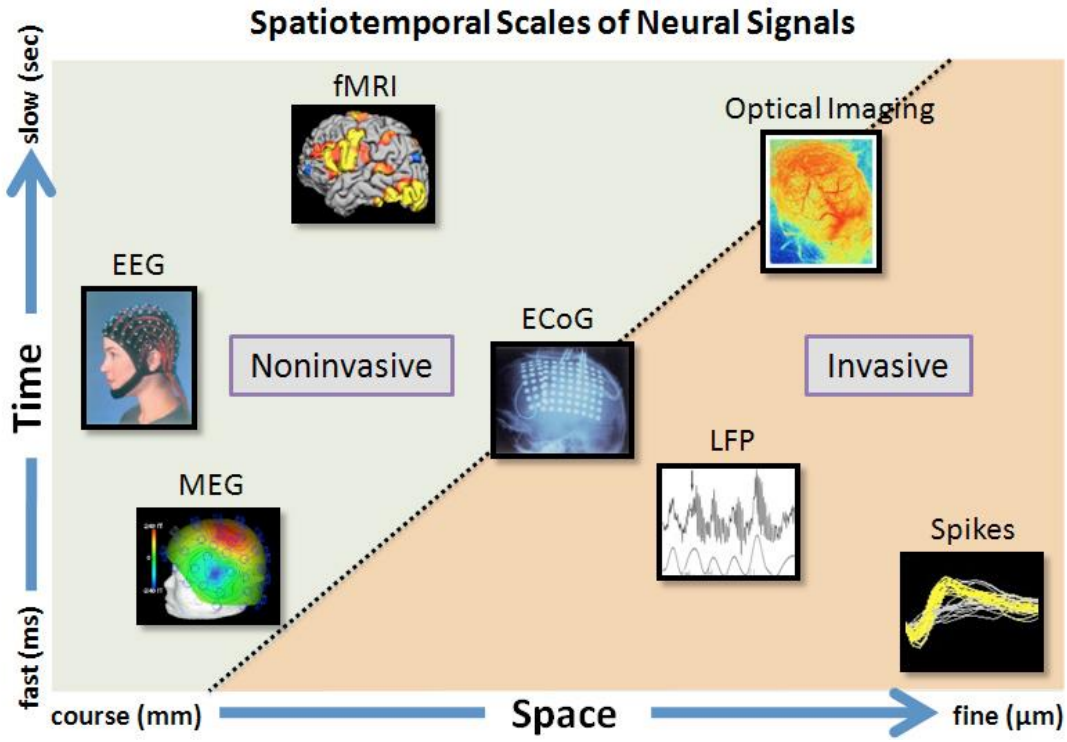

Figure 1.1 Characteristics of different methods for measuring brain activity. The vertical and horizontal axes represent the temporal and spatial resolutions, respectively[10].

1.2 Neuronal electrode

As previously stated, electrical recordings provide excellent temporal and spatial resolution, making them particularly useful for understanding brain function. As a result, using the new MEMS technology, numerous types of brain electrodes have been constructed. Needle and film electrodes are generally utilized for in vivo studies[11]–[13].

Because the electrode measures signals from the surface of the brain tissue, the standard film type electrode allows for less invasive recording (Figure 1.2). Penetration-type electrodes, on the other hand, penetrate brain tissue. Despite being invasive, insertion-type electrodes give great spatial and temporal resolution because they measure electrical signals in the vicinity of the neuron[14]–[19].

Utah electrode arrays (Figure 1.3) and Michigan electrodes (Figure 1.4) are examples of insertion-type electrodes. The planer procedure is used to fabricate the Michigan electrode, which was created by Michigan University. In this case, multiple microelectrodes (each sized 40 μm × 15 μm) are arranged on the surface of a shank needle. The length and shape of the shank needle are freely adjustable in the planar process.

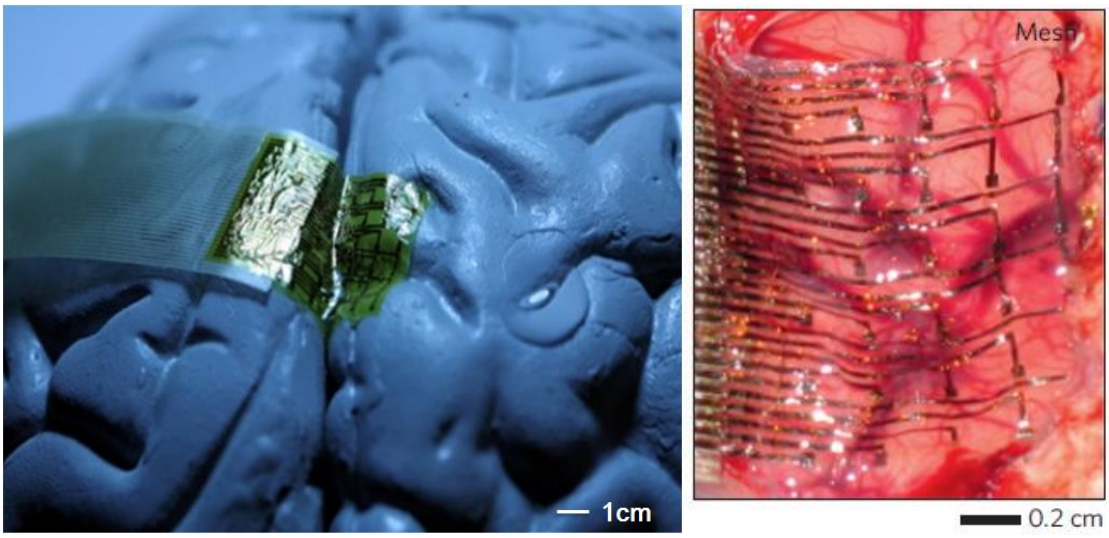

Figure 1.2 Example of a thin film ECoG device supported by a water-soluble material (silk fibroin). The film is ~2.5 μm thick[11].

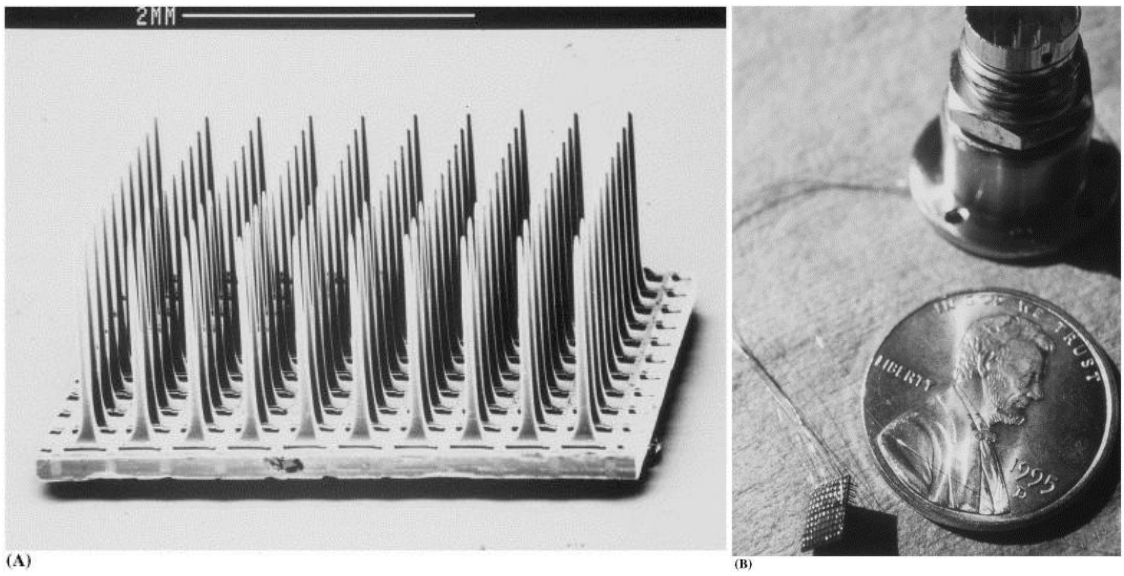

Figure 1.3 Utah electrode array. The electrode diameter and length are ~100 μm and ~1.5 mm, respectively[12].

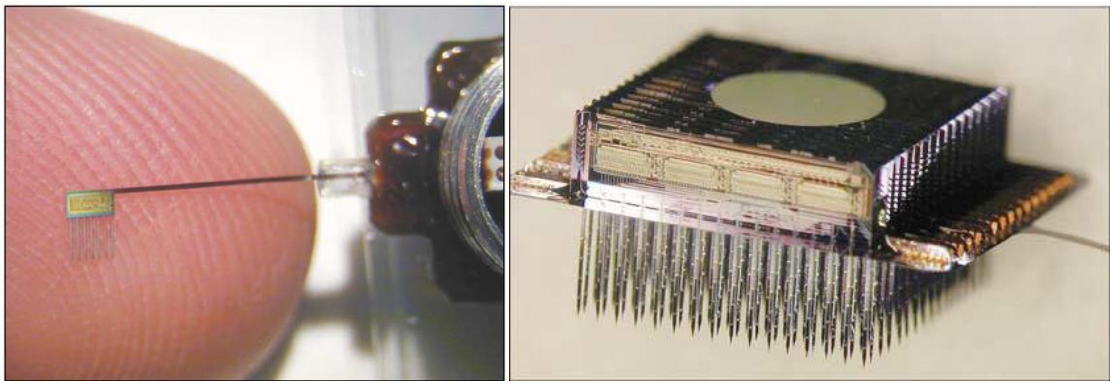

Figure 1.4 A Michigan electrode. Each electrode in the array is sized 40 µm × 15 µm. 2D electrode array (left) and 3D electrode array pattern (right)[13].

Furthermore, recent advancements in complementary metal-oxide-semiconductor (CMOS) technology have allowed for the incorporating recording electrodes into integrated multiplexing circuits in the same silicon-probe shaft, including "Neuropixels" (Figure 1.5)[20]–[24]. The Neuropixels' probe features 960 recording electrodes, each measuring 12 µm × 12 µm and spaced (center to center) by 25 µm, fabricated with a custom 130 nm CMOS process on a single, 10 mm long and 70 µm wide, shank. The probe can be programmed to actively switch between and address the electrodes via 384 independent recording channels[25].

Despite the huge number of independently addressable recording sites in the probe's depth dimension, the fact that Neuropixels is built on a Michigan-type design means that large-scale mapping along lateral dimensions is challenging. Four 16-channel polyimide electrode arrays were integrated into one 64-channel module for a 3D method, and 16 of these modules were stacked into a 1,024-channel recording system for large-scale, multisite mapping of brain activity (Figure 1.6)[26]. Deep-brain neural activity recording with these penetrating silicon probes has high invasiveness[27], [28]. "NeuroGrid" with flexible planar electrodes was developed (Figure 1.7) to lessen invasiveness to brain tissue. The size of the NeuroGrid electrodes was reduced to that of neuronal soma, allowing the detection of LFPs and single-unit action potentials from superficial cortical neurons[29]. Injection of a flexible mesh device into the brain cortex is another option (Figure 1.8)[30]. By using a controlled stereotaxic syringe injection, the flexible mesh electronics can be precisely delivered in vivo into target brain regions[31].

Because of their low invasiveness and many recording sites, these neuronal electrodes are intended to elucidate brain function. However, if the next step necessitates more recording systems, signals can be chronically recorded. I describe chronic recording with a minimally invasive device in detail in Section 1.3.

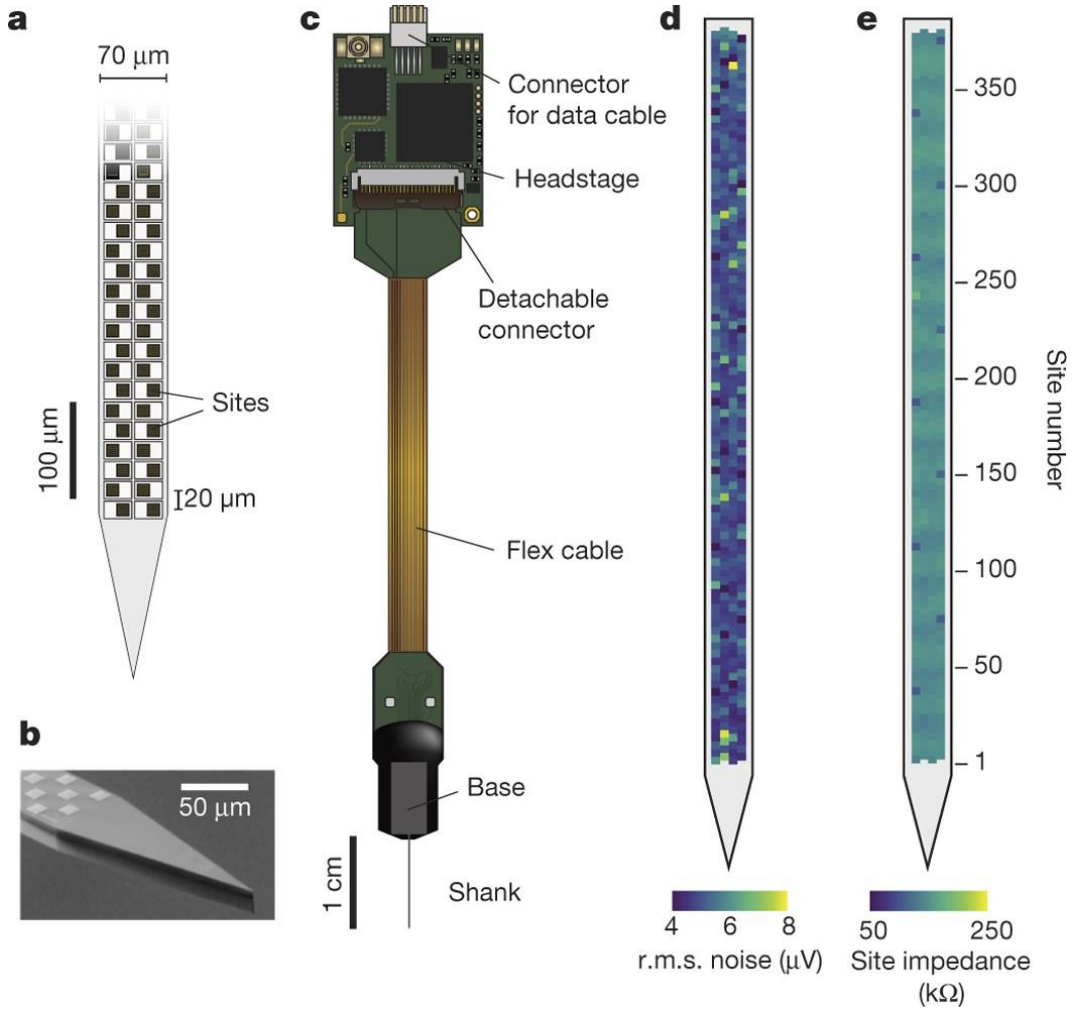

Figure 1.5 Neuropixels. The electrode has 960 recording electrodes, each measuring 12 µm × 12 µm and spaced (centre to centre) by 25 µm, fabricated with a custom 130 nm CMOS process on a single, 10 mm long and 70 µm wide, shank[25].

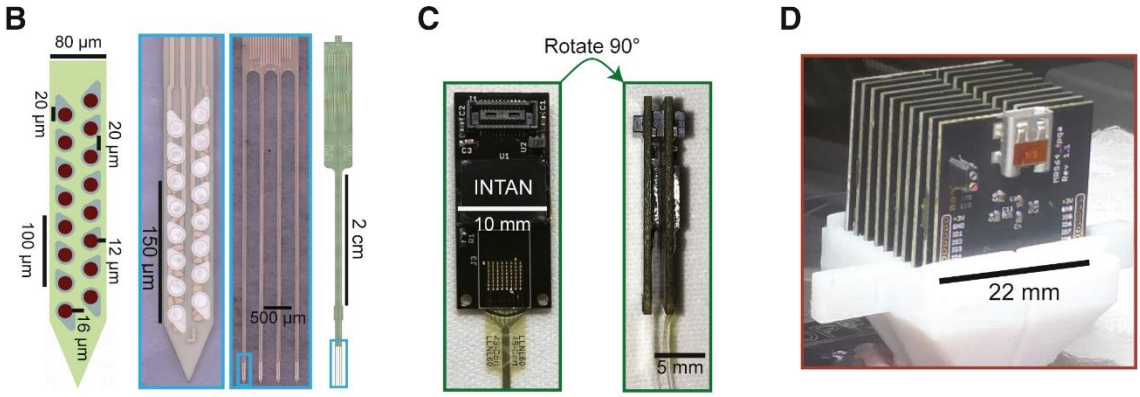

Figure 1.6 Polymer electrode array. Four 16-channel polyimide electrode arrays were assembled into one 64-channel module, and 16 of these modules were stacked into a 1,024-channel recording system[26].

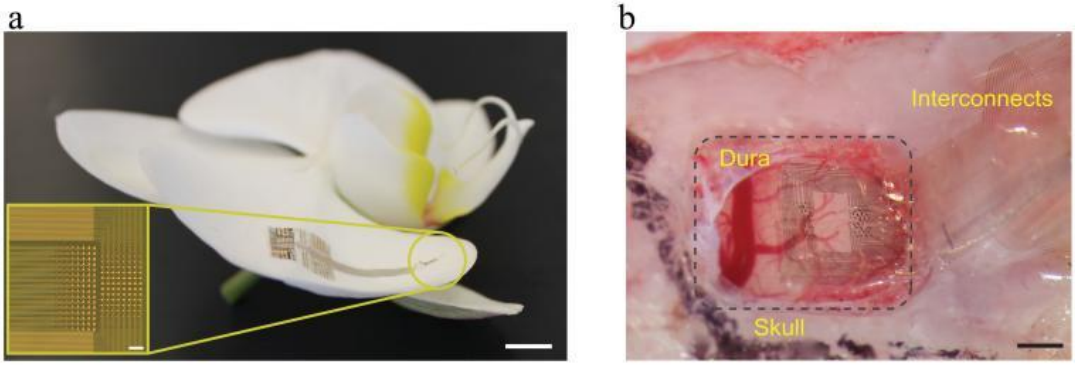

Figure 1.7 NeuroGrid. The electrode has a density that matches the average size of neuronal bodies and neuronal density (10 × 10 µm^2 electrode surface area and 30 µm inter-electrode spacing)[29].

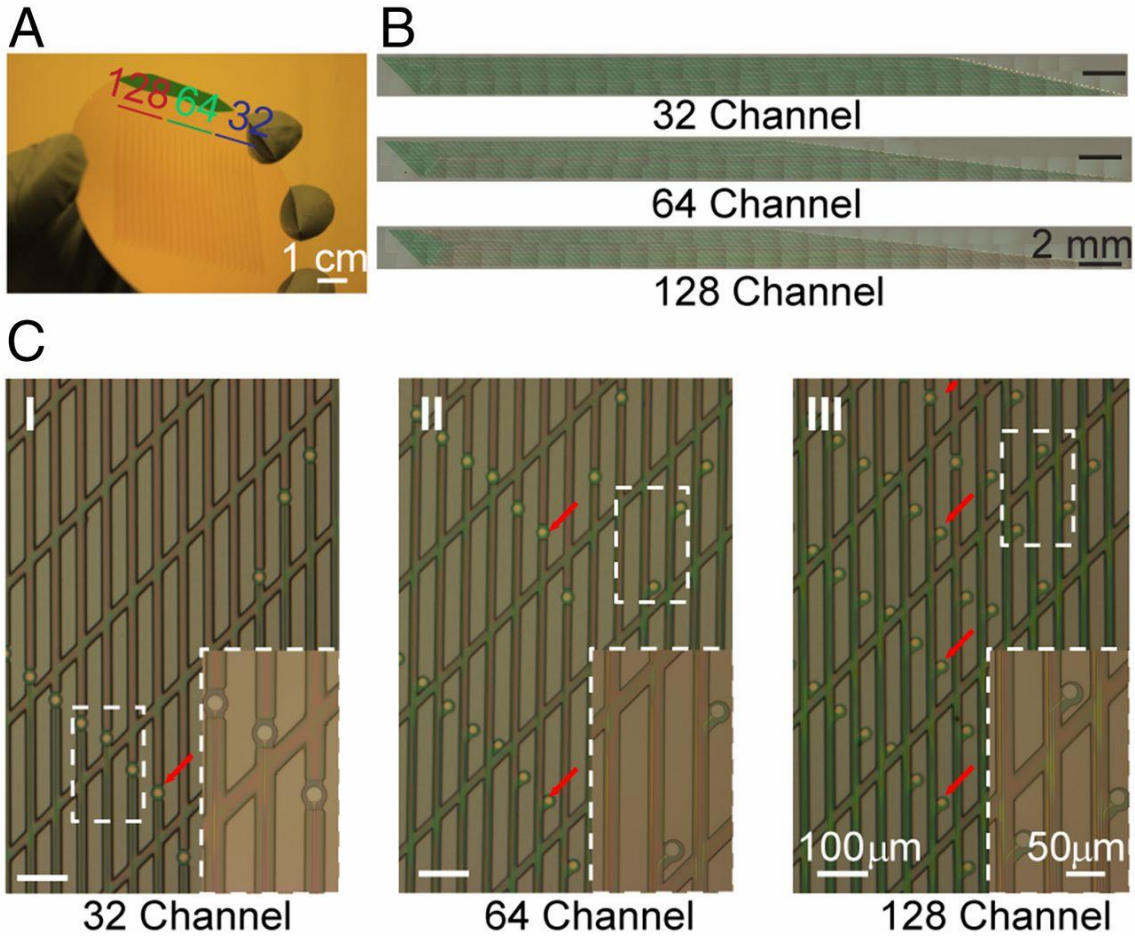

Figure 1.8 Mesh electronics. The electrode has total mesh width, W =2 mm; longitudinal SU-8 polymer element width, w1 =20 μm[30].

1.3 Implantable electrodes for long-period recording

The brain is a dynamic system that exhibits constant changes in neuronal activity and connections at many temporal scales, ranging from milliseconds for single-unit action potentials to months and years for circuit-level modifications during learning and long-term memory formation[32]. Therefore, to comprehend the complex brain system, a recording method with a long duration of reliable and high signal-to-noise ratio (SNR) neural recording is required. Maintaining high SNR recordings from thousands of neurons, on the other hand, proved difficult, and biocompatibility and reliability concerns frequently resulted in electrode failure only a few weeks after implantation[33]–[35]. Failure modes of brain electrodes can be classified into mechanical and biological failure modes (Figure 1.9)[34]–[37]. The former comprises electrical and environmental insulation degradation, the interconnection between interface parts and implanted

electrodes, and mechanical failure of the different layers constituting the device[33], [36]. As a result, packing and encapsulating solutions have emerged as critical features of neural electrode design. The loss of recorded signals can be caused by neuronal death and the formation of glial scars around implanted electrodes, which are composed of reactive astrocytes and activated microglia[35], [38]. Several factors have been reported to contribute to this inflammatory response, including tissue damage during device penetration[34], [35], an elastic mismatch between neural electrodes and neural tissue in the context of relative micromotion[36], [39], [40], chronic breach of the blood-brain barrier[41] and materials neurotoxicity[42].

Some of the neuronal electrodes can be implantable chronically (Table 1.1), but these devices have several challenges. For example, NeuroGrid can detect spike signals (depth in 200 μm) from the brain surface. However, recorded signals necessitate complex data analysis, such as spike clustering[29]. Despite having a great number of recording sites on Neuropixels and polymer electrode arrays, the implantation method; that is, the device platform attached to the cranium (Figure 1.10), causes harm to brain tissue due to the device's relative micromotion (Figure 1.11)[36], [39], [40]. Furthermore, because these devices have large platform sizes, recording with a mouse is limited.

Flexible substrate devices such as Mesh electronics and Nanoelectronic thread (NET) electrodes are expected to reduce invasiveness after device implantation, however, device penetration or implantation method into biological tissue is a challenge. Mesh electronics with injection approach demonstrating repeated recordings over an extended period of time utilizing mouse brain tissue. The injection method, on the other hand, has various challenges, including device placement and an early injury to brain tissue during the injection (Figure 1.12)[30], [31]. Nanoelectronic thread (NET) electrodes with a hole at the end of the probe enable to penetrate the biological tissue using a guide needle to catch the hole of thread (Figure 1.13). However, these penetration methods require the withdrawal of the guide needle, which causes misalignment of the electrode device and makes accurate implantation difficult[17].

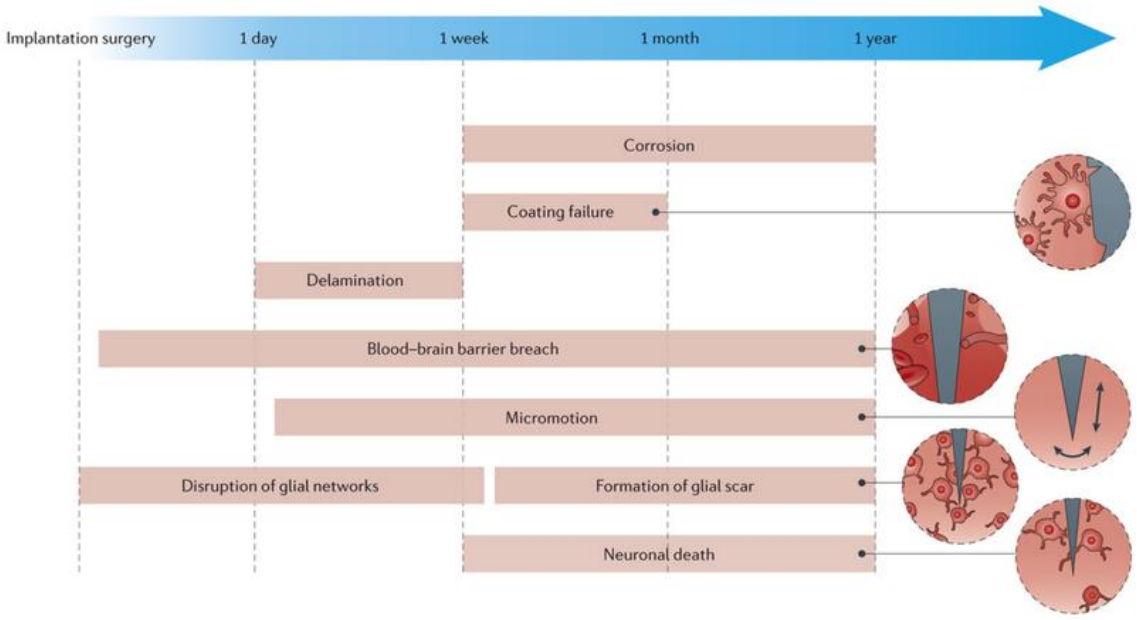

Figure 1.9 Mechanisms of neuronal electrode failure[37].

Table 1.1 Comparison of different properties of electrode.

	Multiplexity	Stability	Animal
NeuroGrid[29]	120-256 channels	10 days	Rat
Neuropixels[25]	960 channels	60 days	Rat
Polymer electrode array[26]	1,024 channels	10 days	Rat
Mesh electronics[30]	16-128 channels	8 months	Mouse
NET electrode[17]	8 channels	4 months	Mouse

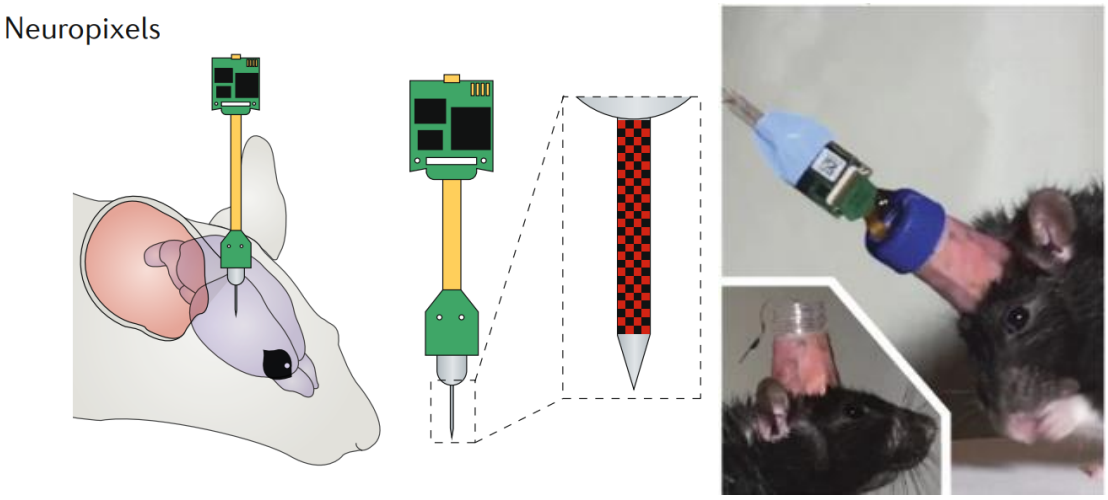

Figure 1.10 Implantation method with Neuropixels using rat[6], [25].

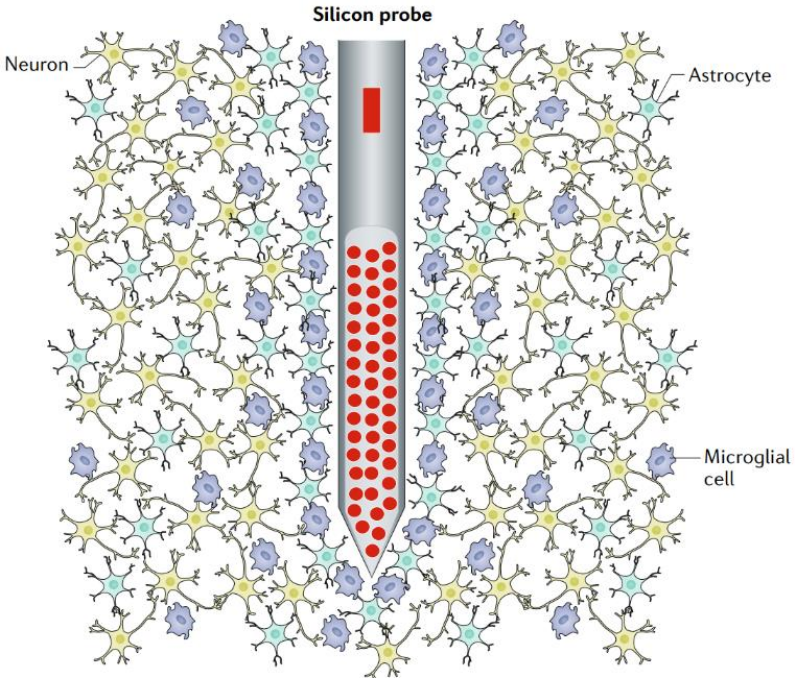

Figure 1.11 Inflammation of neuronal electrode-brain tissue interface[6].

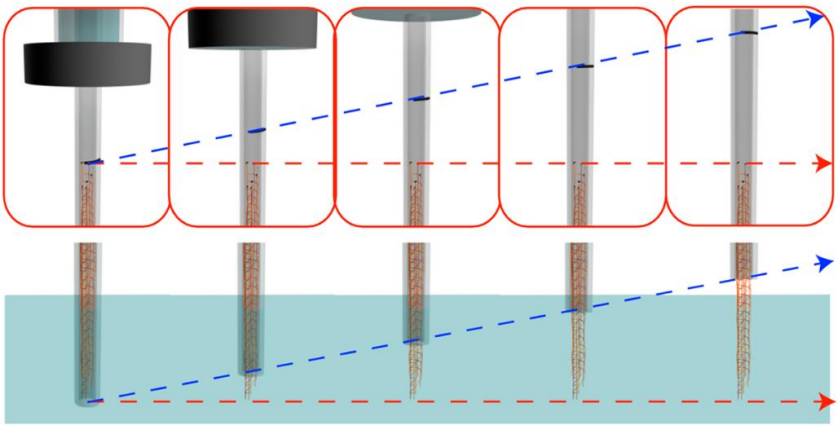

Figure 1.12 Injection method of mesh electrode[31].

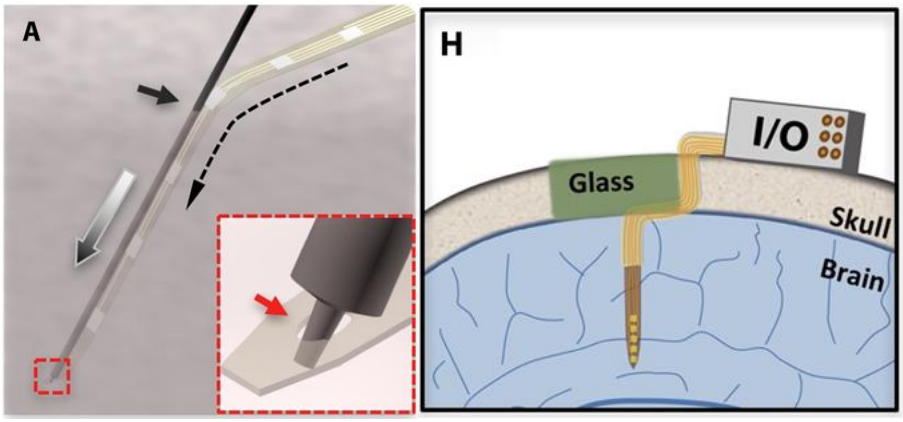

Figure 1.13 Device insertion method using guide needle[17].

1.4 Objective of the present study

To understand brain function, it is important to record neuronal activity in the brain with great spatial and temporal resolution over a lengthy period of time. Several key human disorders, including Parkinson's disease, Alzheimer's disease, and major depressive disorders, require an understanding of the basic neurological system from a mammal model. Mice have frequently been utilized as a model organism in the study of certain human diseases. However, the conventional study employing mice provides data that is difficult to quantitatively evaluate using behavioral tests.

Recent advances in microelectromechanical system technology allow us to fabricate multi-channel neural electrode devices and record electrical signals such as spikes and LFPs. However, these devices have some challenges with the failure mechanism of the brain electrode, which includes mechanical and biological origins.

In this study, I provide several of the neuronal electrode and implant systems for chronic recording with high spatial and temporal resolution using mice (Figure 1.14). The proposed methodology in this study offers advantages of i) minimized initial tissue damage during device penetration ii) enabling accurate insertion position and iii) providing flexibility to biological tissue during implantation.

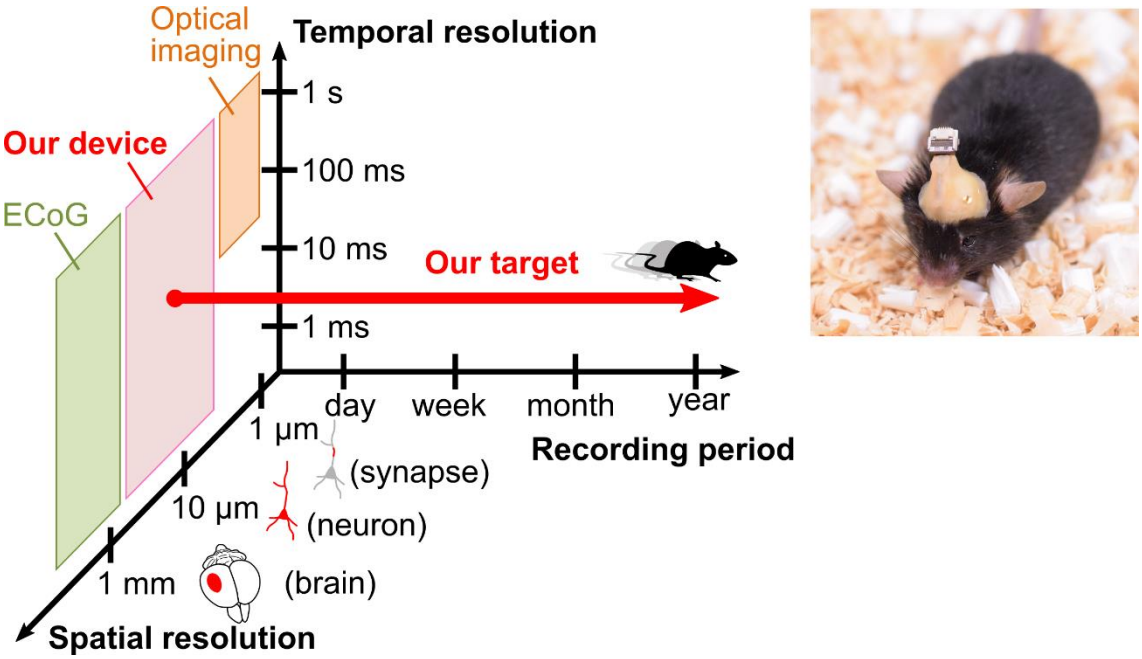

Figure 1.14 The objective of the present study: high spatial and temporal resolution recording with a long period for mice.

1.5 Organization of the thesis

This thesis summarizes several of the neuronal electrode and implant systems for chronic recording with high spatial and temporal resolution using mice. This thesis consists of all 6 chapters, and its organization is as follows.

In chapter 1, the method of measuring the neural activity, especially, the advantages of the electrical measurement method and neural electrode, the device implantation for chronic recording, and failure mode of the neural electrode including the mechanical origin and biological origin were introduced. The objective of this research was also shown.

In chapter 2, the device penetration method for reducing tissue damage using dissolvable materials and comparison of dissolvable materials and selection are described.

Chapter 3 introduced the parylene-thread microelectrode based on film fabrication and surgical procedure based on the sewing mechanism. The acute and chronic in vivo experiments were also described using the parylene-thread microelectrode in mice.

Chapter 4 introduced a "floating" electrode architecture using a 5-μm-diameter microneedle electrode. The device packaging and surgical procedure for achieving the "floating" electrode were described. The results including in vivo chronic experiment recording with SNR for 6 months and damage analysis using immunohistochemistry were also described.

Chapter 5 introduced a microneedle-electrode-assembled flexible-film device for chronic in vivo recording with high spatiotemporal resolution multi-signal and low invasive implantation. The device fabrication and packaging for high spatiotemporal resolution recording were described. In addition, acute and chronic in vivo experiments were also described using the device in mice. Finally, damage analysis using immunohistochemistry was also described.

In chapter 6, the findings obtained in this research and future prospects of this device are shown and summarized in this research.

Reference

[1] S. Herculano-Houzel, "The human brain in numbers: a linearly scaled-up primate brain," *Frontiers in human neuroscience*, vol. 3, p. 31, 2009.

[2] E. R. Dorsey *et al.*, "Projected number of people with Parkinson disease in the most populous nations, 2005 through 2030," *Neurology*, vol. 68, no. 5, pp. 384–386, 2007.

[3] G. Adelman, S. G. Rane, and K. F. Villa, "The cost burden of multiple sclerosis in the United States: a systematic review of the literature," *Journal of medical economics*, vol. 16, no. 5, pp. 639–647, 2013.

[4] P. E. Greenberg *et al.*, "The economic burden of depression in the United States: how did it change between 1990 and 2000?," *Journal of clinical psychiatry*, vol. 64, no. 12, pp. 1465–1475, 2003.

[5] E. R. Kandel, J. H. Schwartz, T. M. Jessell, S. Siegelbaum, A. J. Hudspeth, and S. Mack, *Principles of neural science*, vol. 4. McGraw-hill New York, 2000.

[6] G. Hong and C. M. Lieber, "Novel electrode technologies for neural recordings," *Nature Reviews Neuroscience*, vol. 20, no. 6, pp. 330–345, 2019.

[7] R. A. Poldrack and M. J. Farah, "Progress and challenges in probing the human brain," *Nature*, vol. 526, no. 7573, pp. 371–379, 2015.

[8] M.-T. Ke, S. Fujimoto, and T. Imai, "SeeDB: a simple and morphology-preserving optical clearing agent for neuronal circuit reconstruction," *Nature neuroscience*, vol. 16, no. 8, pp. 1154–1161, 2013.

[9] W. Yang and R. Yuste, "In vivo imaging of neural activity," *Nature methods*, vol. 14, no. 4, pp. 349–359, 2017.

[10] Y. J. Kim *et al.*, "A study on a robot arm driven by three-dimensional trajectories predicted from non-invasive neural signals," *Biomedical engineering online*, vol. 14, no. 1, pp. 1–19, 2015.

[11] D. Kim *et al.*, "Dissolvable films of silk fibroin for ultrathin conformal bio-integrated electronics.," *Nature Materials*, vol. 9, no. 6, pp. 511–517, 2011, doi: 10.1038/nmat2745.Dissolvable.

[12] P. J. Rousche and R. A. Normann, "Chronic recording capability of the Utah Intracortical Electrode Array in cat sensory cortex," *Journal of Neuroscience Methods*, vol. 82, no. 1, pp. 1–15, 1998.

[13] K. D. Wise, D. J. Anderson, J. F. Hetke, D. R. Kipke, and K. Najafi, "Wireless

implantable microsystems: high-density electronic interfaces to the nervous system," *Proceedings of the IEEE*, vol. 92, no. 1, pp. 76–97, 2004.

[14] S. Takeuchi, T. Suzuki, K. Mabuchi, and H. Fujita, "3D flexible multichannel neural probe array," *Journal of micromechanics and microengineering*, vol. 14, no. 1, p. 104, 2003.

[15] T. il Kim *et al.*, "Injectable, cellular-scale optoelectronics with applications for wireless optogenetics," *Science*, vol. 340, no. 6129, pp. 211–216, 2013.

[16] B. J. Kim *et al.*, "3D Parylene sheath neural probe for chronic recordings," *Journal of neural engineering*, vol. 10, no. 4, p. 045002, 2013.

[17] L. Luan *et al.*, "Ultraflexible nanoelectronic probes form reliable, glial scar–free neural integration," *Science Advances*, vol. 3, no. 2, pp. 1–10, 2017.

[18] E. Musk, "An integrated brain-machine interface platform with thousands of channels," *Journal of medical Internet research*, vol. 21, no. 10, p. e16194, 2019.

[19] K. Yamashita *et al.*, "Flexible parylene-thread bioprobe and the sewing method for in vivo neuronal recordings," *Sensors and Actuators B: Chemical*, vol. 316, p. 127835, 2020.

[20] H. P. Neves *et al.*, "The NeuroProbes project: a concept for electronic depth control," in *2008 30th Annual International Conference of the IEEE Engineering in Medicine and Biology Society*, 2008, p. 1857.

[21] T. Torfs *et al.*, "Two-dimensional multi-channel neural probes with electronic depth control," *IEEE transactions on biomedical circuits and systems*, vol. 5, no. 5, pp. 403–412, 2011.

[22] K. Seidl, M. Schwaerzle, I. Ulbert, H. P. Neves, O. Paul, and P. Ruther, "CMOS-based high-density silicon microprobe arrays for electronic depth control in intracortical neural recording–characterization and application," *Journal of Microelectromechanical Systems*, vol. 21, no. 6, pp. 1426–1435, 2012.

[23] M.-Y. Cheng, L. Yao, K. L. Tan, R. Lim, P. Li, and W. Chen, "3D probe array integrated with a front-end 100-channel neural recording ASIC," *Journal of Micromechanics and Microengineering*, vol. 24, no. 12, p. 125010, 2014.

[24] R. Fiáth *et al.*, "Large-scale recording of thalamocortical circuits: in vivo electrophysiology with the two-dimensional electronic depth control silicon probe," *Journal of neurophysiology*, vol. 116, no. 5, pp. 2312–2330, 2016.

[25] J. J. Jun *et al.*, "Fully integrated silicon probes for high-density recording of neural

activity," *Nature*, vol. 551, no. 7679, pp. 232–236, 2017.

[26] J. E. Chung *et al.*, "High-density, long-lasting, and multi-region electrophysiological recordings using polymer electrode arrays," *Neuron*, vol. 101, no. 1, pp. 21–31, 2019.

[27] R. Feiner and T. Dvir, "Tissue–electronics interfaces: from implantable devices to engineered tissues," *Nature Reviews Materials*, vol. 3, no. 1, pp. 1–16, 2017.

[28] J. W. Salatino, K. A. Ludwig, T. D. Y. Kozai, and E. K. Purcell, "Glial responses to implanted electrodes in the brain," *Nature Biomedical Engineering*, vol. 1, no. 11, pp. 862–877, 2017.

[29] D. Khodagholy *et al.*, "NeuroGrid: Recording action potentials from the surface of the brain," *Nature Neuroscience*, vol. 18, no. 2, pp. 310–315, 2015.

[30] T.-M. Fu, G. Hong, R. D. Viveros, T. Zhou, and C. M. Lieber, "Highly scalable multichannel mesh electronics for stable chronic brain electrophysiology," *Proceedings of the National Academy of Sciences*, vol. 114, no. 47, pp. E10046–E10055, 2017.

[31] G. Hong, T.-M. Fu, T. Zhou, T. G. Schuhmann, J. Huang, and C. M. Lieber, "Syringe injectable electronics: Precise targeted delivery with quantitative input/output connectivity," *Nano letters*, vol. 15, no. 10, pp. 6979–6984, 2015.

[32] C. Herry and J. P. Johansen, "Encoding of fear learning and memory in distributed neuronal circuits," *Nature neuroscience*, vol. 17, no. 12, pp. 1644–1654, 2014.

[33] K. Scholten and E. Meng, "Materials for microfabricated implantable devices: a review," *Lab on a Chip*, vol. 15, no. 22, pp. 4256–4272, 2015.

[34] M. P. Ward, P. Rajdev, C. Ellison, and P. P. Irazoqui, "Toward a comparison of microelectrodes for acute and chronic recordings," *Brain research*, vol. 1282, pp. 183–200, 2009.

[35] V. S. Polikov, P. A. Tresco, and W. M. Reichert, "Response of brain tissue to chronically implanted neural electrodes," *Journal of Neuroscience Methods*, vol. 148, no. 1, pp. 1–18, 2005, doi: 10.1016/j.jneumeth.2005.08.015.

[36] J. C. Barrese *et al.*, "Failure mode analysis of silicon-based intracortical microelectrode arrays in non-human primates," *Journal of neural engineering*, vol. 10, no. 6, p. 066014, 2013.

[37] R. Chen, A. Canales, and P. Anikeeva, "Neural recording and modulation technologies," *Nature Reviews Materials*, vol. 2, no. 2, pp. 1–16, 2017.

[38] T. D. Y. Kozai, A. S. Jaquins-Gerstl, A. L. Vazquez, A. C. Michael, and X. T. Cui, "Brain tissue responses to neural implants impact signal sensitivity and intervention strategies," *ACS chemical neuroscience*, vol. 6, no. 1, pp. 48–67, 2015.

[39] H. Lee, R. v Bellamkonda, W. Sun, and M. E. Levenston, "Biomechanical analysis of silicon microelectrode-induced strain in the brain," *Journal of neural engineering*, vol. 2, no. 4, p. 81, 2005.

[40] G. Lind, C. E. Linsmeier, and J. Schouenborg, "The density difference between tissue and neural probes is a key factor for glial scarring," *Scientific reports*, vol. 3, no. 1, pp. 1–7, 2013.

[41] T. Saxena *et al.*, "The impact of chronic blood–brain barrier breach on intracortical electrode function," *Biomaterials*, vol. 34, no. 20, pp. 4703–4713, 2013.

[42] G. Kotzar *et al.*, "Evaluation of MEMS materials of construction for implantable medical devices," *Biomaterials*, vol. 23, no. 13, pp. 2737–2750, 2002.

Chapter 2

Surgical procedure for microelectrode devices

2.1 Introduction

To understand brain functions, it is important to record neuronal activity in the brain with great spatial and temporal resolution over a lengthy period of time. Several inflammatory responses are elicited by implanted devices, including tissue damage during device penetration[1], [2], elastic mismatch between neural electrodes and neural tissue in the context of relative micromotion[3]–[5], chronic breach of the blood–brain barrier[6] and materials neurotoxicity[7]. In this Chapter, device penetration and implantation method for reducing tissue damage using dissolvable are detailed.

2.2 Penetration and implantation procedures

Figure 2.1 depicts standard device placement and insertion. Even though flexible film devices can be placed on brain tissue with tweezers (Figure 2.1a), the resolution of recorded signals are insufficient. The insert-type electrode, on the other hand, can record high-resolution signals. Traditional implant methods for in vivo chronic recording, however, involve tissue injury due to micromotion caused by the device connected to the

cranium after insertion (Figure 2.1b). As a result, I propose different approaches for implanting devices into brain tissue utilizing dissolvable material for non-invasive chronic recording.

Figure 2.2 shows the device placement using a dissolvable material. Dissolvable materials can “catch” and “release” the device without mechanical vibration by utilizing the “solid phase” via the “liquid phase” condition (Figure 2.2a). Furthermore, some dissolvable compounds can be melted with a solution such as phosphate-buffered saline (PBS) and entirely removed from brain tissue. These properties allow high-aspect-ratio devices[8]–[11] to be inserted into the brain without causing device failure or inflammation (Figure 2.2b). Furthermore, using biocompatible materials, minimal invasion, and continuous recording can be expected. Dissolvable materials with biocompatibility are discussed in length in section 2.3.

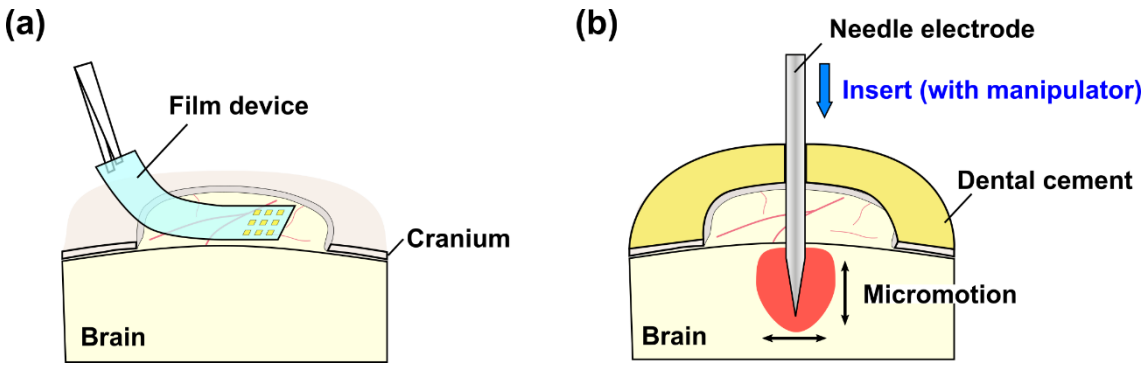

Figure 2.1 Conventional device placement and implantation. (a) Film device placement using tweezers. (b) Implantation method of needle electrode fix to cranium.

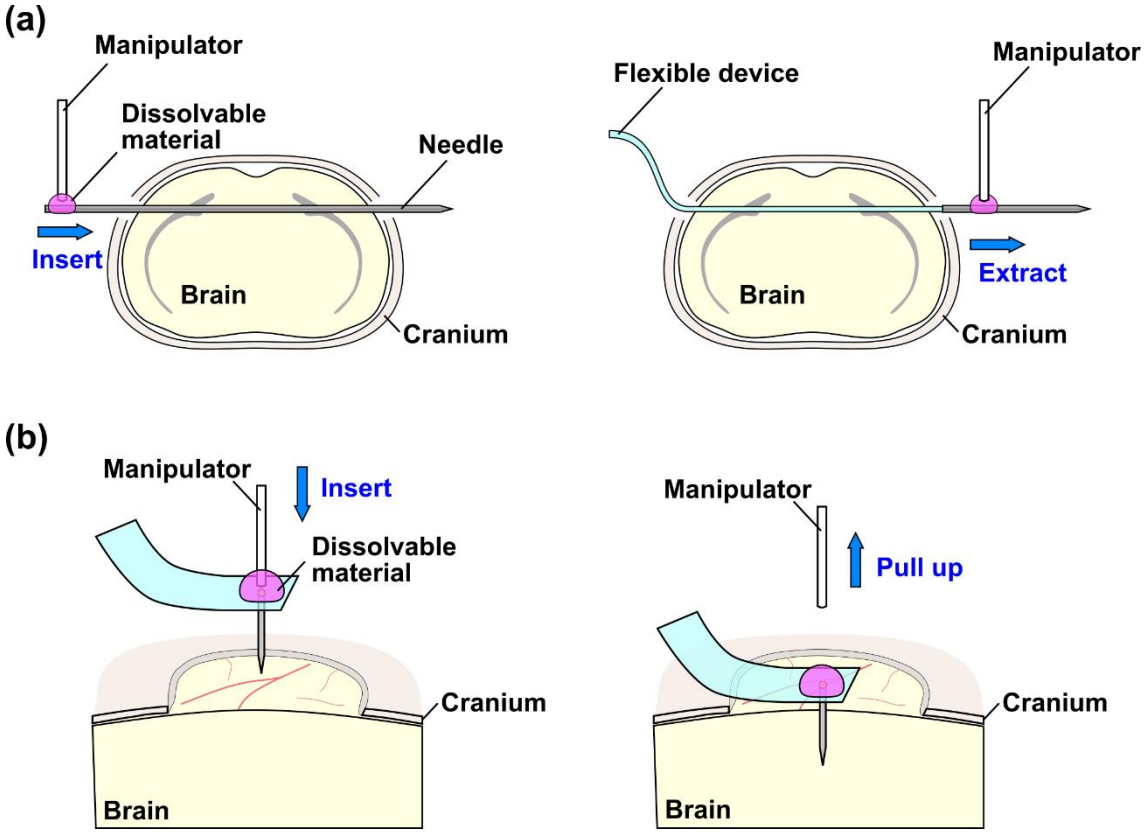

Figure 2.2 Device placement using dissolvable material. (a) Surgical method enables to "catch" and "release" without mechanical vibration. (b) Device placement for high-aspect-ratio electrode device.

2.3 Dissolvable materials with biocompatibility

A comparison of dissolvable materials with biocompatibility is shown in Table 2.1 and Figure 2.3. By heating paraffin wax below 60 °C, it transforms into a liquid phase and then into a solid phase for a short time at room temperature. Although paraffin wax has a quick response time, it requires a high temperature during device implantation on brain tissue (Table 2.1 and Figure 2.3a). Silk fibroin solution is made from B.mori cocoons that have been boiled, dried, and salted[12], [13]. The silk fibroin solution is crystallized in the air (< 24 hours) to produce a homogeneous silk film (Figure 2.3b)[14]–[16]. The silk film degrades proteolytically in water at ambient temperature (< 2 weeks) (Table 2.1)[16], [17]. At normal temperature, silk fibroin can dissolve. The silk fibroin solution, on the other hand, takes ~24 hours to silk film and takes ~2 weeks to dissolve. These time scales result in a misalignment in the surgical process. Polyethylene glycol (PEG) exhibits a liquid phase (~50 °C) when a PEG powder is heated, which is a solid

phase at ambient temperature. Furthermore, PEG dissolves quickly in PBS (Table 2.1 and Figure 2.3c)[18]. Furthermore, the degradation rate of PEG allows for the mixing of different molecular weights of PEG. These features are suitable for altering the time scale with device implantation during surgical operations.

Table 2.1 Comparison of different materials with biocompatibility.

	Melting point	Solidification time	Dissolving time
Paraffin wax	~ 60 ℃	Few seconds	×
Silk fibroin	×	~ 24 hours	~ weeks
Polyethylene glycol	~ 50 ℃	Few seconds	~ minutes

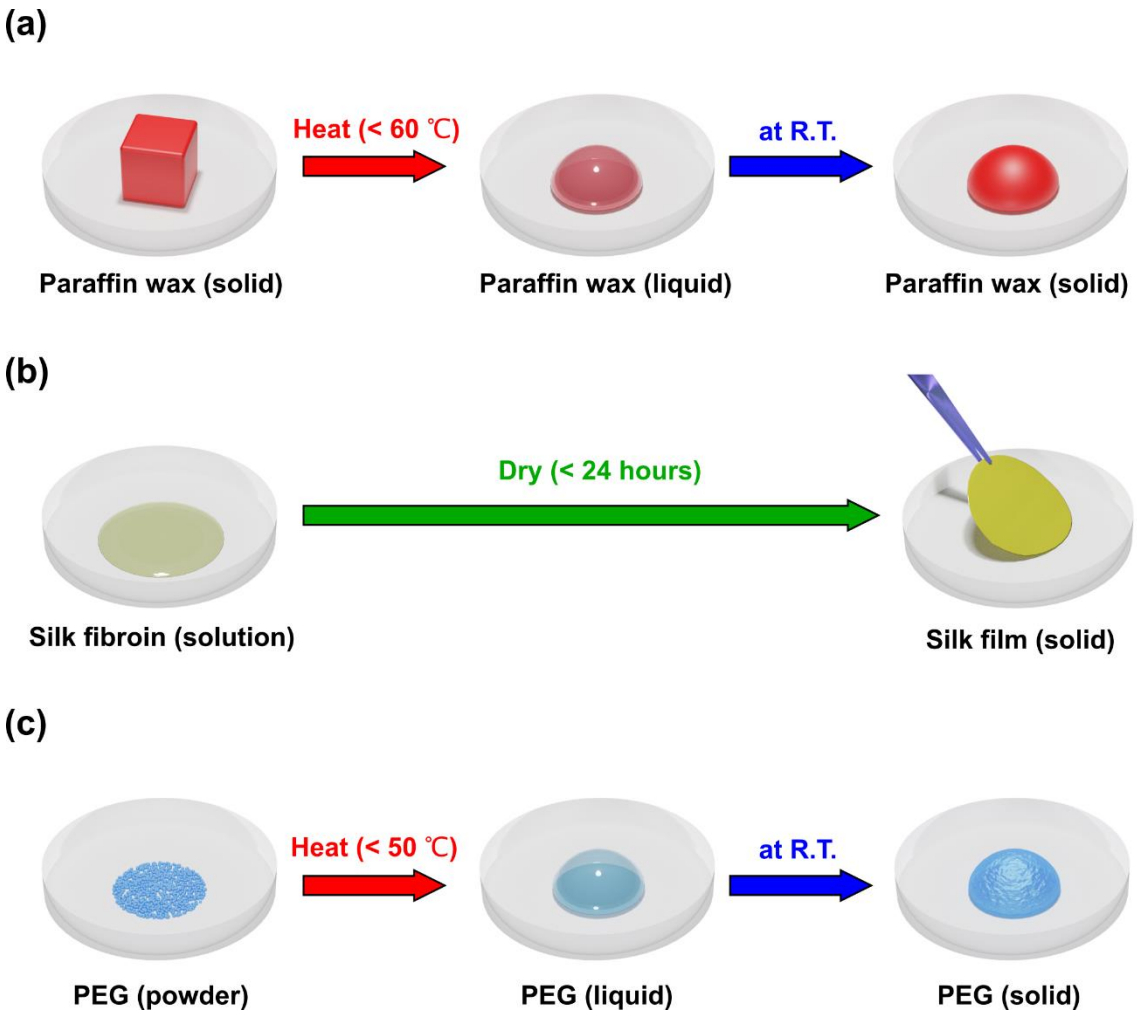

Figure 2.3 Comparison of biocompatibility materials for use device implantation. (a) Paraffin wax, (b) silk fibroin and (c) polyethylene glycol (PEG).

2.4 Conclusions

This Chapter discussed how to use dissolvable material to reduce tissue injury during device penetration and implantation. Using the states of "solid phase" and "liquid phase," the dissolvable materials may "capture" and "release" the device without mechanical vibration.". Polyethylene glycol is a dissolvable substance that is compatible with device insertion for surgical operations due to the time scale. In the next chapter, I will investigate low-invasive chronic recording with a flexible parylene-thread microelectrode and a surgical method involving PEG.

Reference

[1] M. P. Ward, P. Rajdev, C. Ellison, and P. P. Irazoqui, "Toward a comparison of microelectrodes for acute and chronic recordings," *Brain research*, vol. 1282, pp. 183–200, 2009.

[2] V. S. Polikov, P. A. Tresco, and W. M. Reichert, "Response of brain tissue to chronically implanted neural electrodes," *Journal of Neuroscience Methods*, vol. 148, no. 1, pp. 1–18, 2005.

[3] J. C. Barrese *et al.*, "Failure mode analysis of silicon-based intracortical microelectrode arrays in non-human primates," *Journal of neural engineering*, vol. 10, no. 6, p. 066014, 2013.

[4] H. Lee, R. v Bellamkonda, W. Sun, and M. E. Levenston, "Biomechanical analysis of silicon microelectrode-induced strain in the brain," *Journal of neural engineering*, vol. 2, no. 4, p. 81, 2005.

[5] G. Lind, C. E. Linsmeier, and J. Schouenborg, "The density difference between tissue and neural probes is a key factor for glial scarring," *Scientific reports*, vol. 3, no. 1, pp. 1–7, 2013.

[6] T. Saxena *et al.*, "The impact of chronic blood–brain barrier breach on intracortical electrode function," *Biomaterials*, vol. 34, no. 20, pp. 4703–4713, 2013.

[7] G. Kotzar *et al.*, "Evaluation of MEMS materials of construction for implantable medical devices," *Biomaterials*, vol. 23, no. 13, pp. 2737–2750, 2002.

[8] H. Sawahata *et al.*, "Single 5 μm diameter needle electrode block modules for unit recordings in vivo," *Scientific Reports*, vol. 6, p. 35806, 2016.

[9] A. Fujishiro, H. Kaneko, T. Kawashima, M. Ishida, and T. Kawano, "In vivo neuronal action potential recordings via three-dimensional microscale needle-electrode arrays," *Scientific Reports*, vol. 4, pp. 1–9, 2014.

[10] Y. Kubota *et al.*, "Long nanoneedle-electrode devices for extracellular and intracellular recording in vivo," *Sensors and Actuators B: Chemical*, vol. 258, pp. 1287–1294, 2018.

[11] T. D. Y. Kozai *et al.*, "Ultrasmall implantable composite microelectrodes with bioactive surfaces for chronic neural interfaces," *Nature materials*, vol. 11, no. 12, pp. 1065–1073, 2012.

[12] U.-J. Kim, J. Park, H. J. Kim, M. Wada, and D. L. Kaplan, "Three-dimensional aqueous-derived biomaterial scaffolds from silk fibroin," *Biomaterials*, vol. 26, no.

15, pp. 2775–2785, 2005.

[13] Q. Lu *et al.*, "Silk fibroin electrogelation mechanisms," *Acta biomaterialia*, vol. 7, no. 6, pp. 2394–2400, 2011.

[14] D. Kim *et al.*, "Dissolvable films of silk fibroin for ultrathin conformal bio-integrated electronics.," *Nature Materials*, vol. 9, no. 6, pp. 511–517, 2011..

[15] S. Yagi *et al.*, "Dissolvable Base Scaffolds Allow Tissue Penetration of High-Aspect-Ratio Flexible Microneedles," *Advanced healthcare materials*, vol. 4, no. 13, pp. 1949–1955, 2015.

[16] A. Lecomte *et al.*, "Silk and PEG as means to stiffen a parylene probe for insertion in the brain: Toward a double time-scale tool for local drug delivery," *Journal of Micromechanics and Microengineering*, vol. 25, no. 12, 2015.

[17] H. Jin *et al.*, "Water-stable silk films with reduced β-sheet content," *Advanced Functional Materials*, vol. 15, no. 8, pp. 1241–1247, 2005.

[18] S. Felix *et al.*, "Removable silicon insertion stiffeners for neural probes using polyethylene glycol as a biodissolvable adhesive," in *Conf. Proc. IEEE Eng. Med. Biol. Soc*, 2012, vol. 2012, pp. 871–874.

Chapter 3

Parylene-thread microelectrode

3.1 Introduction

The electrode substrate's flexibility decreases penetration-induced tissue damage[1]–[4]. Furthermore, decreasing the total needle geometry (diameter or width) reduces the degree of tissue inflammation. Micro-electro-mechanical system (MEMS) devices based on flexible materials were created to combine these features. However, because they were to be placed into biological tissue, their application was difficult. Furthermore, in electrophysiology, the accurate penetration of the needle as well as the microelectrodes contained within it is a significant factor. Moreover, these microelectrode locations should be fixed for long-term recording (e.g., persistent device implantation). Several techniques have been proposed to penetrate the flexible needle[5]–[8]; however, as the next step, the penetration method requires features of minimized tissue damage and the precise position control of the microelectrodes during the penetration and fixation of these electrodes towards the chronic recording.

The method described in this Chapter is based on a traditional stitching mechanism. It entails the use of a “thread-like” flexible parylene substrate device with microelectrodes, which allows for accurate penetration and implantation into the brain and other biological tissues with the assistance of a guiding microneedle. A tungsten

microneedle is attached to the tip of a parylene-thread microelectrode. The tungsten microneedle, like conventional sewing, plays a role during tissue penetration and guides the flexible device into the tissue; however, the tungsten needle is wholly withdrawn from the tissue. I also suggest a stitching method that manipulates the parylene-thread microelectrode with a dissolvable substance to reduce physical stress to brain tissue during device penetration. The proposed methodology has the advantages of i) reduced tissue injury during device penetration; ii) accurate positioning of the microelectrodes by guiding the tungsten needle, and; iii) implantation capabilities by attaching each side of the threaded part to the cranium.

3.2 Design and fabrication

I developed a parylene-thread microelectrode with a length of 1,500 μm and 150 μm width thread section with a 500 μm spacing array of three Pt microelectrodes (10 μm × 40 μm). The overall length of the parylene device geometry was 33,000 μm, including the three Pt-electrode pads for external connections (Figure 3.1).

A parylene film MEMS method was used to make the proposed parylene-thread microelectrode (Figure 3.2)[9]–[11]. The device process was initiated with a 5-μm thick parylene film on a Si substrate by vacuum deposition equipment (model PDS2010, LABCOTER). As both the microelectrode-site and the device interconnection, a platinum (Pt) layer was formed on the parylene film by sputtering and etching with argon (Ar) plasma (Figure 3.2 (i,ii)). The Pt layer was subsequently covered using another parylene layer of 5 μm parylene, that was followed by parylene patterning using oxygen (O_2) plasma with a titanium (Ti)-mask (Figure 3.2 (iii–v)). Finally, the parylene film was released from the substrate using ethanol (Figure 3.2 (vi)).

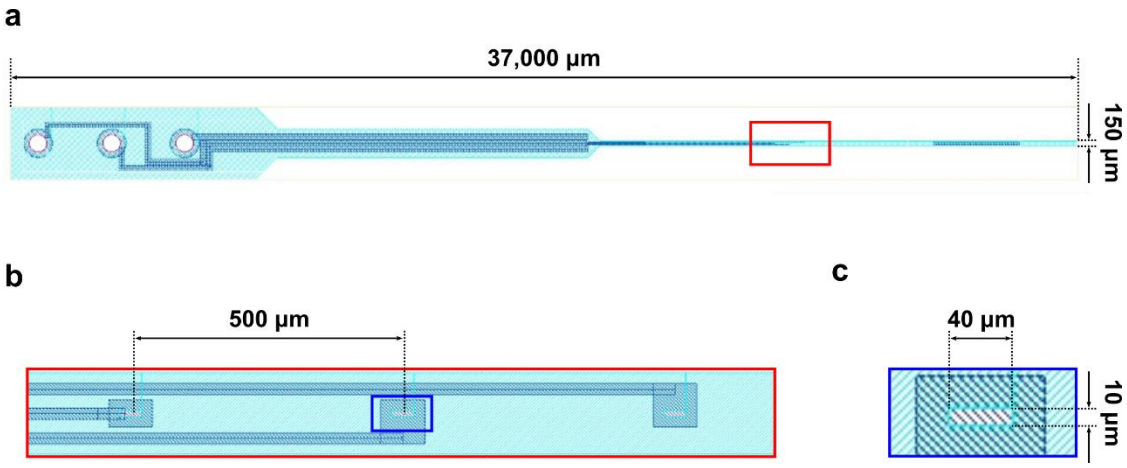

Figure 3.1 Design of the parylene-thread microelectrode. (a) Entire image of the design of the parylene-thread microelectrode array. (b) Enlarged view of the microelectrode. (c) Enlarged view of the microelectrode with a size of 10 × 40 μm.

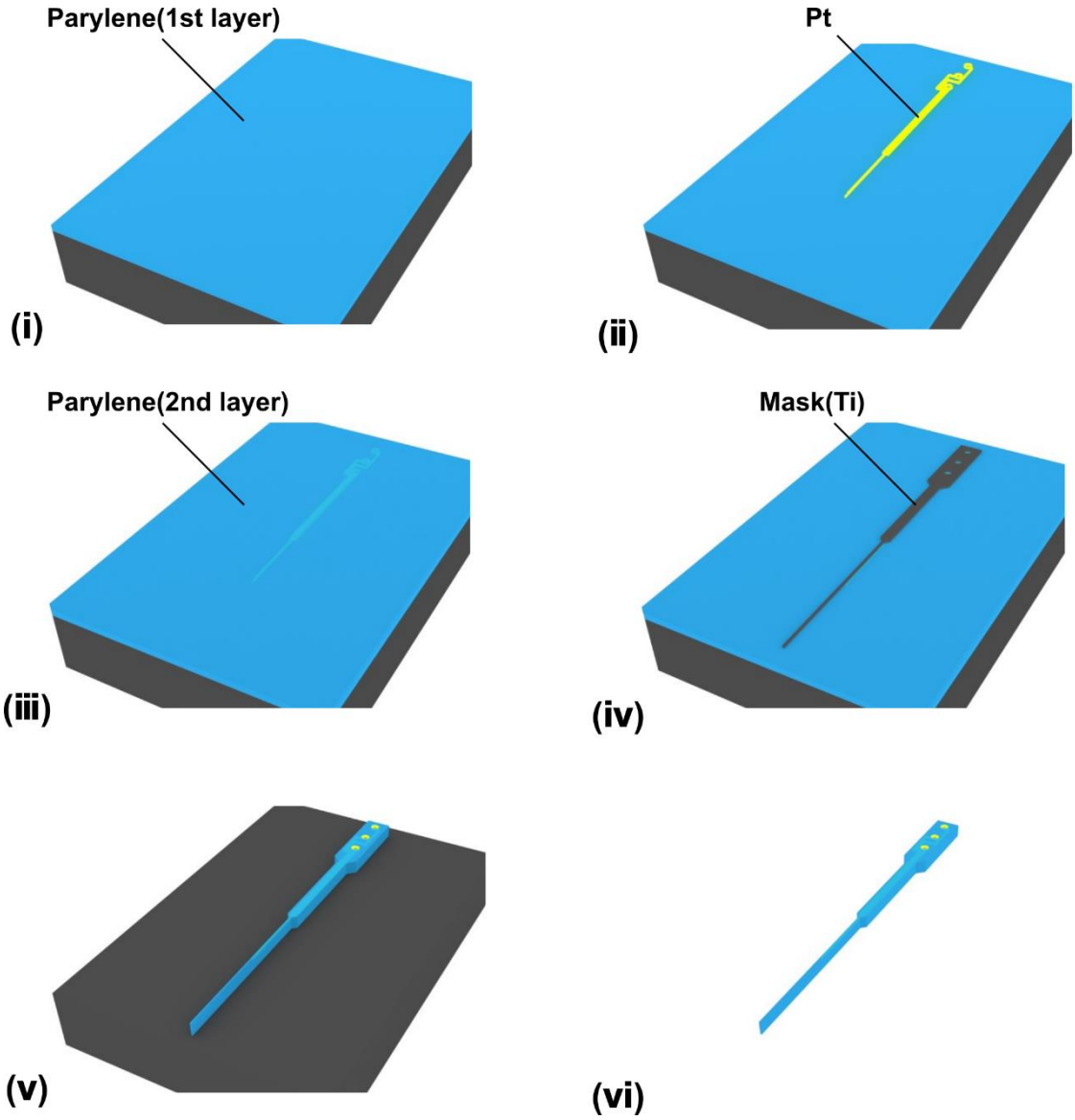

Figure 3.2 Fabrication process of parylene-thread microelectrode: (i) first, parylene deposition on a substrate (Si); (ii) Pt layer as both the electrode-site and the device interconnection that was formed on parylene by sputtering and etching; (iii) second, parylene deposition; (iv, v) parylene patterning by O_2 plasma with a Ti-mask; and (vi) release of parylene film from the substrate using ethanol.

3.3 Device packaging and electrical characteristics

Figure 3.3a depicts the thread portion of the fabricated parylene-thread microelectrode with a thickness of 10 μm (parylene thickness was measured by using spectroscopic film thickness measurement system). Each size of the fabricated Pt-electrodes shows ~15 μm × 40 μm (Figure 3.3b, c), which are larger than the designed

values (10 μm × 40 μm). This size difference is due to the over-etching of the top parylene layer (5 μm) in O_2 plasma etching, step "v" in Figure 3.2. The process can be improved by compensating the exceeded parylene etching.

Figure 3.4 depicts the packaging device in which the tip portion of the thread-bioprobe is connected to an tungsten microneedle [two types of diameters used: 150 μm (Figure 3.4b) and 50 μm in animal experiment] by a ultraviolet (UV)-curable resin with the geometry of <150 μm in width. On the other device-sided each microelectrode's pad is connected to conventional pin connectors (three channels). The Pt-microelectrode's impedance characteristics at 10 Hz – 10 kHz, measured in phosphate buffered saline (PBS) at room temperature, ranged from 69 ± 16 kΩ to 12 ± 3 MΩ [500 ± 100 kΩ (mean ± SD) at 1 kHz]. These were further reduced from 19 ± 2 kΩ to 1 ± 0.2 MΩ [54 ± 6 kΩ (mean ± SD) at 1 kHz] by additional plating with a low impedance material of platinum black (Pt black) (Figure 3.5)[12]–[14]. These values are sufficiently low for measuring the neuronal activity[13]–[15]. As the actual sewing of the device into the tissue, a device characterization of twist test was also conducted while the electrode impedance was measured. Herein, the parylene-thread microelectrode was twisted in five turns, showing no significant change in the electrode's impedance (Figure 3.6).

I also explored the amplitude attenuation of recorded neuronal signals associated with the electrodes' impedance characteristics and a recording system with a preamplifier (ZC64, Tucker-Davis Technologies, USA, input resistance = 1×10^{14} Ω), as measuring the output/input signal amplitude ratios of the thread-bioprobe device with the recording system (Figure 3.7). By applying test signals of 300 μV peak-to-peak sinusoidal waves from 1 Hz – 10 kHz, the measured output/input ratios ranged from 69% to 89% (averages of 3 electrodes) (84% at 1 kHz for spike recording), while the measured root mean square noise voltage was 26.4 μVrms. Considering the used test signals (300 μV, 1 kHz), the calculated signal-to-noise ratio of the recording system was 18 dB.

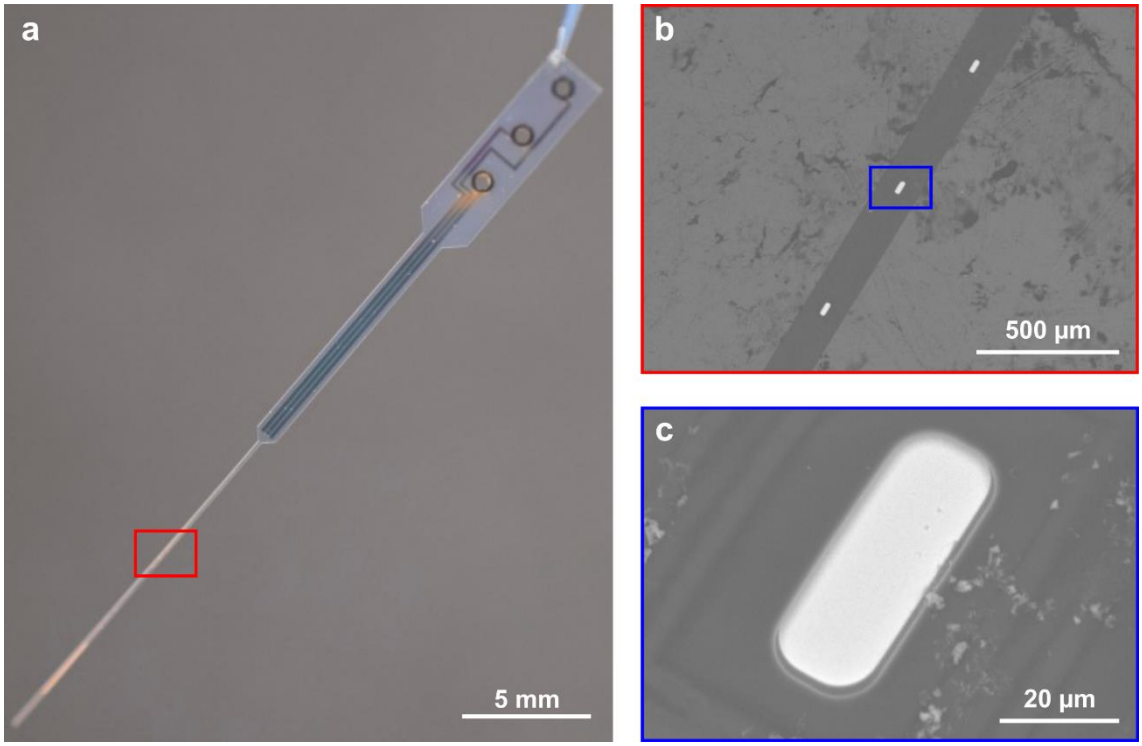

Figure 3.3 Fabricated parylene-thread microelectrode. (a) Photograph of overview of the parylene-thread microelectrode. (b, c) Insets of red and blue squares that denote the SEM images of an array of three Pt microelectrodes and one electrode in the device, respectively.

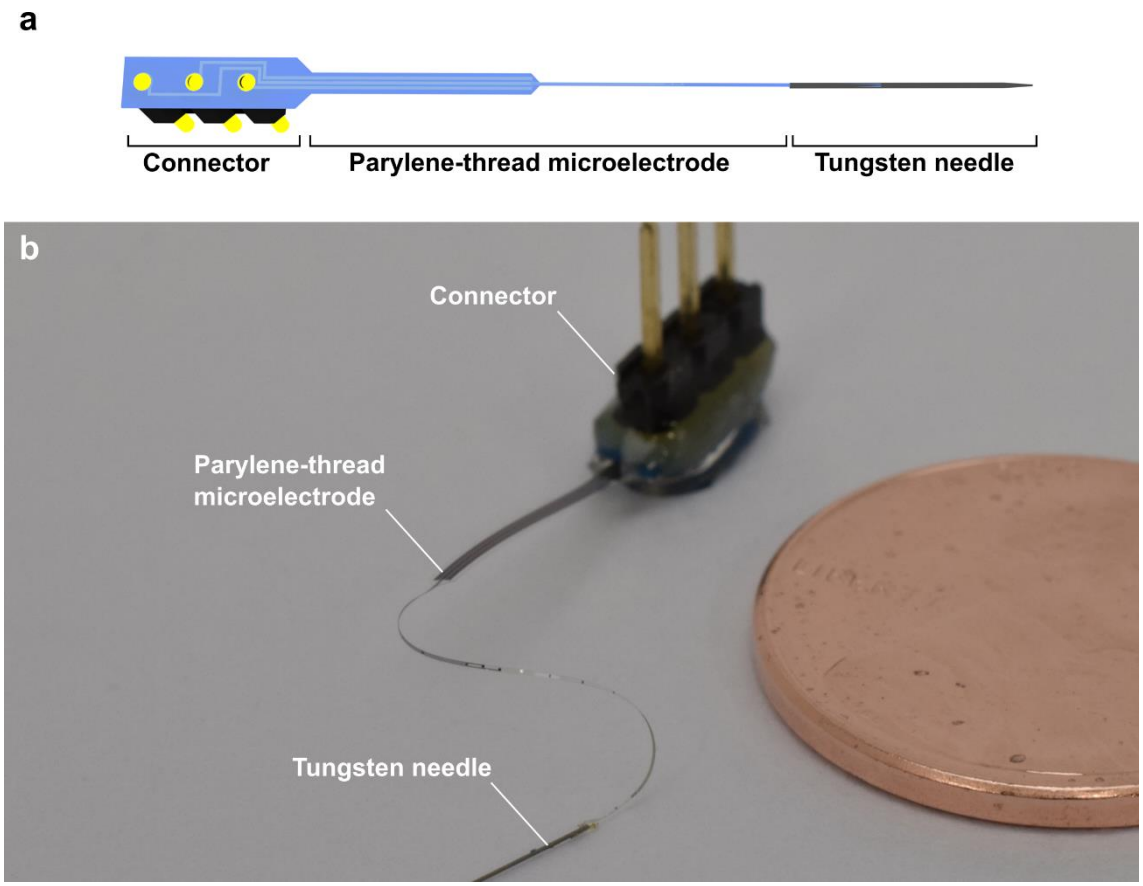

Figure 3.4 Schematic and photograph showing the packaging device. The tip portion of the parylene-thread microelectrode was connected to a tungsten microneedle; further, each electrode's pad at the other device-side is connected to conventional pin connectors (three channels).

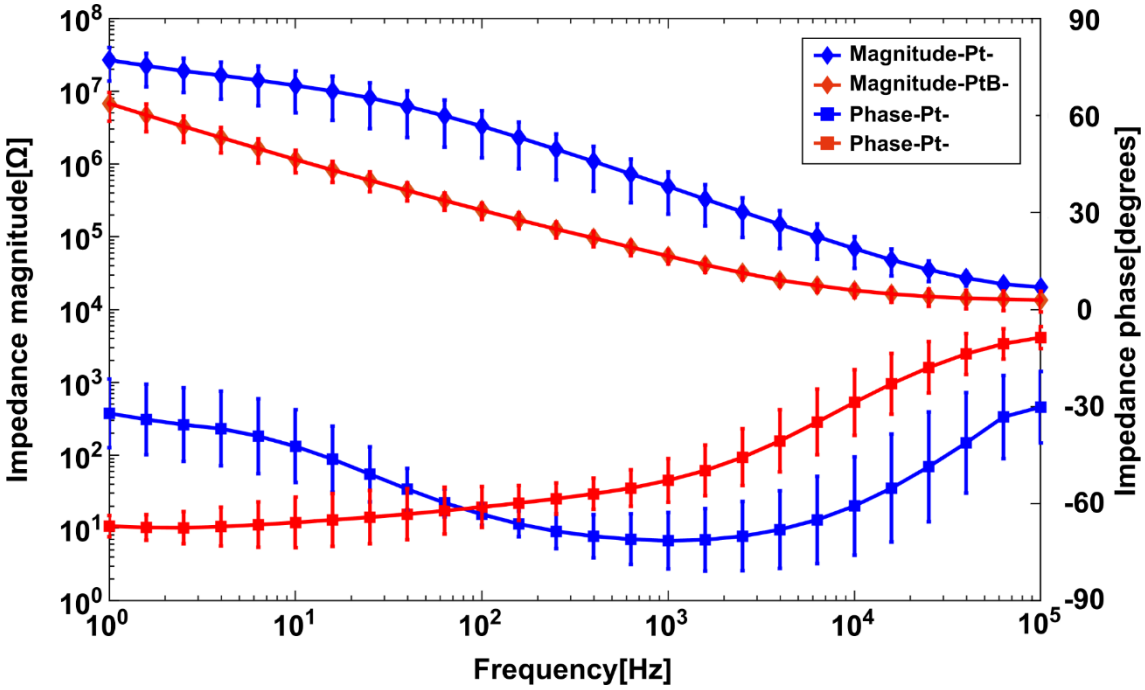

Figure 3.5 The impedance characteristics of Pt black plated microelectrodes measured in phosphate buffered saline (PBS) at room temperature.

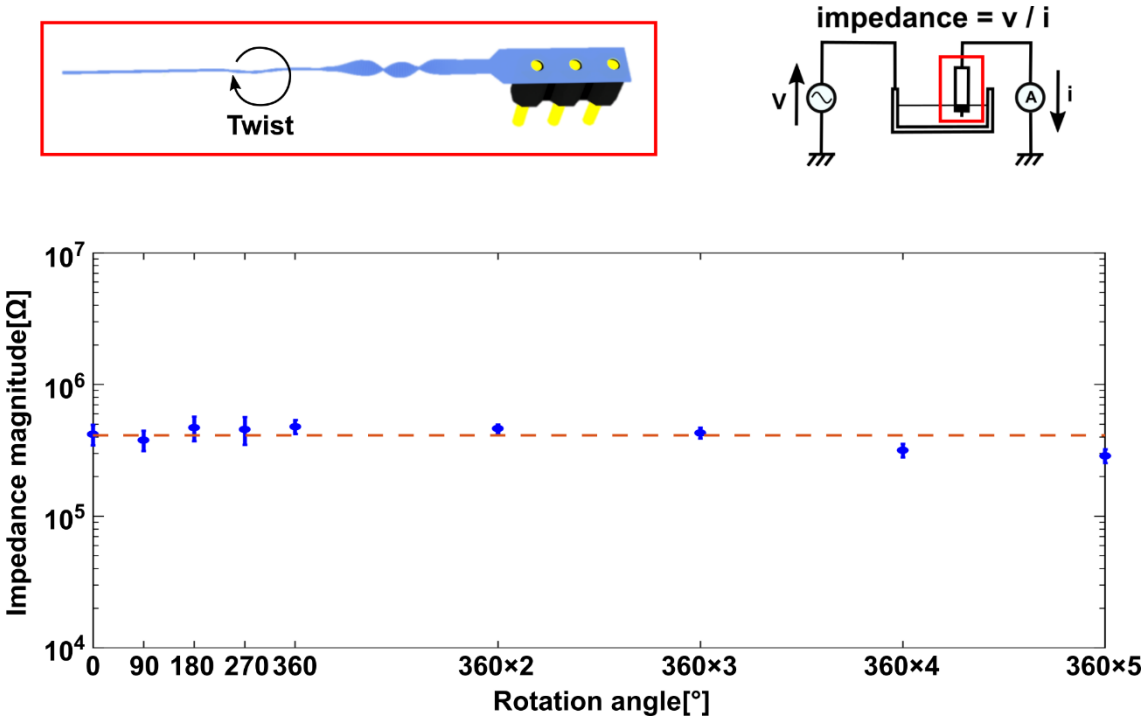

Figure 3.6 The impedance characteristics of the twisted parylene-thread microelectrode. The parylene-thread is twisted in five turns (360 × 5), showing no significant change in the electrode's impedance.

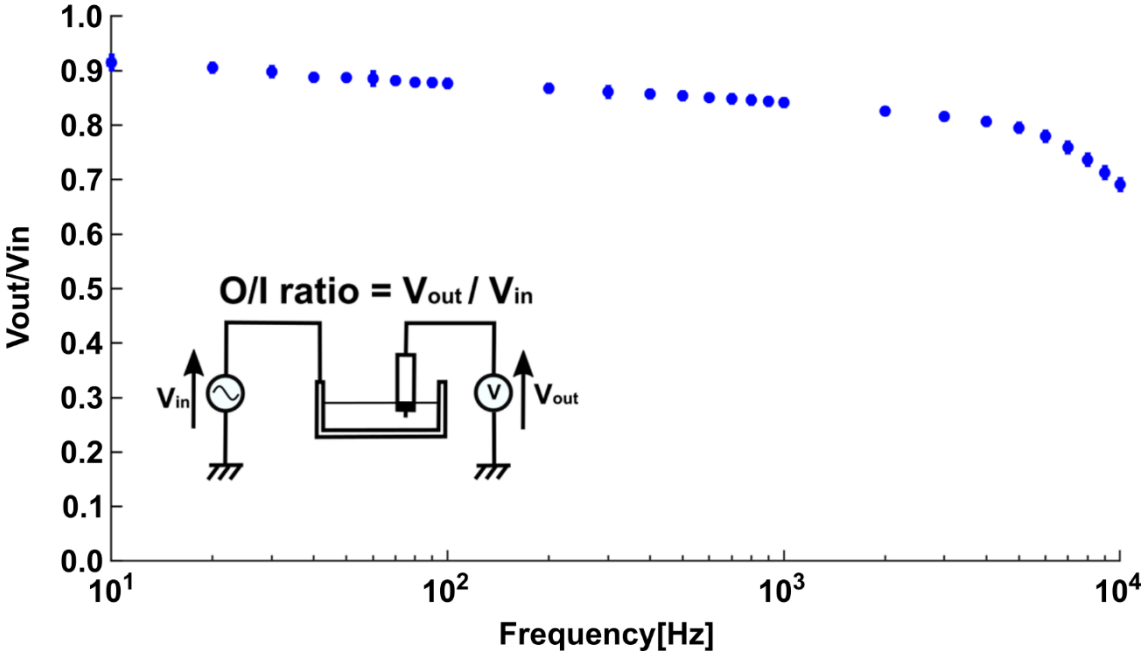

Figure 3.7 Output/input signal amplitude ratios of Pt black microelectrodes measured in PBS. Test signals of 300 μV peak-to-peak sinusoidal waves from 1 Hz to 10,000 Hz Are applied to the PBS.

3.4 Sewing method and EMG signal recording

Figure 3.8 shows the sewing and signal recording capabilities of the fabricated parylene-thread microelectrode using hindlimb muscle of the mouse. The mouse (male, 20–25 g) was anesthetized by intraperitoneal injection of urethane (50 μl of 10% solution per 10 g body weight) and chlorprothixene (100 μl of 0.5% solution per 10 g body weight). For the device sewing in the biological tissue, I used the tungsten microneedle with a diameter of 50 μm, which was manipulated by hand with tweezers. By guiding the tungsten needle, the fabricated thread-bioprobe was punched and embedded into the medial gastrocnemius (MG) muscle. Figure 3.8b depicts two of the three Pt black microelectrodes that were placed on the muscle surface while the other one was embedded in the muscle. For multichannel recording, three microelectrodes were embedded in the muscle (picture not depicted).

During the recording, the nerve corresponding to the MG muscles was electrically stimulated with a current ranging from +0.1 to +1.0 mA, 0.1 mA step, with a 100 μs duration at 1 s intervals (100 trials for each current range). No response was observed

from these three microelectrodes to the stimuli ranging from +0.1 to +0.2 mA (Figure 3.9a). However, a response could be observed at the current stimulation of +0.3 mA; further, a response clearly appeared at the current stimuli of more than +0.5 mA (Figure 3.9b). Furthermore, these recorded signals were observed to be nonlinear (Figure 3.10) and the latency of responses is approximately 5 ms, the waveforms that were recorded via the three microelectrodes were considered to be the electromyography (EMG) signals that were generated by the current stimuli to the nerve.

I further investigated the device displacement through the cycling tests of the muscle stimulation. Figure 3.11 shows a set of photographs before and after the stimulation for 500 trials. Herein, two of the three microelectrodes (Pt black) were placed on the muscle surface for the displacement observation, while the other one (upper right in each picture) was embedded in the muscle. The device displacement analysis was performed by measuring the distance between the positions of an electrode and a blood vessel as shown in the photograph. After 500 trials, this distance was measured as approximately 3 μm.

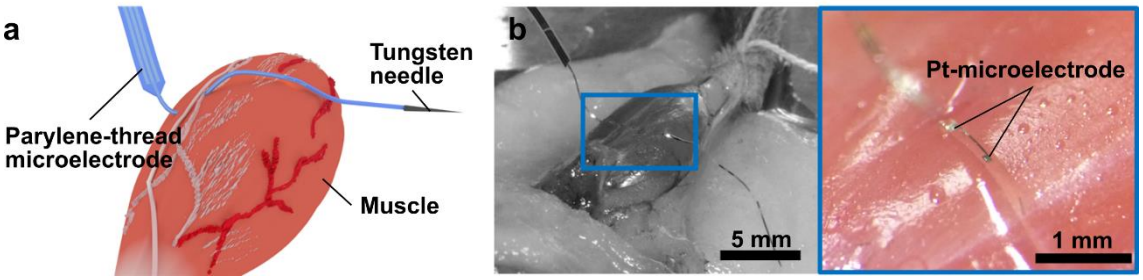

Figure 3.8 (a) Schematic and (b) photographs of the parylene-thread microelectrode, which was sewn to the MG muscle in the mouse's leg by guiding the tungsten microneedle.

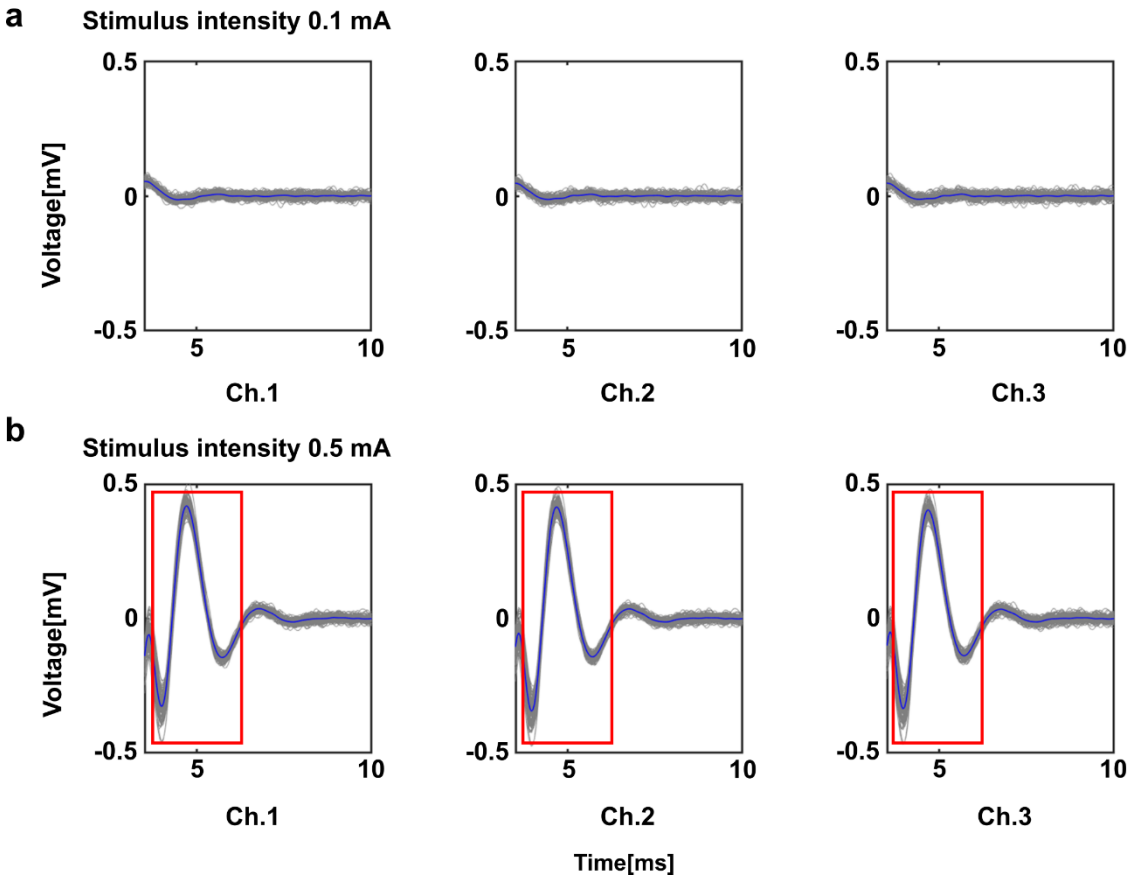

Figure 3.9 Signal waveforms recorded from the muscle via three Pt black microelectrodes embedded in the muscle. During the electrical stimuli to the corresponding nerve: 0.1 mA (a) and 0.5 mA (b).

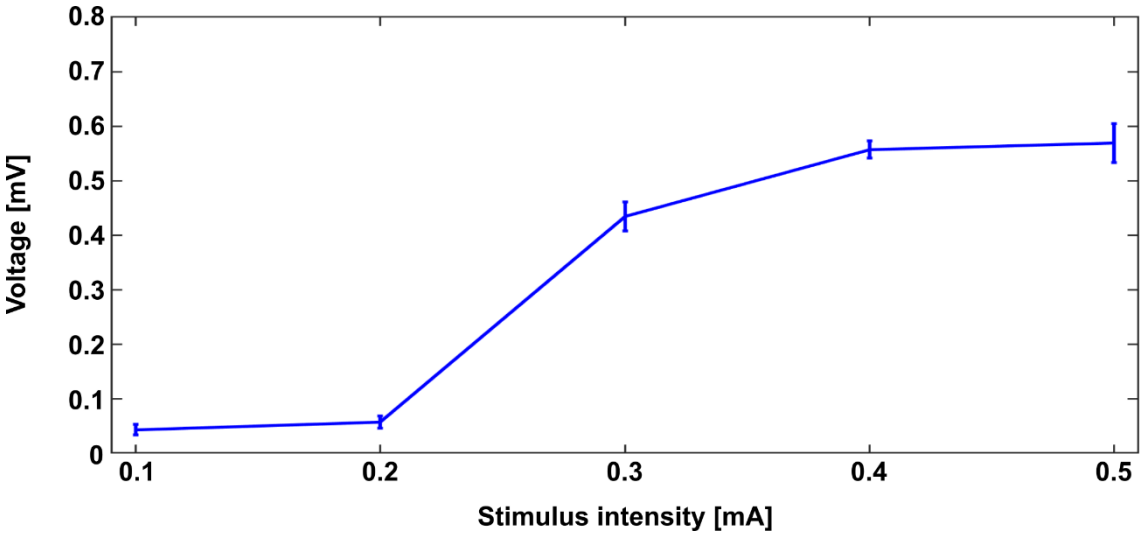

Figure 3.10 Stimulus intensity-dependent EMG signal amplitudes.

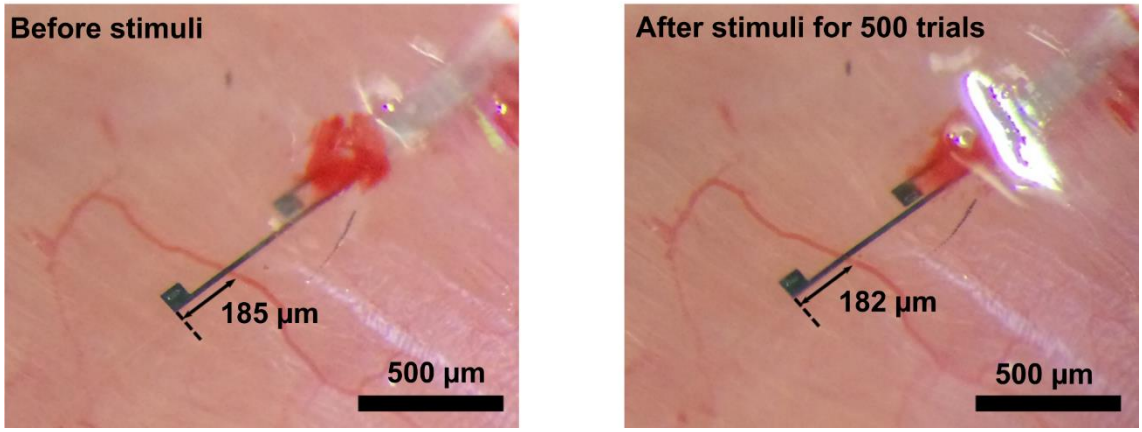

Figure 3.11 Device displacement during the muscle stimuli for 500 trials. The device displacement was analyzed by measuring the distance between the microelectrode and the blood vessel in each photograph (before and after).

3.5 Surgical procedure for brain tissue

The multichannel neuronal signal recording within the tissue for both acute and chronic cases can be obtained by applying the designed parylene-thread microelectrode; however, the tissue damage associated with the device penetration via the tungsten needle by hand (as earlier demonstrated using muscle, Figure 3.8-Figure 3.11) should be minimized. To overcome the issue of tissue damage, a surgical sewing method of using a dissolvable material of PEG is proposed. Because PEG shows both the liquid and solid phases at varying temperatures (~60 °C), it enables the 'catch' and 'release' of the tungsten needle during manipulation.

Figure 3.12 shows the proposed surgical procedure in the sewing of the parylene-thread microelectrode into the gelatin brock. The tungsten microneedle, which was held by a manipulator (first manipulator) via PEG, penetrated the gelatin (Figure 3.12(i)). The tip portion of the tungsten needle was subsequently caught using a liquid–PEG of the other manipulator (second manipulator, Figure 3.12(ii)), which was cooled and solidified for holding of the needle. By dropping solution (PBS) on the PEG at the first manipulator, the tungsten needle was released from the manipulator; however, the needle was held by the second manipulator (Figure 3.12(iii)). The tungsten needle was continuously pulled using the second manipulator, resulting in a parylene-thread and that was placed inside the gelatin block (Figure 3.12(iv)).

Furthermore, I observation of the needle's displacement during the needle

manipulation of "catch" and "release" (Figure 3.13). Both "catch" and "release" of displacement of the needle during the surgical procedure showed without significant differences (< 50 μm), respectively.

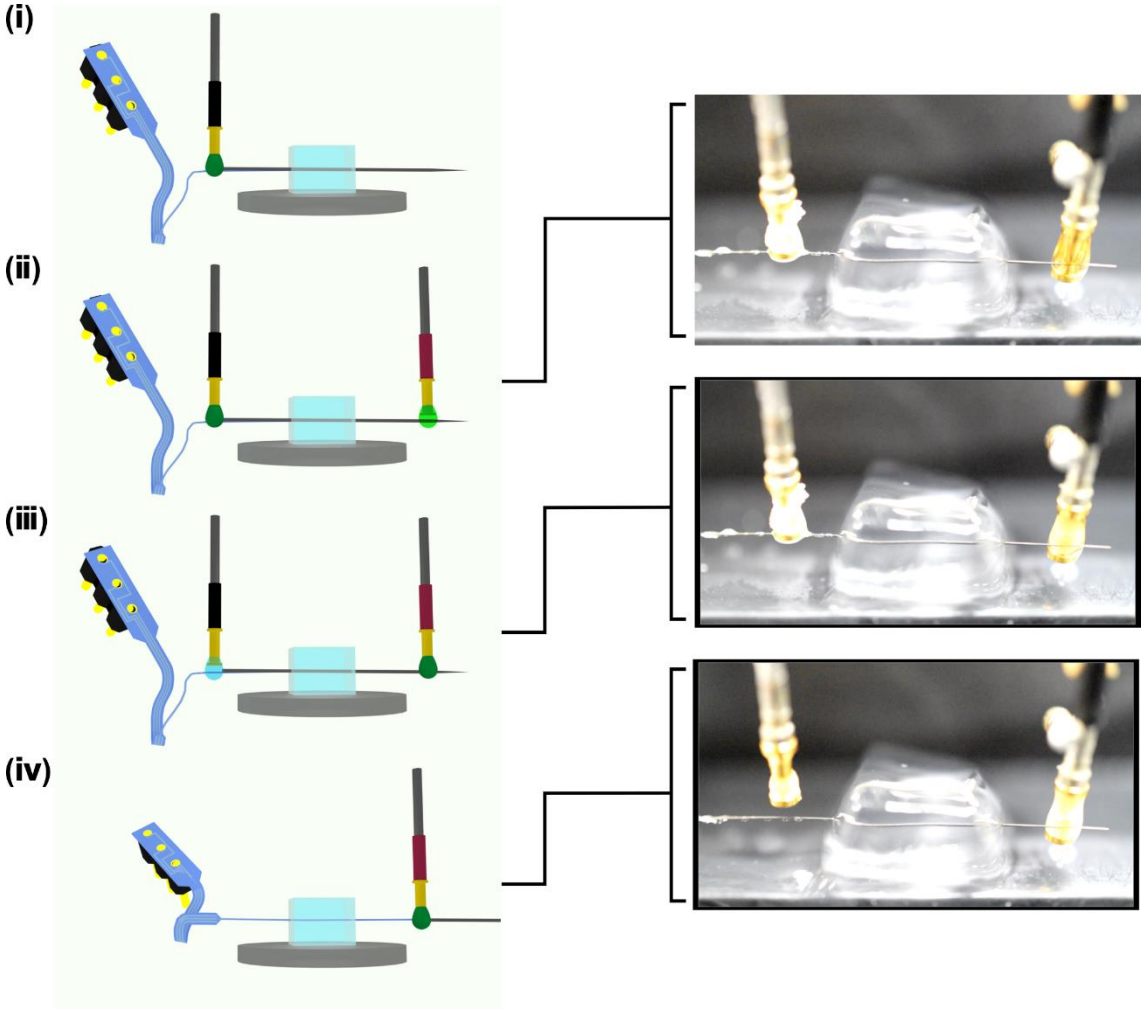

Figure 3.12 Schematics and photographs of surgical procedure with “catch” and “release” of the tungsten needle using the gelatin block: (i)The tip portion of the tungsten needle is caught using a liquid-PEG of the other manipulator (ii), which was cooled and solidified for holding the needle (iii). By dropping solution (PBS) on the PEG at the first manipulator, the tungsten needle is released from the manipulator, while the needle is held by the second manipulator (iv).

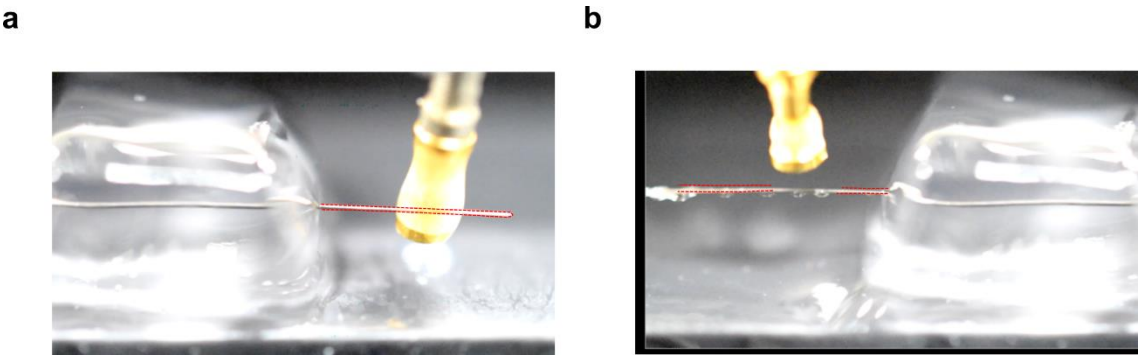

Figure 3.13 Photographs of observation of the needle's displacement during the needle manipulation of (a) "catch" and (b) "release." Measured displacement of the needle during the surgical procedure was within 50 µm. The diameter of the used tungsten needle is 150 µm.

3.6 Acute in vivo neuronal recording

Figure 3.14 shows the proposed surgical procedure in the sewing of parylene-thread microelectrode into the mouse brain tissue. The tungsten microneedle, which was held by a manipulator (first manipulator) via PEG, penetrated the tissue and passed through the two holes of cranial opening (Figure 3.14(i)). The tip portion of the tungsten needle was subsequently caught using a liquid–PEG of the other manipulator (second manipulator, Figure 3.14(ii)), which was cooled and solidified for holding of the needle. By dropping solution (PBS) on the PEG at the first manipulator, the tungsten needle was released from the manipulator; however, the needle was held by the second manipulator (Figure 3.14(iii)). The tungsten needle was continuously pulled using the second manipulator, resulting in the parylene-thread microelectrode and that was placed inside the mouse's brain tissue (Figure 3.14(iv)). As a surgical advantage, the positions of microelectrodes in the tissue can be monitored precisely by the second manipulator.

Figure 3.15 depicts the cranial opening area in which the parylene-thread microelectrode penetrated the brain tissue. Herein, the cranial opening area measured 1–3 mm in diameter, and the device's footprint in the tissue was approximately 150 µm in diameter (the diameter of the tungsten needle is 50 µm; the width and thickness of the parylene device are 150 and 10 µm, respectively). Using this surgical procedure, the tissue damage can be minimized, as confirmed by the minor bleeding in the tissue after the trials more than five times.

The in vivo acute neuronal recording capability was also demonstrated using the mouse's brain (Figure 3.16a). The mouse (male, 20–25 g) was anesthetized by intraperitoneal injection of urethane (50 µl of 10% solution per 10 g body weight) and chlorprothixene (100 µl of 0.5% solution per 10 g body weight). To record the visual response, after the cranial opening (3.2–3.5 mm on the lateral side and 4.0 mm on the caudal side from the bregma, having a diameter of 1–3 mm), the fabricated parylene-thread microelectrode consisting of Pt-black plated three microelectrodes was inserted into the tissue and placed in the cortical layers of the primary visual cortex (V1) on the right hemisphere (~ 2.5 mm on the lateral side and 4.0 mm on the caudal side from the bregma) by manipulating the tungsten microneedle (50 µm diameter) with PEG (Figure 3.16b). With the needle's guide, each microelectrode (Pt black, 10 × 40 μm^2 in area) was precisely positioned in the tissue achieving lateral distances of 3.0 mm for Ch. 1, 2.5 mm for Ch. 2, and 2.0 mm for Ch. 3 along with the device penetration (Figure 3.16b).

As a visual stimulus, a light emitting diode (LED) array, consisting of nine white LEDs on a 20-mm wide substrate, was used. While visual stimuli were applied to the mouse's eye for 0.5 s, neuronal responses were repeatedly recorded via the three embedded microelectrodes in the tissue (Figure 3.17). The second panel in Figure 3.17 represents low frequency-band (filtering = 10–500 Hz), whereas third panel shows high frequency-band (filtering = 500–3,000 Hz) waveforms recorded by each microelectrode. The low frequency-band waveform signals appeared at around 0.25 s, which were consistent with the latency of the visual response, were subjected to be the LFP evoked by the visual stimuli. Bottom two panels show raster plots and peri-stimulus time histograms (PSTHs), respectively, taken from each high frequency-band signals. The detection thresholds for each channel were 4 times the standard deviation (σ) of the mean signal – 0.5 to −1.0 s before the stimulus onset. However, no significant responses to the visual stimulus were obtained. This was probably due to the creation of a gap between the recording electrodes and their neuronal signal sources[1], [16]–[18] (the geometries of our device are 50 µm diameter for tungsten needle, 150 µm width for parylene-thread, and 150 µm width for the resin junction, Figure 3.18).

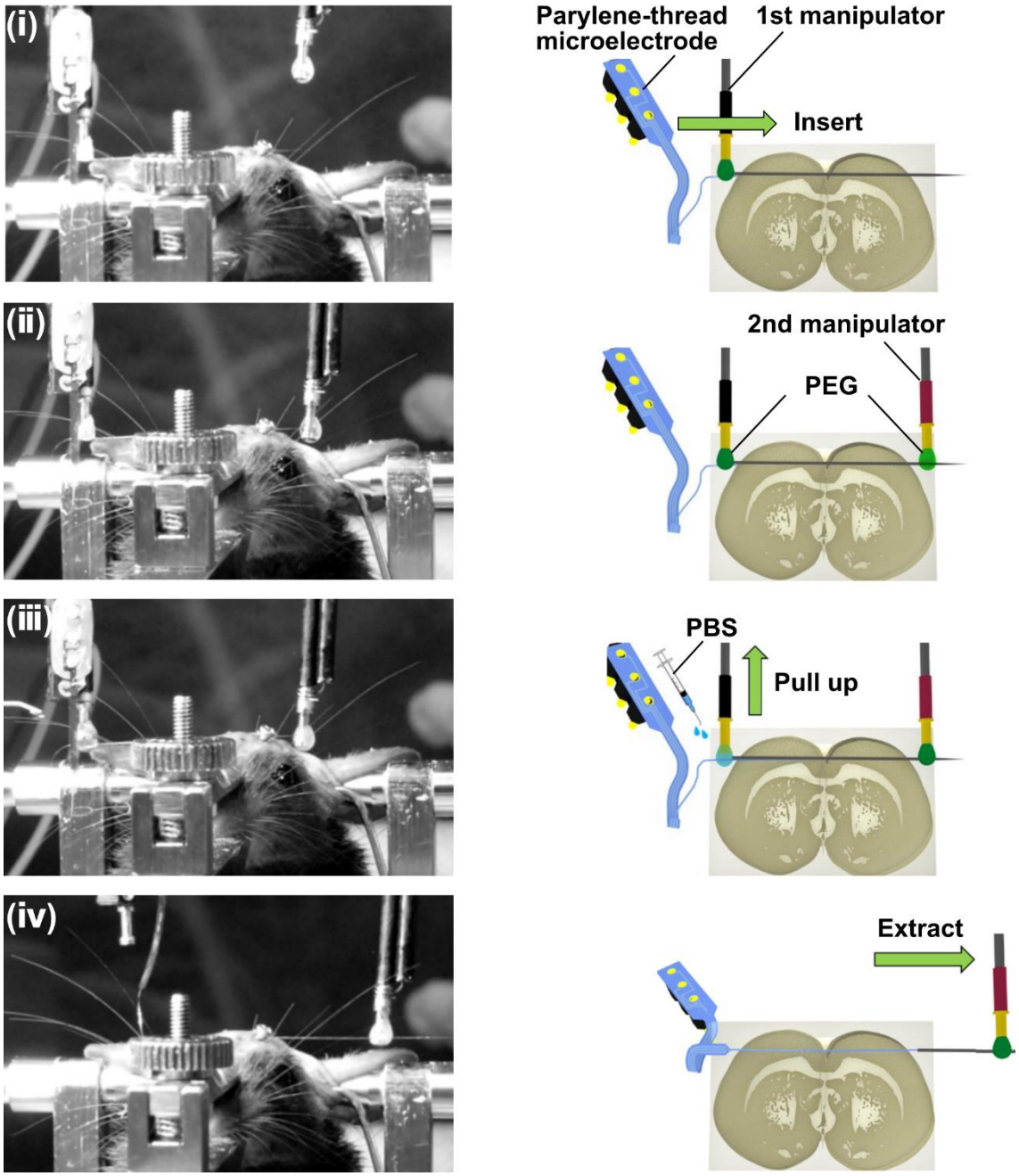

Figure 3.14 Schematic and photographs of each step in the surgical procedure: (i) tungsten microneedle penetrates through the tissue while the needle is held with PEG at first manipulator; (ii) the tip portion of the tungsten needle that is caught using the second manipulator with PEG; (iii) release of the tungsten needle from the first manipulator by dipping PBS to the PEG; and (iv) continuous pulling of the tungsten needle with the second manipulator for placing the parylene-thread microelectrode within the tissue.

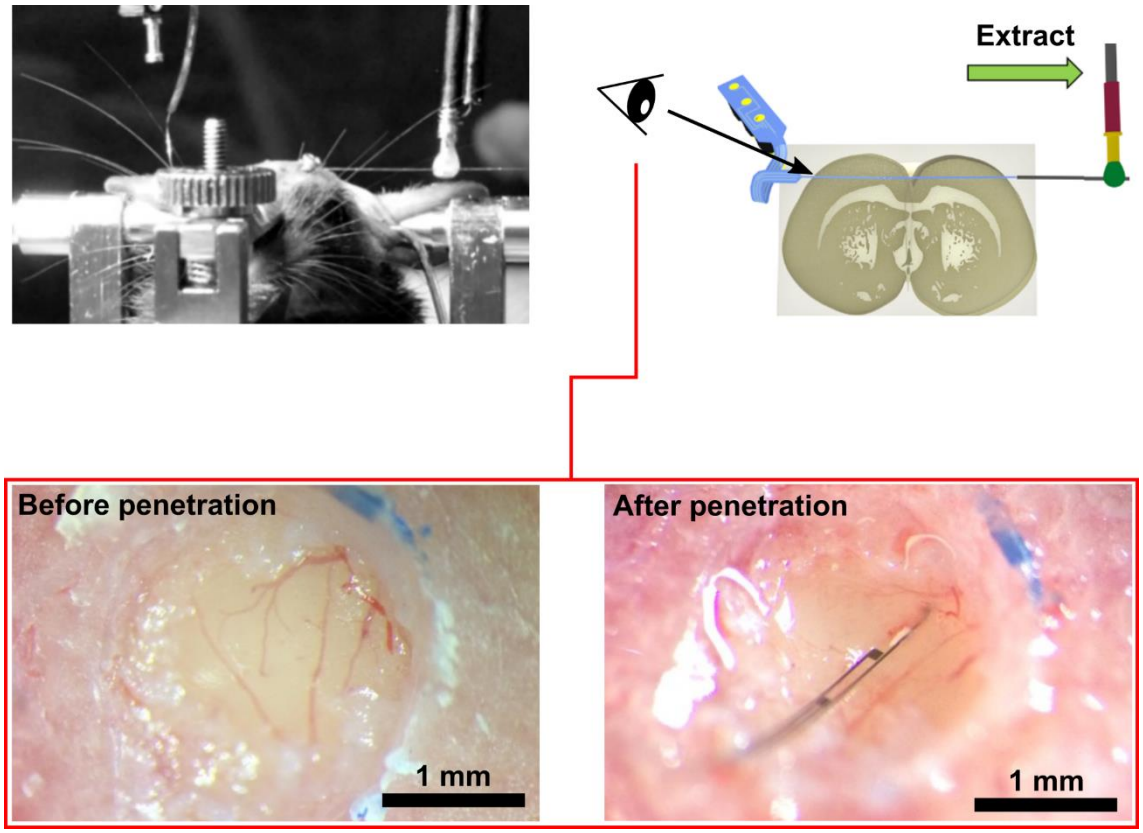

Figure 3.15 Photographs depicting the cranial opening area of the brain tissue before and after device penetration.

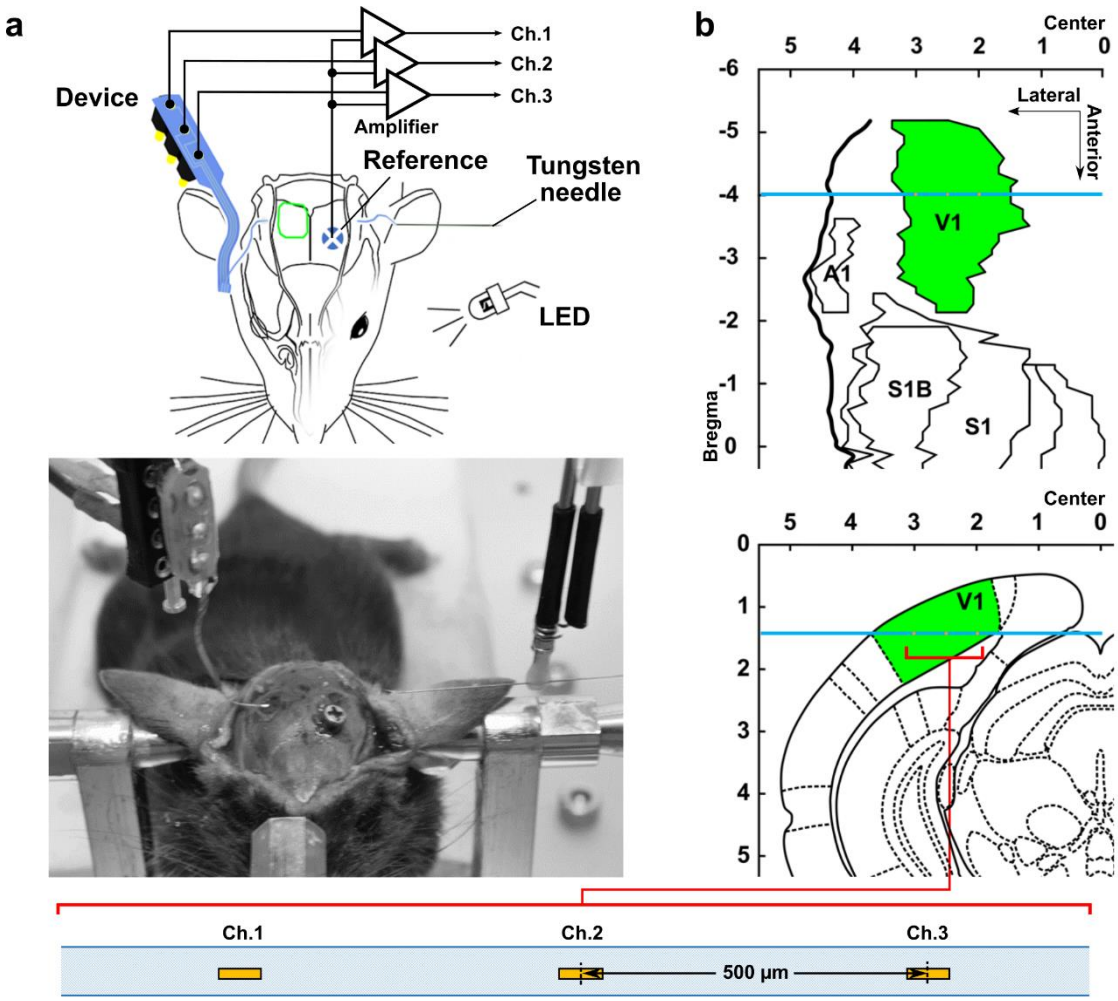

Figure 3.16 Acute in vivo neuronal recording using mouse brain. a) Schematic of the recording setup and photograph of the bioprobe device sewn to the brain tissue by guiding the tungsten microneedle with PEG. An LED array was used for visual stimulation. b) Tangential and coronal schematics of the primary visual cortex (V1) based on stereotaxic coordinate, illustrating the position of the thread-bioprobe in the tissue. Blue lines and yellow dots in both schematics represent the footprint of thread-bioprobe and microelectrodes (Pt black), respectively.

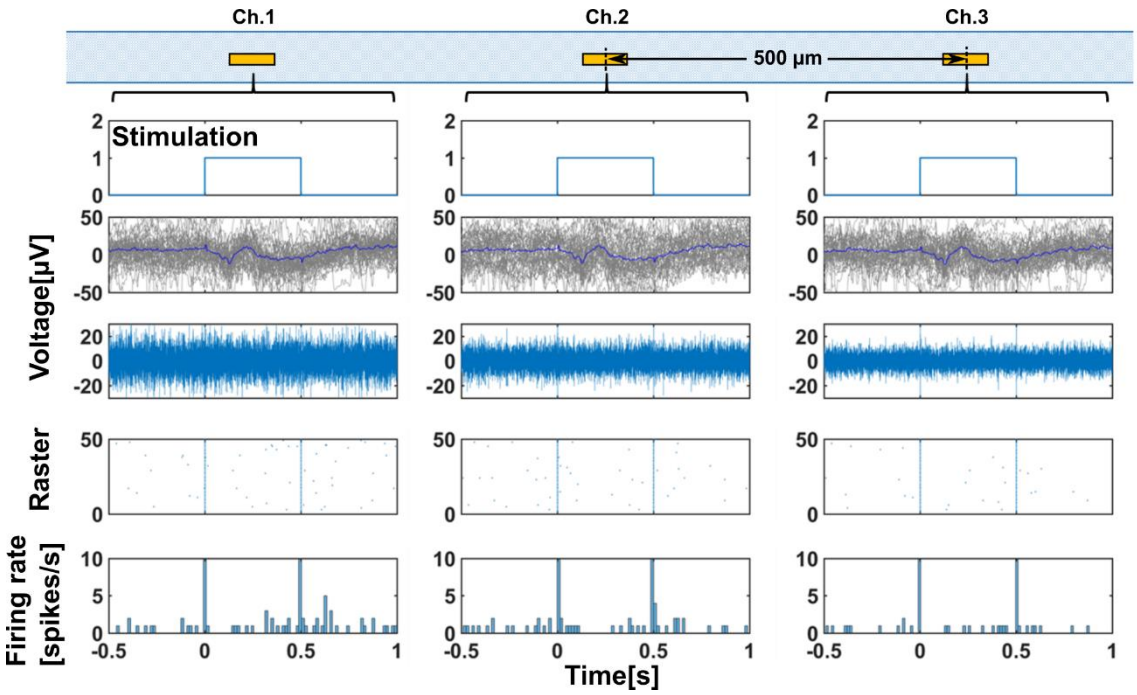

Figure 3.17 Signal waveforms recorded from the V1 via three embedded microelectrodes in the tissue. Top panels represent timing of the optical stimulation. Second and third panels are low-frequency-band (filtering = 10–500 Hz, n = 50 trials) and high frequency-band (filtering = 500–3,000 Hz, single trial) signal waveforms, responsibility. Bottom two panels are raster plots and PSTHs, respectively, taken from the high frequency signals (n = 50 trials). The detection thresholds for each channel was 4 times the standard deviation (σ) of the mean signal − 0.5 to −1.0 s before the stimulus onset.

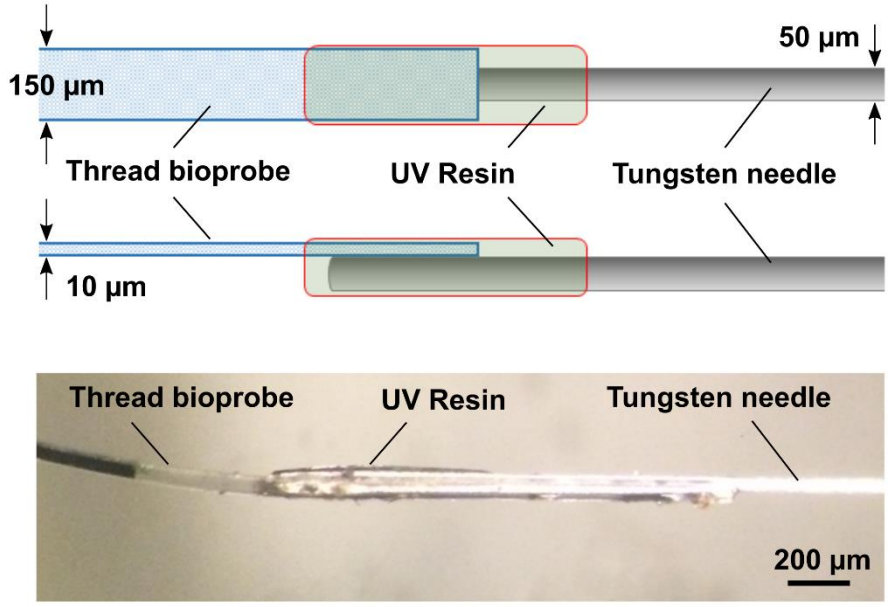

Figure 3.18 UV-curable resin junction. Shcematics show the top and side views of the UV-resin junction between the parylene-threrad microelectrode (150 µm width and 10 µm thick) and the tungsten microneedle (50 µm diameter), respectively. Bottom photograph shows the side view of the UV-resin junction. The resin formed the connection geometry of <150 µm in width.

3.7 Chronic in vivo neuronal recording

The chronic in vivo neuronal recording ability was also demonstrated using the mouse's brain (Figure 3.19). The mouse (male, 20–25 g) was anesthetized by isoflurane, and Pt black plated three microelectrodes were inserted into the mouse brain tissue using the surgical procedure similar to the acute recording. Using dental resin, the parylene-thread microelectrode and pin-connector were attached to the cranium. Here, a gelatin sponge was placed around the thread-bioprobe to protect the brain surface from infection. An array of LEDs was used to record the visual responses as used in the acute recording.

Signals from the free moving mouse were recorded a week after the parylene-thread microelectrode implantation (Figure 3.20). Visual stimuli were applied to the mouse's eye for 0.5 s, and the responses were continuously recorded by the three microelectrodes. The second and third panels in Figure 3.20 represent low frequency-band (filtering = 10–500 Hz) and high frequency-band (filtering = 500–3000 Hz) waveforms recorded by each microelectrode, respectively. The two panels at the bottom

show raster plots and histograms, respectively, obtained from each high frequency-band signals (the detection threshold of each channel was 4σ of the mean signal – 0.5 to −1.0 s before the stimulus onset). These waveform signals, which appeared at around 0.25 s were consistent with the latency of the visual response, and were subjected to be the LFPs (second panels in Figure 3.20) and spikes (third panels in Figure 3.20) evoked by the visual stimuli.

In order to observe the influence of the surgical procedure of sewing on the mouse, the change in the mouse's body weight was continuously monitored for two weeks (Figure 3.21). Initially, decrease in mouse's weight was observed for three consecutive days after surgery and a recovery on the seventh day. This suggested that the proposed surgical method of sewing of the fabricated parylene-thread microelectrode was applicable to the chronic recording on the mouse.

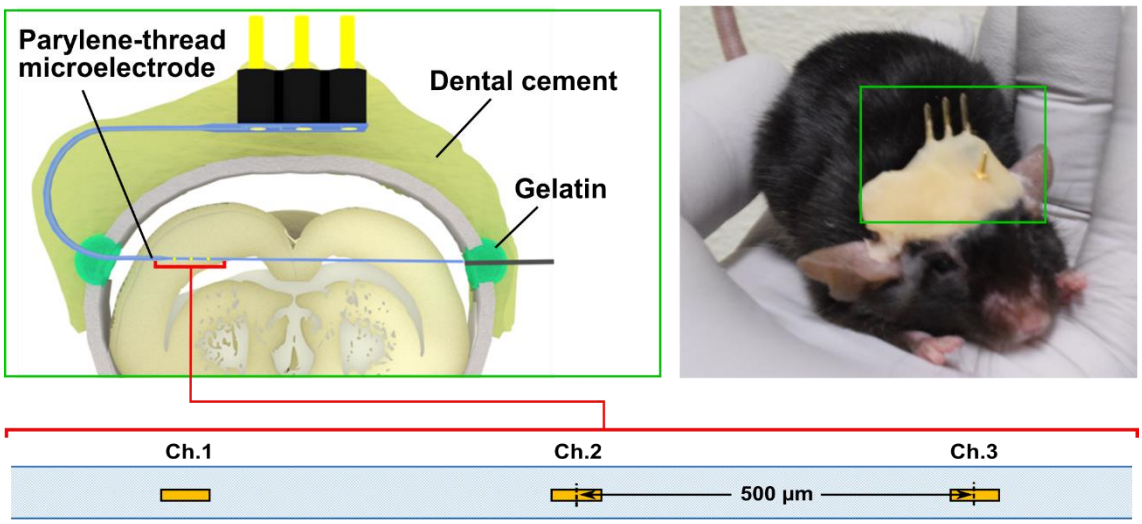

Figure 3.19 Schematic of the surgical procedure for the chronic recording and the photograph of the mouse that was implanted thread-bioprobe. The parylene-thread bioprobe device was implanted in the visual cortex (V1) in the right hemisphere of the mouse. For the recording of the visual responses from the mouse, I used an array of white LEDs.

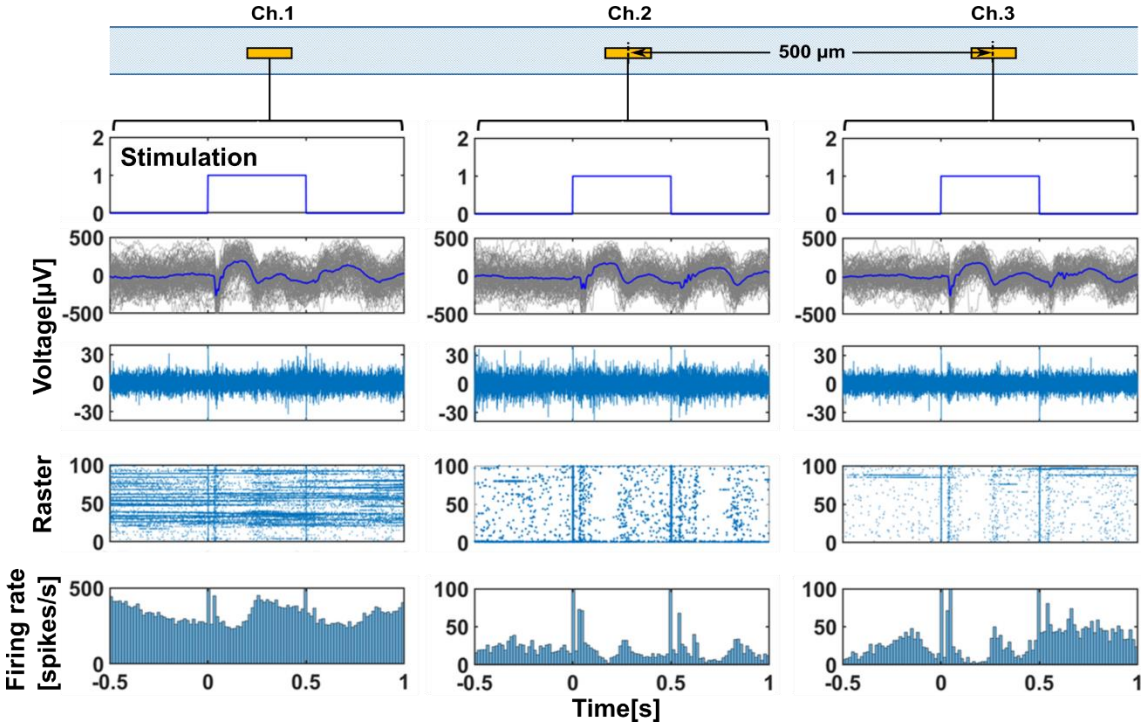

Figure 3.20 Waveforms recorded from the free moving mouse a week after the implantation via three microelectrodes in the V1. Top panels represent timing of the optical stimulation. Second and third panels are low-frequency-band (filtering = 10–500 Hz, n = 50 trials) and high frequency-band (filtering = 500–3,000 Hz, single trial) signal waveforms, responsibility. Bottom two panels are raster plots and PSTHs, respectively, taken from the high frequency signals (n = 50 trials) The detection thresholds for each channel was 4 times the standard deviation (σ) of the mean signal − 0.5 to −1.0 s before the stimulus onset.

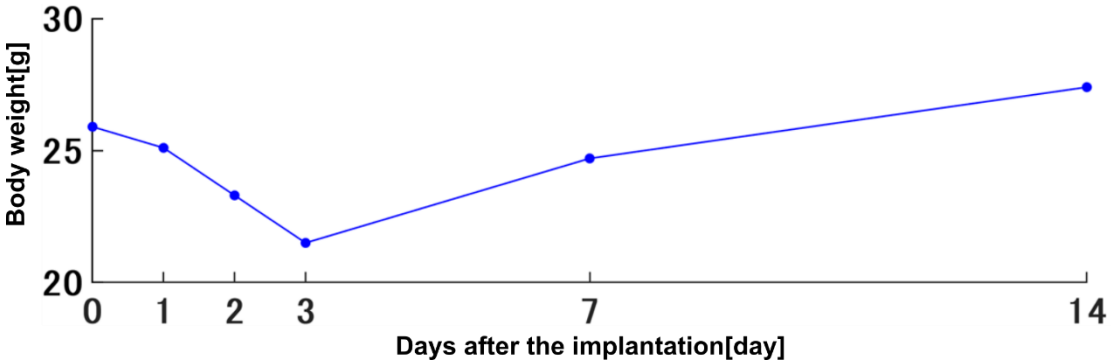

Figure 3.21 Mouse's weight depending on the day after the implantation of thread-device.

3.8 Discussion

The parylene–based flexible thread-bioprobe device was designed and fabricated. The tip portion of the device was connected to the tungsten microneedle with a UV-curable resin, enabling the device penetration into the tissue. The resin formed between the tip of parylene-thread and the root of tungsten needle, achieves a connection geometry of <150 μm in width (Figure 3.18). As demonstrated in both the recordings using mouse's brain tissue as well as limb muscle, these tissues could be punched with a flexible thread-bioprobe following the guidance of the tungsten microneedle. During the tissue penetration, no separation of the tungsten needle from the parylene-thread was observed, indicating that the junction of UV-curable resin is strong enough to sustain tissue punching.

The penetrating and recording capabilities of the fabricated parylene–based flexible device were confirmed on the limb muscle of the mouse. During the electrical stimulation, the limb showed large displacement associated with the relaxation and contraction. However, as confirmed from the recording sessions for 500 trials, no significant electrode displacements (<5 μm, Figure 3.11) could be observed because the thread-device was sewn to the muscle. The advantage of being able to sew microelectrodes with the tissue can be applied to other organs and tissues that exhibit large displacement and deformation (e.g., pulsation). As to the position of microelectrodes within the muscle, because of the diameter of the guiding tungsten needle (50 μm diameter), it was assumed that the thread-bioprobe penetrated the tissue between fascicles (a group of muscle cells) in the skeletal muscle (groups of fascicles). Compared to the device placement over the surface of the skeletal muscles, such an electrode positioning within the skeletal muscles enables us to detect signals inside the muscle,

offering advantages for further analysis in muscles (e.g., three-dimensional signal mapping of the muscle).

In terms of physical effects on the brain tissue, the device features of small geometry and flexibility offer various advantages, including less destabilization of intracranial pressure, reduction of the infection risk, and less amount of damage of the brain tissue and blood vessels located beneath the bone. Theoretically, the required opening area of craniotomy is considered to be adequate with the cross-sectional areas for both the tungsten needle (50 μm diameter) and the parylene-thread device (150-μm wide and 10-μm thick). In addition, because the tungsten microneedle exhibited sufficient hardness, it was not necessary to remove the dura matter, reducing the risk of infection during long-period recordings.

The advantages of the proposed surgical procedure of sewing with PEG include the reduction of the physical influence on the tissue and the risk of infection as well as precise position control of the flexible microelectrode in the tissue. Since the "catch" and "release" of tungsten microneedle was done in dissolvable PEG, its displacement of the tungsten-needle during the sewing ranged within 50 μm (Figure 3.13b), greatly reduced compared to conventional ways with undesirable physical stress on the needle. While recording the brain tissue, precise placement of microelectrodes is considered to be important for determining the recording region. As demonstrated in case of device penetration using a mouse brain tissue, both the direction and the distance of the tungsten needle's penetration were determined by referring to the bregma and the lambda, while the position of three microelectrodes (500 μm apart) in the tissue were determined by manipulating the tungsten needle (Figure 3.16b). For performing acute recording, the position of the thread-bioprobe as well as microelectrodes in the tissue could be fixed by the manipulator system after extracting the tungsten needle from the tissue. In the chronic recordings, each side of the thread-bioprobe's portion was fixed to the cranium with dental resin while the thread-bioprobe was passed through the two narrow openings (1–3 mm diameter) in the cranium at each side. This method enabled the fixation of the flexible device within the tissue with little or no significant misalignment or displacement during the implantation.

Based on the parylene-MEMS process, the geometry of the fabricated thread-bioprobe can further be reduced by decreasing both factors, such as sizes of the recording site (10 μm × 40 μm area) and the device interconnection (20-μm width) with reduced

mask patterns. Since contact printing–based photolithography was used, these pattern sizes will be reduced through i) electron beam–based lithography and ii) multiple layers of device interconnection. It is also possible to combine both processes. These fabrication processes also enable the increase in the number of microelectrodes, permitting the application of the device in bio-signal recording applications.

3.9 Conclusions

The parylene-thread microelectrode was fabricated in this Chapter, and the tissue was penetrated by guiding the tungsten microneedle using the sewing mechanism. I was able to obtain EMG signals from a mouse's MG muscle as well as neuronal signals of LFP and spike from its visual cortex in vivo using the thread-bioprobe. The proposed thread-bioprobe device exhibits unique characteristics such as flexibility, electrodeposition controllability, and implantation capabilities and will contribute to both acute and chronic in vivo electrophysiological recordings. To avoid physical stress on the tissue, a flexible thread device stitching method using a dissolvable PEG substance has been devised. These characteristics of both the flexible thread device and the surgical procedure were previously unattainable using traditional methods and devices.

Reference

[1] V. S. Polikov, P. A. Tresco, and W. M. Reichert, "Response of brain tissue to chronically implanted neural electrodes," *Journal of Neuroscience Methods*, vol. 148, no. 1, pp. 1–18, 2005.

[2] T. Kim *et al.*, "Injectable, cellular-scale optoelectronics with applications for wireless optogenetics," *Science*, vol. 340, no. 6129, pp. 211–216, 2013.

[3] H. S. Sohal *et al.*, "The sinusoidal probe: a new approach to improve electrode longevity," *Frontiers in neuroengineering*, vol. 7, p. 10, 2014.

[4] J. Liu *et al.*, "Syringe-injectable electronics," *Nature Nanotechnology*, vol. 10, no. 7, pp. 629–635, 2015.

[5] L. Luan *et al.*, "Ultraflexible nanoelectronic probes form reliable, glial scar–free neural integration," *Science Advances*, vol. 3, no. 2, pp. 1–10, 2017, doi: 10.1126/sciadv.1601966.

[6] A. Lecomte *et al.*, "Silk and PEG as means to stiffen a parylene probe for insertion in the brain: Toward a double time-scale tool for local drug delivery," *Journal of Micromechanics and Microengineering*, vol. 25, no. 12, 2015.

[7] S. Felix *et al.*, "Removable silicon insertion stiffeners for neural probes using polyethylene glycol as a biodissolvable adhesive," in *Conf. Proc. IEEE Eng. Med. Biol. Soc*, 2012, vol. 2012, pp. 871–874.

[8] L. W. Tien, F. Wu, M. D. Tang-Schomer, E. Yoon, F. G. Omenetto, and D. L. Kaplan, "Silk as a multifunctional biomaterial substrate for reduced glial scarring around brain-penetrating electrodes," *Advanced Functional Materials*, vol. 23, no. 25, pp. 3185–3193, 2013.

[9] S. Yamagiwa, M. Ishida, and T. Kawano, "Flexible parylene-film optical waveguide arrays," *Applied Physics Letters*, vol. 107, no. 8, pp. 1–6, 2015.

[10] Y. Morikawa *et al.*, "Ultrastretchable Kirigami Bioprobes," *Advanced healthcare materials*, vol. 7, no. 3, p. 1701100, 2018.

[11] S. Yamagiwa, M. Ishida, and T. Kawano, "Self-curling and-sticking flexible substrate for ECoG electrode array," in *Micro Electro Mechanical Systems (MEMS), 2013 IEEE 26th International Conference on*, 2013, pp. 480–483.

[12] H. Oka, K. Shimono, R. Ogawa, H. Sugihara, and M. Taketani, "A new planar multielectrode array for extracellular recording: application to hippocampal acute slice," *Journal of neuroscience methods*, vol. 93, no. 1, pp. 61–67, 1999.

[13] A. Fujishiro, H. Kaneko, T. Kawashima, M. Ishida, and T. Kawano, “In vivo neuronal action potential recordings via three-dimensional microscale needle-electrode arrays,” *Scientific Reports*, vol. 4, pp. 1–9, 2014.

[14] H. Sawahata *et al.*, “Single 5 μm diameter needle electrode block modules for unit recordings in vivo,” *Scientific Reports*, vol. 6, p. 35806, 2016.

[15] T. Harimoto *et al.*, “Enlarged gold-tipped silicon microprobe arrays and signal compensation for multi-site electroretinogram recordings in the isolated carp retina,” *Biosensors and Bioelectronics*, vol. 26, no. 5, pp. 2368–2375, 2011.

[16] R. Biran, D. C. Martin, and P. A. Tresco, “Neuronal cell loss accompanies the brain tissue response to chronically implanted silicon microelectrode arrays,” *Experimental Neurology*, vol. 195, no. 1, pp. 115–126, 2005.

[17] H. Szarowski *et al.*, “Brain responses to micro-machined silicon devices,” *Brain Research*, vol. 983, pp. 23–35, 2003.

[18] D. J. Edell, V. van Toi, V. M. McNeil, and L. D. Clark, “Factors influencing the biocompatibility of insertable silicon microshafts in cerebral cortex,” *IEEE Transactions on Biomedical Engineering*, vol. 39, no. 6, pp. 635–643, 1992.

Chapter 4

Floating microneedle-electrode device

4.1 Introduction

Recent advances in microelectromechanical system technology enable us to fabricate extracellular needle electrodes with a diameter of less than 10-μm (e.g., <3 μm[1], [2] for in vitro recording, 8.6 μm[3], 5 μm[4], [5], 300 nm[6] for in vivo recording), thereby minimizing tissue response. In addition, in chronic applications, the physical stress at the interface between the device substrate [e.g., silicon (Si)] and tissue surfaces induce sustained inflammation and tissue response. In particular, the large geometry of the device substrate enhances areas of craniotomy and tissue damage. The approach reported in this Chapter involves using an electrode device that has a 5-μm-diameter needle electrode on a 1 × 1 × 0.5 mm^3 substrate; in addition, a surgical procedure for the chronic device implantation is proposed. Because of brain tissue pulsation, conventional implantations, in which the electrode is fixed to the cranium, cause significant chronic inflammation[4] (Figure 4.1a). To avoid these difficulties, a floating architecture for implantable devices, such as Smart dust on the tissue (nerve or muscle)[7], [8] can be offered. By utilizing the surgical technique, the electrode device is implanted in the brain without being fixed to the cranium, resulting in a floating 5-μm-diameter needle

electrode on the tissue to follow the pulsations Figure 4.1b). For physical stress reduction in the tissue during the electrode penetration, the device is attached to the manipulator with a material that dissolves. I demonstrated the device implantation in mice and chronic experiments while evaluating the signal quality and tissue damages.

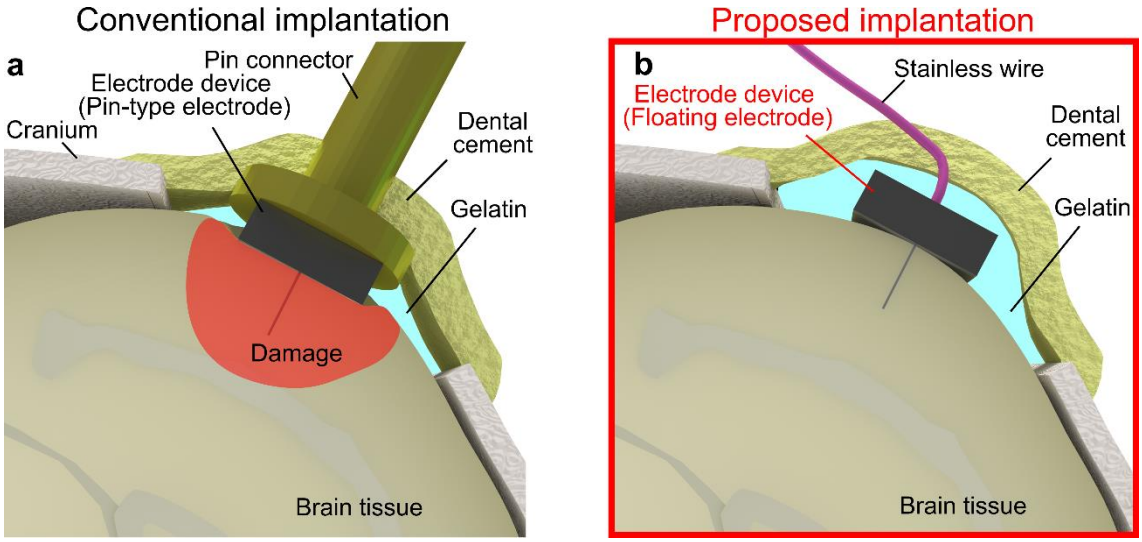

Figure 4.1 Comparison of electrode implantation. a) Schematic showing conventional implantation, in which the electrode is fixed to the cranium of the brain. b) Schematic showing the proposed implantation, in which the electrode packaged with a flexible lead is implanted in the brain without fixing to the cranium, achieving a "floating electrode" on the tissue.

4.2 Microneedle-electrode device

I used a device that has a 5 µm diameter and 400 µm length microneedle electrode at the center of the 1 × 1 mm^2 Si substrate [n-type (111)-Si, resistivity = <0.02 Ω cm, thickness = 525 µm][4], [9] (Figure 4.2). I used a Si growth technology [gold (Au)-catalyzed vapor–liquid–solid growth of Si[10]] to fabricate the Si microneedle, which was then metalized with platinum (Pt) and titanium (Ti) (total Pt/Ti thickness = 200 nm) followed by the device encapsulation with a biocompatible insulator of parylene-C (1 µm in thickness, with the exception of the tip by plasma process). Insets of red and blue squares in Figure 4.2 show SEM images of the overall and tip section of the fabricated microneedle electrode. The tip and bottom diameters of the microneedle were 1 and 10 µm, respectively.

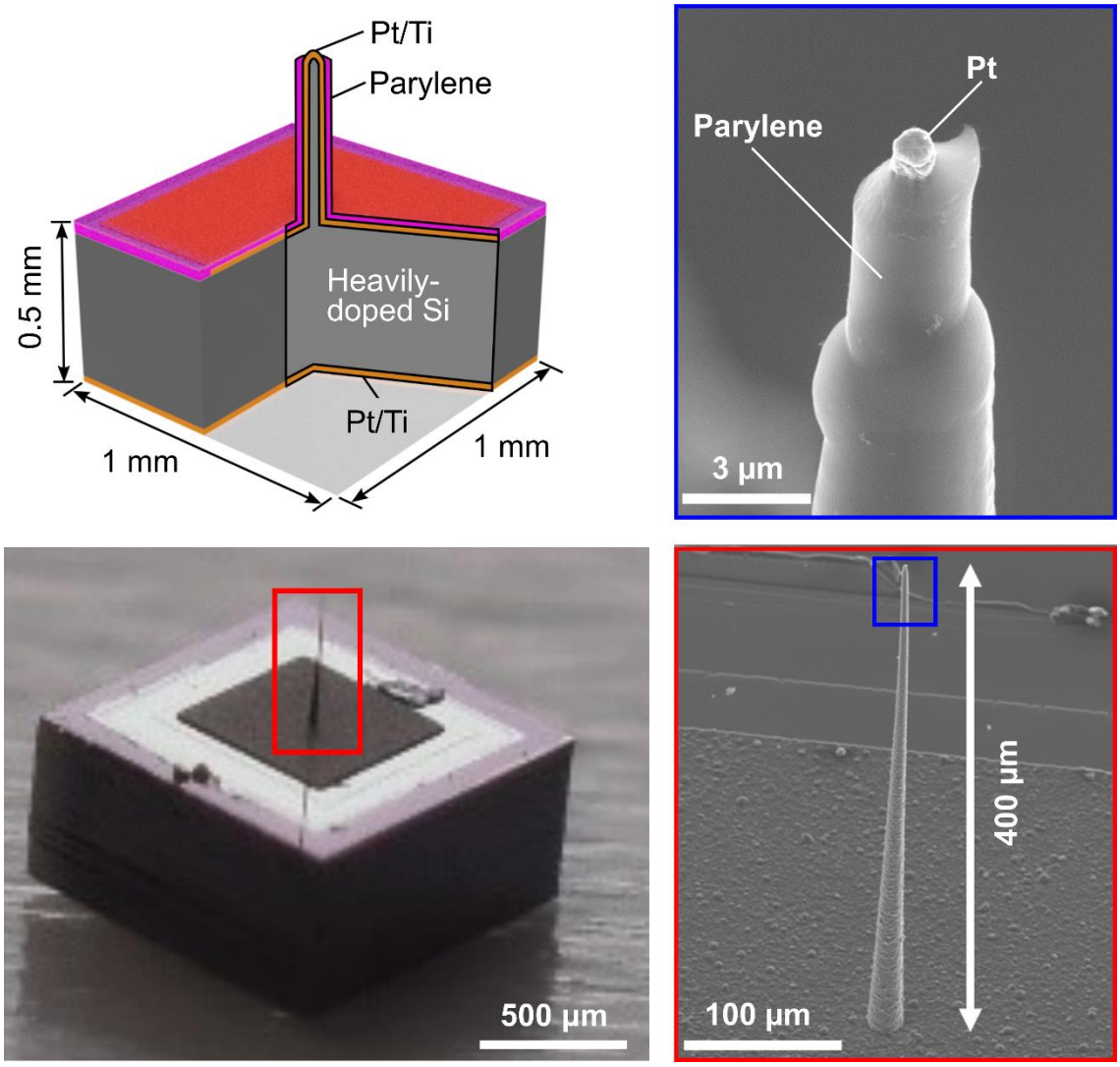

Figure 4.2 Schematic and photograph of an electrode device. The electrode device has a 5 μm diameter and 400 μm length microneedle electrode at the center of the 1 × 1 mm^2 Si substrate. Insets of red and blue squares that denote the SEM images of the microneedle electrode.

4.3 Device packaging and electrical characteristics

Figure 4.3a show the device package with PEG paste. The PEG paste [two types of PEG with different melting characteristics were mixed, PEG 1000 : PEG 4000 = 1 : 1 (165-09085 for PEG 1000, 162-09115 for PEG 4000, FUJIFILM Wako Pure Chemical Corporation, Japan)] is then applied to the tip of a pin connector, and the fabricated electrode device with the stainless wire is assembled. The PEG solidifies at room temperature and is ready for use in animal experiments.

Figure 4.3b illustrates an electrode device packaged with PEG paste and equipped with a stainless wire for the recording ["Pin connector (to recording system)" in Figure 4.3b]. Owing to the small geometry of the recording site of Pt, the microneedle electrode showed impedance magnitudes ranging from 290 ± 220 MΩ to 580 ± 38 kΩ at 10 Hz to 10 kHz [5.0 ± 0.8 MΩ (mean ± SD) at 1 kHz] in phosphate-buffered saline (PBS) at room temperature. To reduce the electrode impedance, the microneedle's tip was modified with a low impedance material of Pt black[11], resulting in the impedance magnitudes that ranged from 6.3 ± 6.1 MΩ to 60 ± 12 kΩ [300 ± 150 kΩ (mean ± SD) at 1 kHz][4], [5] (Figure 4.4).

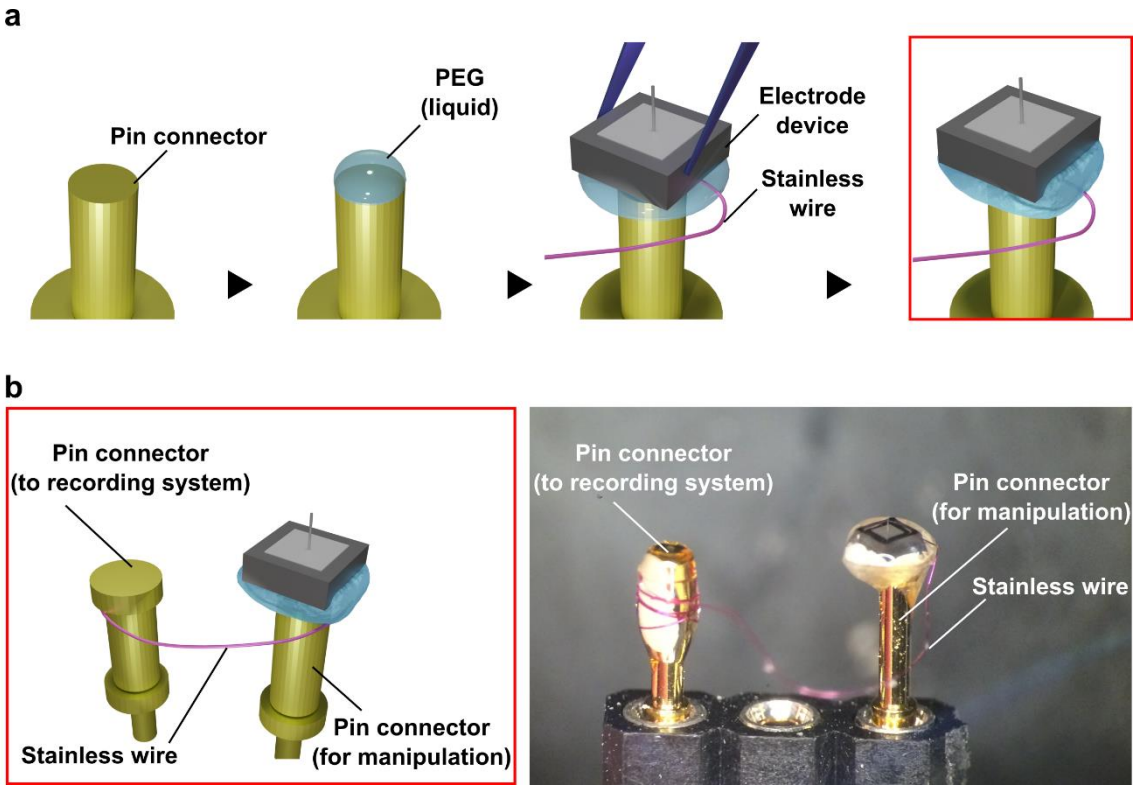

Figure 4.3 Device package using PEG. (a) Assembly of the electrode device on a pin connector via the PEG paste. (b) Schematic and photograph of the packaged electrode device with an output lead (stainless-steel wire).

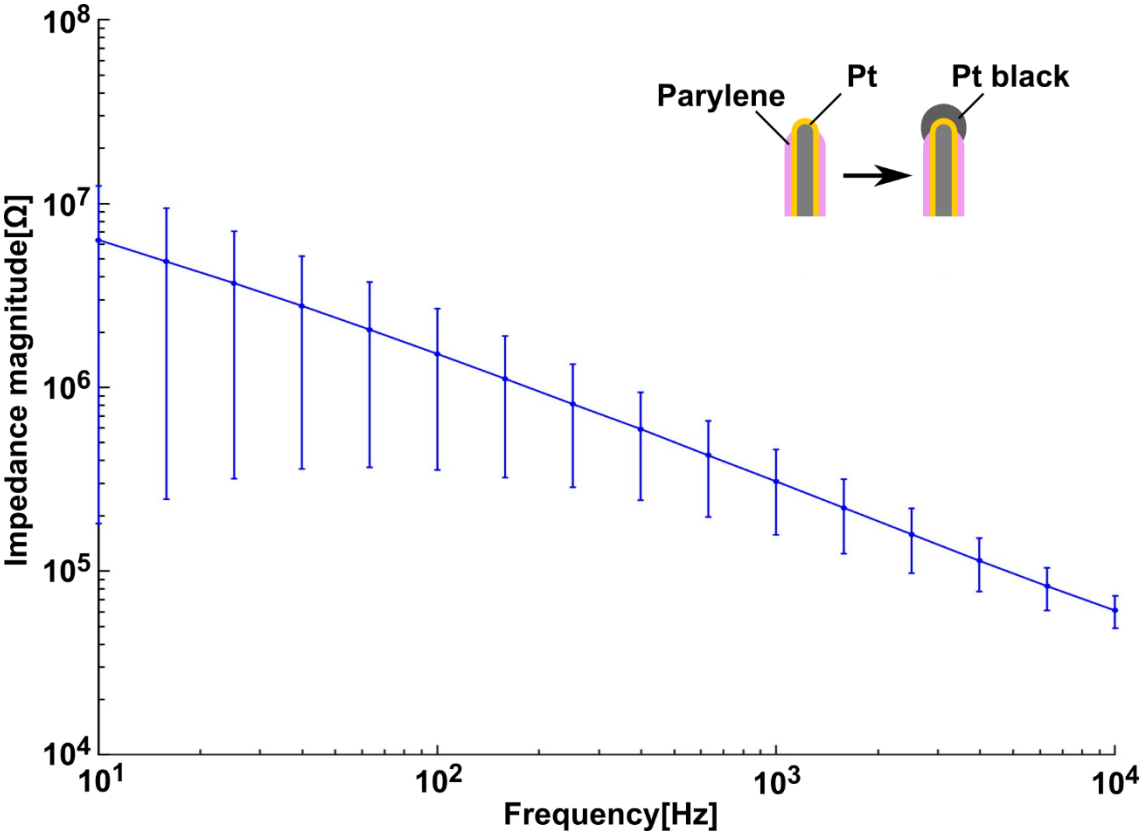

Figure 4.4 Impedance characteristics of Pt black plated microelectrodes measured at room temperature in PBS.

4.4 Surgical procedure

Figure 4.5 shows the proposed surgical procedure for the electrode placement on the mouse's brain tissue and the device detachment by using a dissolvable material of PEG. For the in vivo experiments, mice (wild-type C57 BL/6 mice, 20-30 g in weight) were anesthetized by isoflurane. After the head of a mouse was fixed with stereotaxic apparatus (SR-50, Narishige, Tokyo, Japan), parts of the cranium were removed [primary visual cortex (V1), 2.5 mm on the lateral side and 4.0 mm on the caudal side to the bregma, having a diameter of 1–3 mm]. The floating electrode device was attached to a micromanipulator (MO-10, Narishige) to control needle penetration as well as device placement. The needle electrode penetrated the brain tissue by manipulating the pin connector with a manipulator (Figure 4.5a1). By dropping solution (PBS) on the PEG, the solid-phase PEG is dissolved (Figure 4.5a2). After the PEG is completely dissolved, the electrode's substrate can be detached from the pin connector, and the electrode device remains on the surface of the brain tissue (Figure

4.5a3). The time required in the experimental procedure was within 6 min. Figure 4.5b and c show an electrode device, which was placed on the V1 on the right hemisphere.

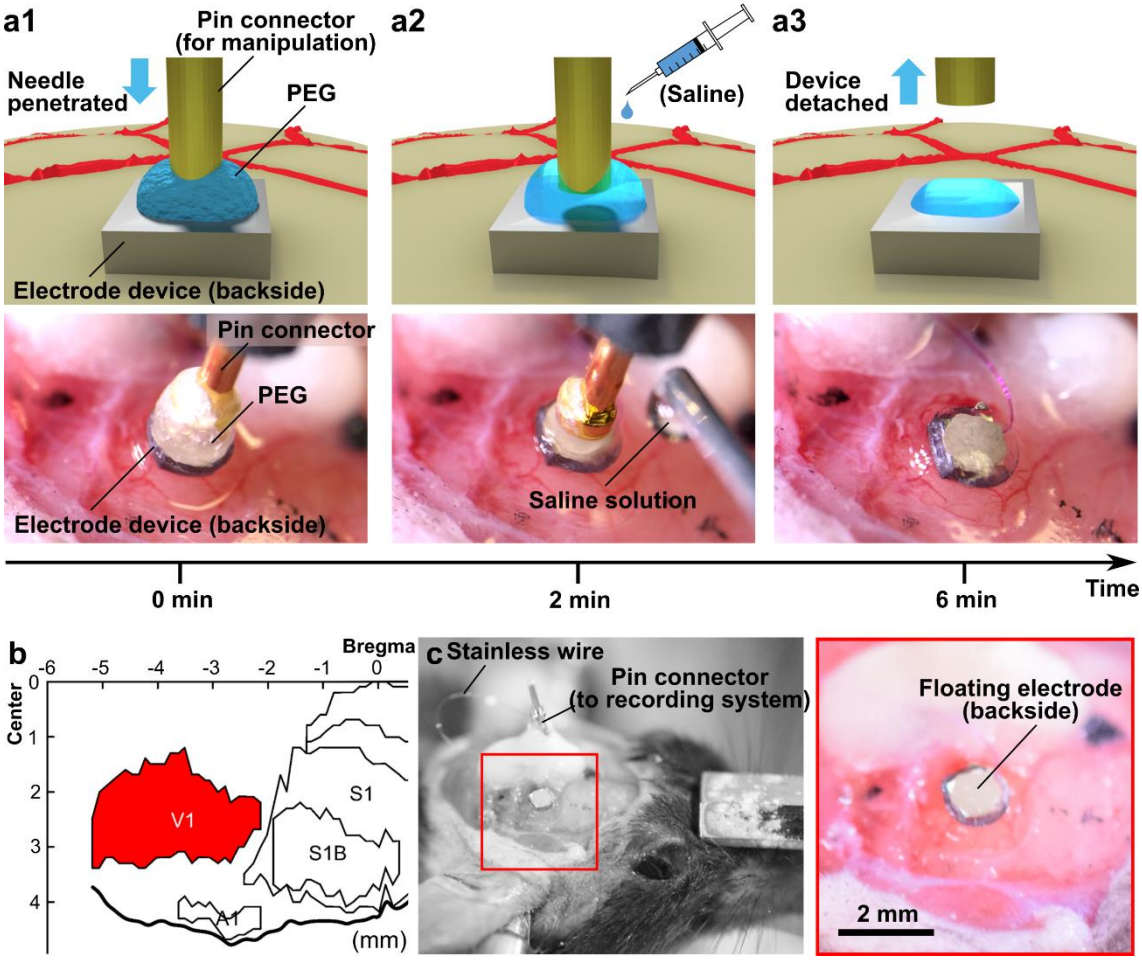

Figure 4.5 Placement of the floating electrode on the brain tissue of a mouse. a) Schematic and photograph of each step in the surgical procedure for the electrode penetration: a1) the needle electrode penetrates the brain tissue of the mouse by manipulating the pin connector; a2) dropping PBS to the PEG for detaching the electrode's substrate from the pin connector; and a3) pulling the pin connector upward for leaving the electrode device on the tissue. b) Schematic showing the area of the device placement in the cortex (visual cortex, V1). c) Photographs of the electrode device after the surgical method.

4.5 Chronic in vivo neuronal recording

After the device placement (in Figure 4.5), the device was covered with a gelatin sponge and dental cement for the chronic recording (Figure 4.6). I assessed chronic recording from mice implanted with pin type and floating electrodes (wild-type C57 BL/6,

20-30 g prior to implantation). Figure 4.7a1 and a2 represent low-frequency (filtering = 10–80 Hz) and high-frequency (filtering = 500–1,000 Hz) band waveforms, respectively, recorded one day after the pin-type electrode was implanted. Figure 4.7a3 and a4 show raster plot diagrams and the peristimulus time histograms (PSTHs), respectively, obtained from the high-frequency band signals, with the amplitude threshold of three standard deviations (SDs, σ) of the mean signal −0.5 to −1.0 s before the stimulus onset. Similar to the results obtained with the pin-type electrode, Figure 4.7b1 and b2 depict waveforms from the low and high-frequency band, respectively, recorded one day after the floating electrode was implanted. Additionally, Figure 4.7b3 and b4 show raster plot diagrams and the PSTHs detected from the high-frequency band signals using an amplitude threshold (3σ of the mean signal, −0.5 to −1.0 s before the stimulus onset). The signals responding to the visual stimuli appeared at approximately 50 ms, for both pin type and floating electrodes, which was consistent with the latency of the mouse's visual response[12]. These results suggest that the recorded signals were subjected to the local field potentials (Figure 4.7a1 and b1) and the spikes (Figure 4.7a2–a4 and b2–b4), which were evoked by the visual stimuli.

Additionally, I evaluated the chronic recording by comparing the signal-to-noise ratio (SNR) of spikes for a period of 7 days (n = 5 mice for pin-type electrode and n = 4 mice for floating electrode, Figure 4.8). The SNR was defined as the peak-to-peak amplitude of the mean waveform 0.005 to 0.1 s after the stimulus onset divided by the 3σ of the noise level. These SNRs are greater than 1.9 (mean) across all electrode types. The duration of the continuous recording on the other hand depended not only on the mouse but also on the type of the implanted electrode. The pin-type electrode demonstrated a decrease in the number of electrodes detecting spike signals (3σ of the mean signal −0.5 to −1.0 s before the stimulus onset) from 5 to 1 on day 7. On the other hand, the floating electrode demonstrated a decrease in the number of electrodes from 4 to 3, indicating that it is more stable with the floating electrode than with the pin-type electrode (Figure 4.9).

I examined the chronic recording from the floating electrode implanted mouse for a longer period of 6 months (n = 1 mouse, wild-type C57 BL/6, female, 27.8 g in weight before implantation). Figure 4.10a1, 2 and b1, 2 represent low-frequency band (filtering = 10–80 Hz) and high-frequency band (filtering = 500–1,000 Hz) waveforms of the periods of 2 weeks and 6 months, respectively, recorded from the same electrode implanted mouse. Large spikes that appeared at 0 and 0.5 s are stimulation-induced

artifacts that represent the timing of LED illumination. Figure 4.10a3, 4 and b3, 4 also show raster plot diagrams and the PSTHs of high-frequency band signals detected at these recording periods (3σ of the mean signal −0.5 to −1.0 s before the stimulus onset). I also analysed the SNR during the recording period (6 months, Figure 4.11), showing the mean SNR of > 2.4 from 2 weeks to 6 months without significant degradations.

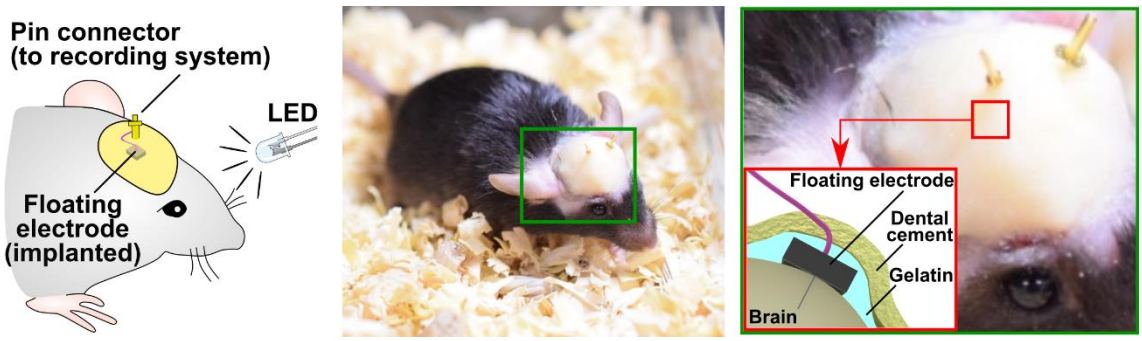

Figure 4.6 Schematic and photographs of chronic in vivo neuronal recording. (a) Schematic of the recording with visual stimulation provided by a light-emitting diode (LED). (b) Photographs of a mouse implanted with a floating electrode. To record visual responses, each device is implanted into the mouse's visual cortex (V1).

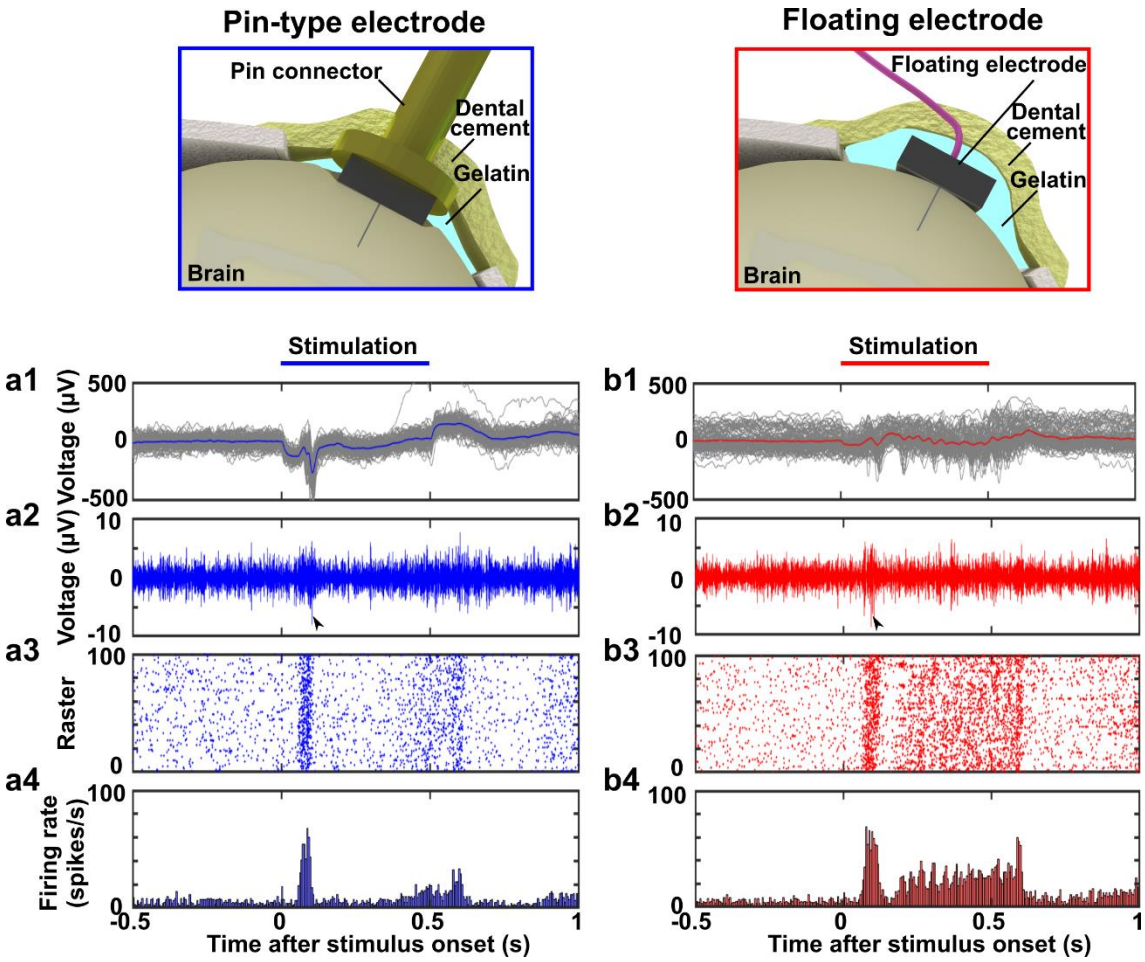

Figure 4.7 Chronic recordings of pin-type and floating electrode 1 day after implantation. (a1-4) Waveforms recorded from the pin-type electrode 1 day after implantation; a1) an average waveform of low-frequency band signals (filtering = 10–80 Hz, n = 100 trials), a2) a single high-frequency band signal from a single trial (filtering = 500–1,000 Hz), and a3, 4) raster plot diagrams and PSTHs extracted from the high-frequency band signals, respectively (n = 100 trials). The detection threshold was set to 3 × the SD (σ) of the mean signal −0.5 to −1.0 s before the stimulus onset. b1–4) Waveforms recorded from the floating electrode 1 day after implantation.

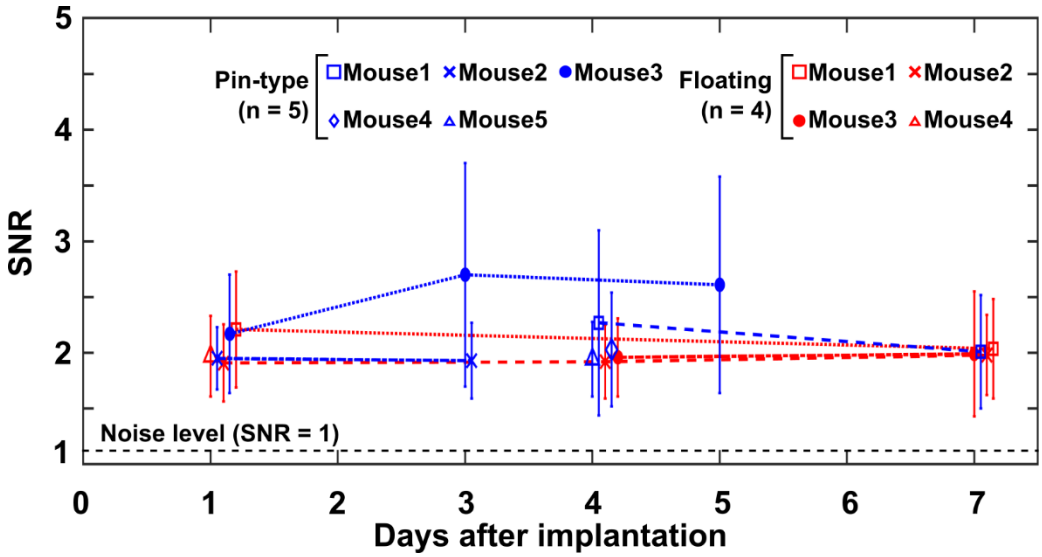

Figure 4.8 SNR of spike detected on each electrode implanted mouse for 7 days (mean ± SD, n = 100 trials for each electrode during the recording period).

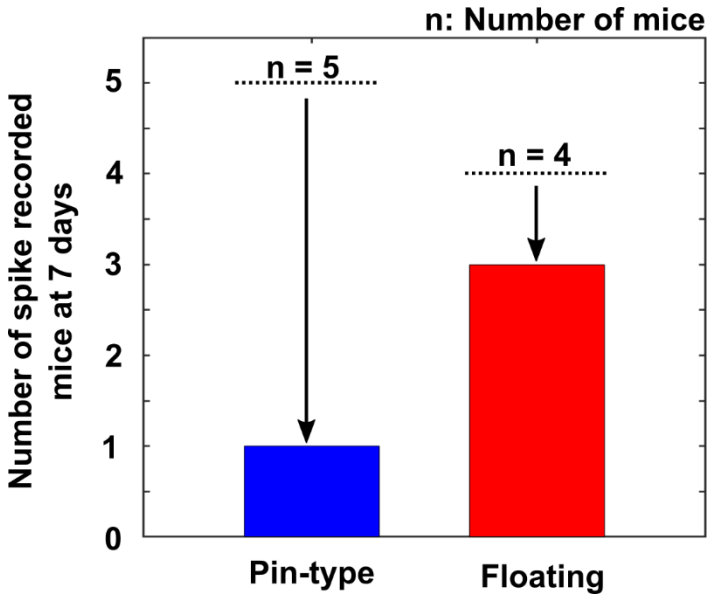

Figure 4.9 Numbers of electrodes detecting spike from each mouse 7 days after implantation.

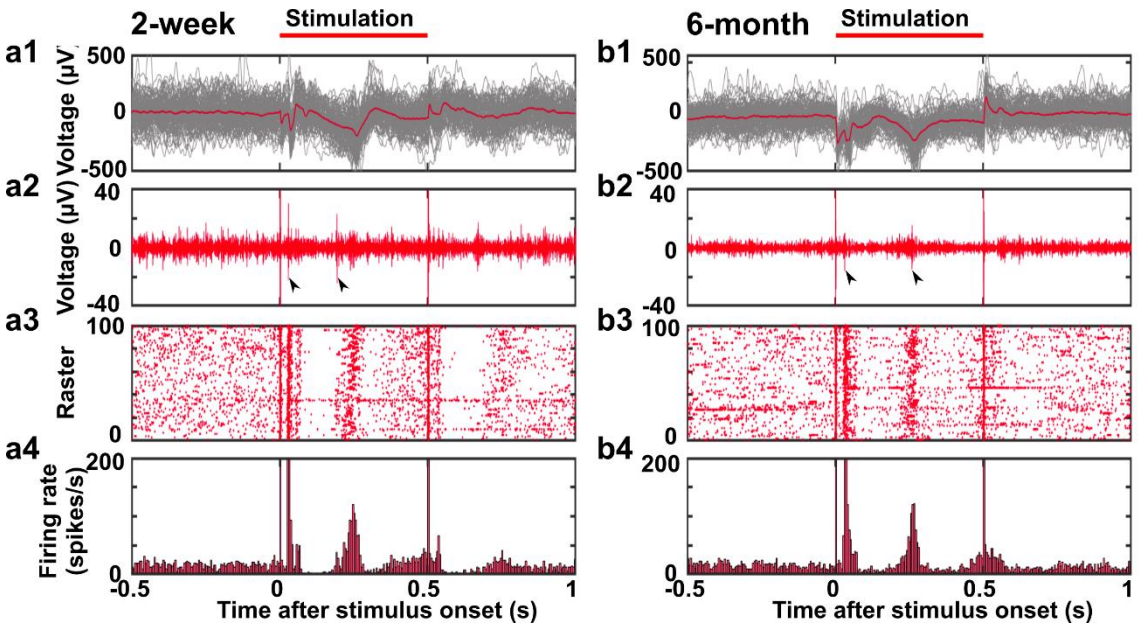

Figure 4.10 Chronic in vivo neuronal recording with the floating electrode for 6 months. a1–4) Waveforms recorded from the freely moving mouse 2 weeks after the implantation. Top panel represents the timing of the optical stimulation: a1) average waveform of low-frequency band signals (filtering = 10–80 Hz, n = 100 trials), a2) a high-frequency band signal from a single trial (filtering = 500–1,000 Hz), and a3,4) raster plot diagrams and PSTHs taken from the high-frequency signals (n = 100 trials). The detection threshold was 3 × the SD (σ) of the mean signal −0.5 to −1.0 s before the stimulus onset. b1–4) Waveforms recorded from the free-moving mouse 6 months after the implantation.

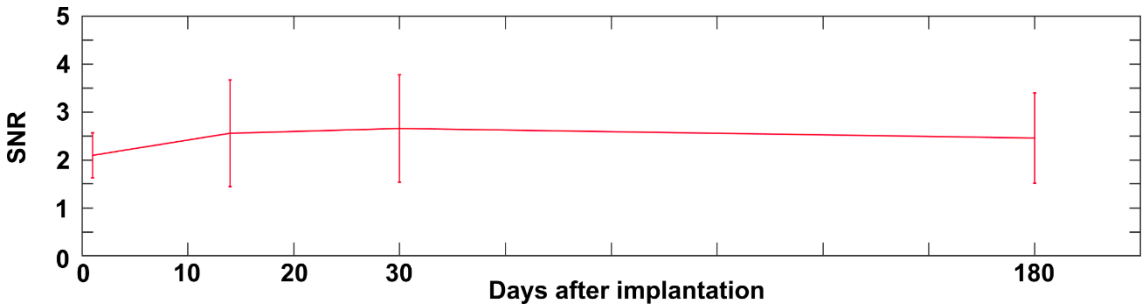

Figure 4.11 SNR of spike detected on the electrode implanted mouse for 180 days (6 months) (mean ± SD, n = 100 trials for each recording period).

4.6 Histological analysis of floating electrode

Additionally, I examined tissue damage associated with the implanted floating device; I also examined tissue damage associated with the pin-type electrode (cranium-fixed electrode) using different mice (n = 3 mice for the floating electrode and n = 3 mice for the pin-type electrode). Figure 4.12a shows the brain tissues (coronal section) two weeks after the pin-type electrode and floating device were implanted. Each slice sample shows a dimple-like damaged area at the location of each electrode. Figure 4.12b shows the quantitative comparison of these damaged areas, which were calculated by smoothing each tissue surface ("damaged area" is depicted in Figure 4.12a with a red dashed line). The floating electrode significantly reduced the damaged area compared to the pin-type electrode (24-slice samples from six mice, t-test, *$p < 0.01$). Figure 4.12c shows the histological outcome (coronal brain section) from the V1 of mice 2 weeks after device implantation, including the distribution of labeled reactive astrocytes (GFAP), microglia (Iba-1), and cell nuclei (DAPI) (24-slice samples from six mice, t-test, *$p < 0.01$). In comparison to the pin-type electrode, the floating device exhibits fewer reactive astrocytes (Figure 4.12d). The microglia (Iba-1) and cell nuclei (DAPI) associated with the floating electrode were compared to those of the pin-type electrode (Figure 4.12e and f), and no statistically significant difference was observed. These histological findings indicate that the floating device is capable of recording for an extended period of time while minimizing tissue responses, compared to the pin-type.

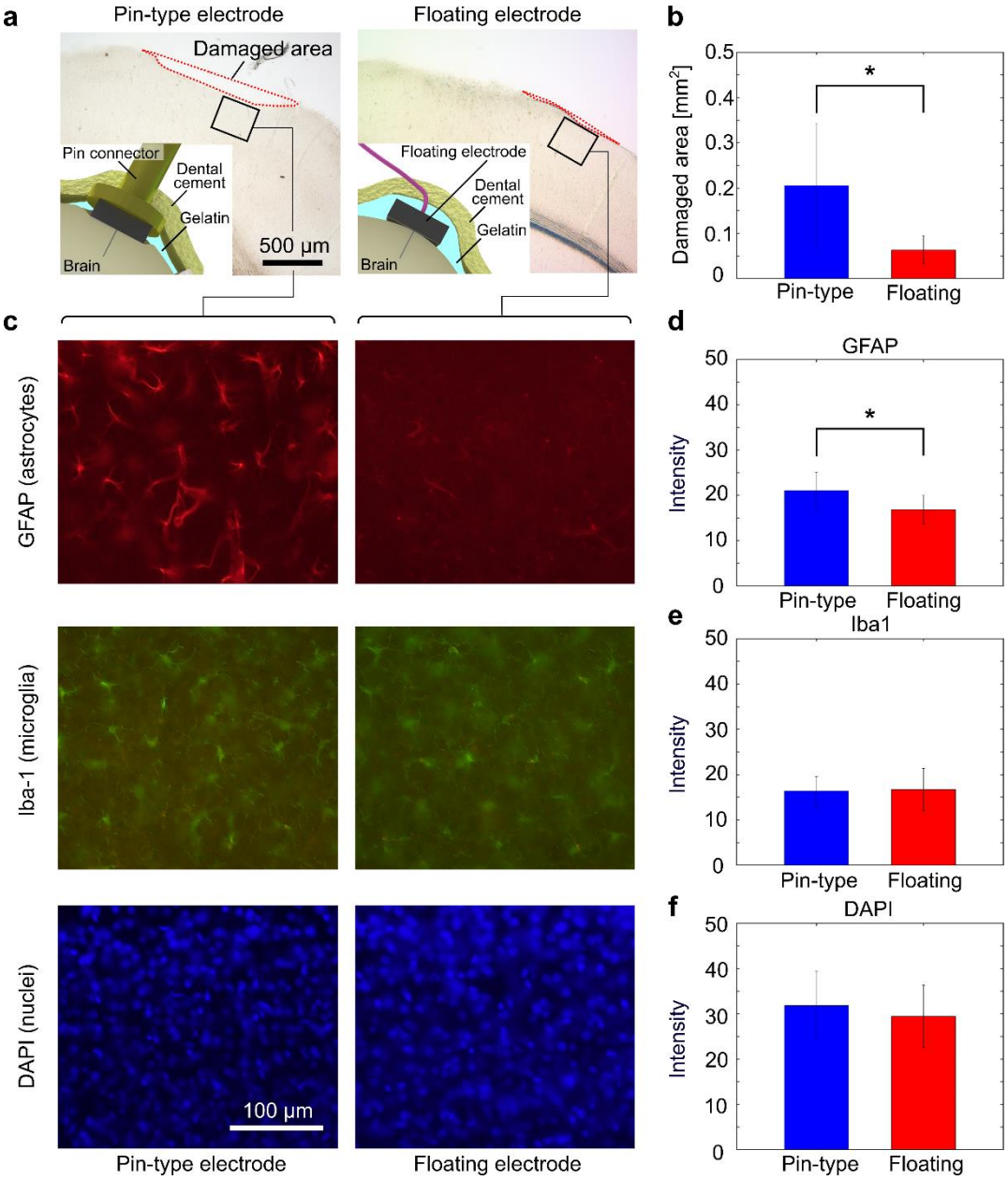

Figure 4.12 Histological comparison of the tissue response to chronically implanted conventional pin type and floating electrodes. a) Photograph of the brain tissues two weeks after the pin-type electrode and floating electrode were implanted. b) Quantitative comparison of damaged areas on pin type and floating electrodes. c) Tissue responses in the visual cortex following 2-week implantation of a pin-type electrode (left panels) and the floating electrode (right panels). Tissues are labeled for reactive astrocytes (GFAP), microglia (Iba-1), and nuclei (DAPI). d-f) Quantitative comparisons of each cell type between the pin type and floating electrodes using fluorescent intensity in an area of 0.1 mm^2, taken from 24 slices of six mice (mean ± SD) (* $p < 0.01$, t-test).

4.7 Discussion

I proposed the penetration of a microelectrode into the brain tissue and the device detachment with dissolvable material of PEG. The advantage of the proposed surgical procedure is the reduction of the physical stress to the tissue during the device placement as well as the detachment from the manipulator[13]. Other material of paraffin wax was also used in our prior work[14]; however, this material needed to be heated for melting (~**6**0°C), while the used PEG dissolves with PBS at room temperature. The time required for the device placement was ~10 min, a period that can be adjusted by changing the molecular weight of the PEG used. As an advanced way to use the dissolvable material, I can use a PEG-containing bioactive agent, which would reduce immune responses of the tissue[15].

For a period of 7 days following implantation, neuronal recordings were demonstrated using the pin type and proposed floating electrodes implanted in mice. Throughout the recording period, the number of pin electrodes detecting spike signals decreased from 5 to 1, while the number of floating electrodes decreased from 4 to 3 (Figure 4.9). The SNR varied between recordings (date and mouse), indicating that there was no significant difference between these two types of electrodes, whereas the recording duration (days) was dependent on the mice. Additionally, I confirmed that some mice did not exhibit spike recording in the early days (1–3 days post implantation); however, these mice displayed spike recording in later days (e.g., 3–7 days post implantation). The temporal loss of spike signals was almost certainly caused by the needle penetration's initial impact, such as compressing and slashing tissue, as well as early responses (e.g., activated microglia[16]). Although additional experiments are required, these results suggest that the floating electrode improves the recording stability.

I also analyzed the SNR during the floating electrode implanted mouse for 6 months. As known, the implanted device fixed to the cranium induces the motion of the needle in the tissue, resulting in continuously repeated injury to the brain tissue[17]–[19]. This continuous injury forms glial scars, which act as an electrically insulating layer around the recording site of the needle electrode. However, the SNRs measured from 2 weeks to 6 months showed no significant degradation. These results suggest that the floating electrode enables following the tissue motion and reduces the continuous injury.

I examined tissue damage associated with the proposed floating electrode and pin-type electrode. The result indicated that the floating device shows a dimple-like damaged

area four times smaller than the damaged area of the pin-type electrode. This result suggested that the device substrate of the pin-type electrode, which is fixed to the cranium, induced pressure to the brain surface during the device implantation. It is known that pressure to the brain tissue causes cerebral ischemia, which results in a blood-brain barrier breach as well as biological inflammation[20], [21]. Alternatively, the floating electrode showed a smaller damaged area in the tissue (Figure 4.12a,b), which could minimize the issues associated with the electrode implantation.

For the further quantitative comparison of reactive astrocytes (GFAP, Figure 4.12d), I confirmed these fewer astrocytes with the floating electrode. This result represents the effect of the floating electrode, which was not fixed to the cranium to enable following the tissue. However, comparisons of other cell types of microglia (Iba-1, Figure 4.12e) and nuclei (DAPI, Figure 4.12f) showed no significant differences between the floating and pin-type electrodes. These phenomena were due to the observation period of 2 weeks, in which microglia formed in response to the injury (over hours and days[18]) and astrocytes became activated afterward (for 2 weeks and beyond[16]). Although the floating electrode showed these less tissue damage than did the pin-type electrode, further minimized tissue damage will be required for future implantation.

For the recording of neuronal activities from the mouse's cortex, I used a single-channel electrode with a 5-μm-diameter microneedle and a device size of 1×1 mm^2 to record neuronal activity from the mouse cortex. Although the floating approach minimized tissue damage (Figure 4.12), the dimensions of this device are insufficient for use with small animals (such as mice in this study) or for arranging them in the multisite recording. I am currently working on fabricating an even smaller device ($< 1 \times 1$ mm^2) using the small design and fabrication process as in this work[4]. The device miniaturization and multisite recording results will be reported in a future publication.

In addition, the floating electrode device presented here includes an additional cable that connects the mouse (electrode device) to the first-stage amplifier of the recording system. This cable may result in the inhabitation of the mouse's behavior as well as a decrease in the recording signal quality due to external noise coupled with the cable. These concerns can be resolved with a wireless electrode recording system[22]–[26].

4.8 Conclusions

In this Chapter, I proposed a chronic neuronal recording in mice, in which a 5-μm-diameter microneedle electrode penetrates the brain tissue with dissolvable material–based detachment, and the device is placed on it without fixing the device to the cranium, achieving the floating electrode architecture. Although the electrode device needs further improvements, such as miniaturization and wireless recording system, the proposed recording technology showed clear advantages of the high SNR during the implantation and the minimized tissue damage.

Reference

[1] A. Hai, J. Shappir, and M. E. Spira, “In-cell recordings by extracellular microelectrodes,” *Nature methods*, vol. 7, no. 3, pp. 200–202, 2010.

[2] L. Grob, H. Yamamoto, S. Zips, P. Rinklin, A. Hirano-Iwata, and B. Wolfrum, “Printed 3D electrode arrays with micrometer-scale lateral resolution for extracellular recording of action potentials,” *Advanced Materials Technologies*, vol. 5, no. 3, p. 1900517, 2020.

[3] T. D. Y. Kozai *et al.*, “Ultrasmall implantable composite microelectrodes with bioactive surfaces for chronic neural interfaces,” *Nature materials*, vol. 11, no. 12, p. 1065, 2012.

[4] H. Sawahata *et al.*, “Single 5 μm diameter needle electrode block modules for unit recordings in vivo,” *Scientific Reports*, vol. 6, p. 35806, 2016.

[5] A. Fujishiro, H. Kaneko, T. Kawashima, M. Ishida, and T. Kawano, “In vivo neuronal action potential recordings via three-dimensional microscale needle-electrode arrays,” *Scientific Reports*, vol. 4, pp. 1–9, 2014.

[6] Y. Kubota, S. Yamagiwa, H. Sawahata, and S. Idogawa, “Sensors and Actuators B : Chemical Long nanoneedle-electrode devices for extracellular and intracellular recording in vivo,” *Sensors & Actuators: B. Chemical*, vol. 258, pp. 1287–1294, 2018.

[7] D. Seo *et al.*, “Wireless recording in the peripheral nervous system with ultrasonic neural dust,” *Neuron*, vol. 91, no. 3, pp. 529–539, 2016.

[8] B. C. Johnson *et al.*, “StimDust: A 6.5 mm 3, wireless ultrasonic peripheral nerve stimulator with 82% peak chip efficiency,” in *2018 IEEE Custom Integrated Circuits Conference (CICC)*, 2018, pp. 1–4.

[9] S. Yamagiwa *et al.*, “Ultra high-aspect-ratio neuroprobe: 5-μm-diameter and 400-μm-length needle detects action potentials in VIVO,” in *2017 IEEE 30th International Conference on Micro Electro Mechanical Systems (MEMS)*, 2017, pp. 553–556.

[10] A. Ikedo, T. Kawashima, T. Kawano, and M. Ishida, “Vertically aligned silicon microwire arrays of various lengths by repeated selective vapor-liquid-solid growth of n-type silicon/n-type silicon,” *Applied Physics Letters*, vol. 95, no. 3, p. 33502, 2009.

[11] H. Oka, K. Shimono, R. Ogawa, H. Sugihara, and M. Taketani, “A new planar

multielectrode array for extracellular recording : application to hippocampal acute slice," vol. 93, pp. 61–67, 1999.

[12] K. Funayama, N. Hagura, H. Ban, and Y. Ikegaya, "Functional organization of flash-induced V1 offline reactivation," *Journal of Neuroscience*, vol. 36, no. 46, pp. 11727–11738, 2016.

[13] K. Yamashita *et al.*, "Flexible parylene-thread bioprobe and the sewing method for in vivo neuronal recordings," *Sensors and Actuators B: Chemical*, p. 127835, 2020.

[14] K. Yamashita, H. Sawahata, S. Yamagiwa, R. Numano, K. Koida, and T. Kawano, "Floating 5-μm-Diameter Needle for Low Invasive Chronic Recording," in *2019 20th International Conference on Solid-State Sensors, Actuators and Microsystems & Eurosensors XXXIII (TRANSDUCERS & EUROSENSORS XXXIII)*, 2019, pp. 302–305.

[15] A. Lecomte *et al.*, "Silk and PEG as means to stiffen a parylene probe for insertion in the brain: Toward a double time-scale tool for local drug delivery," *Journal of Micromechanics and Microengineering*, vol. 25, no. 12, 2015.

[16] H. Szarowski *et al.*, "Brain responses to micro-machined silicon devices," *Brain Research*, vol. 983, pp. 23–35, 2003.

[17] N. J. Michelson *et al.*, "Multi-scale, multi-modal analysis uncovers complex relationship at the brain tissue-implant neural interface: new emphasis on the biological interface," *Journal of neural engineering*, vol. 15, no. 3, p. 33001, 2018.

[18] T. D. Y. Kozai, A. L. Vazquez, C. L. Weaver, S.-G. Kim, and X. T. Cui, "In vivo two-photon microscopy reveals immediate microglial reaction to implantation of microelectrode through extension of processes," *Journal of neural engineering*, vol. 9, no. 6, p. 66001, 2012.

[19] R. Biran, D. C. Martin, and P. A. Tresco, "Neuronal cell loss accompanies the brain tissue response to chronically implanted silicon microelectrode arrays," *Experimental Neurology*, vol. 195, no. 1, pp. 115–126, 2005.

[20] S. Zhang, J. Boyd, K. Delaney, and T. H. Murphy, "Rapid reversible changes in dendritic spine structure in vivo gated by the degree of ischemia," *Journal of Neuroscience*, vol. 25, no. 22, pp. 5333–5338, 2005.

[21] S. M. Wellman, L. Li, Y. Yaxiaer, I. McNamara, and T. D. Y. Kozai, "Revealing spatial and temporal patterns of cell death, glial proliferation, and blood-brain barrier dysfunction around implanted intracortical neural interfaces," *Frontiers in*

neuroscience, vol. 13, p. 493, 2019.

[22] D. Fan *et al.*, "A wireless multi-channel recording system for freely behaving mice and rats," *PloS one*, vol. 6, no. 7, p. e22033, 2011.

[23] T. A. Szuts *et al.*, "A wireless multi-channel neural amplifier for freely moving animals," *Nature neuroscience*, vol. 14, no. 2, pp. 263–269, 2011.

[24] A. Zhou *et al.*, "A wireless and artefact-free 128-channel neuromodulation device for closed-loop stimulation and recording in non-human primates," *Nature biomedical engineering*, vol. 3, no. 1, pp. 15–26, 2019.

[25] M. H. Ghaed *et al.*, "Circuits for a cubic-millimeter energy-autonomous wireless intraocular pressure monitor," *IEEE Transactions on Circuits and Systems I: Regular Papers*, vol. 60, no. 12, pp. 3152–3162, 2013.

[26] S. Idogawa, K. Yamashita, R. Sanda, R. Numano, K. Koida, and T. Kawano, "A lightweight, wireless Bluetooth-low-energy neuronal recording system for mice," *Sensors and Actuators B: Chemical*, vol. 331, p. 129423, 2021.

Chapter 5

Microneedle-electrode-assembled flexible-film device

5.1 Introduction

To elucidate brain function, it is necessary to measure the neural activity in the brain with the high spatial and temporal resolution for long period in chronic. Recent advances in microelectromechanical system technology enable us to fabricate extracellular needle electrodes with a diameter of less than 10-μm[1]–[6], thereby recordable the high-resolution signals for example LFPs and spikes, and minimizing tissue response during device penetration into the biological tissue. However, conventional electrode devices with a substrate based on Si caused inflammation because of the chronic breach with a blood-brain barrier in a chronic recording[7]. In addition, the conventional implantation method that the device fixed to the cranium[8] induced inflammation during the micromotion after implantation.

In chapter 4, the floating system following brain tissue pulsation shows fewer Inflammatory reactions compared to a conventional needle. In this chapter, we proposed a microneedle-electrode-assembled flexible-film device for chronic in vivo recording with high spatiotemporal resolution multi-signal. Furthermore, a surgical method for

penetration of high-aspect-ratio electrode assembled on the flexible film substrate to brain tissue without physical vibration using PEG was also proposed.

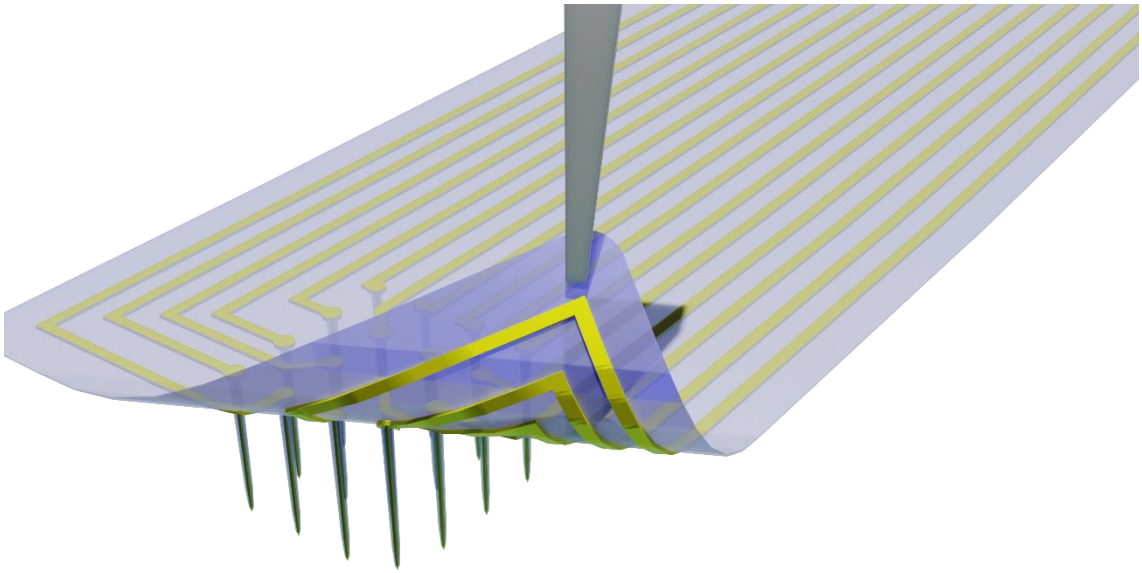

Figure 5.1 Schematic of a microneedle-electrode-assembled flexible-film device.

5.2 Design and fabrication

Figure 5.2 shows layout of the microneedle-electrode-assembled flexible-film device. The device has a 1×4 array of microneedle-electrode (400 um length, < 5 um diameter) is integrated within a 2 × 3.5 mm^2 flexible film.

Figure 5.3 shows fabrication of the microneedle-electrode-assembled flexible-film device. A SiO_2 film is formed on the Si (111) substrate by thermal oxidation (Figure 5.3 (i,ii)), and the portion forming the Si needle is selectively patterned (Figure 5.3 (iii)). An Au film is formed on the patterning resist, and the Au dots are selectively formed by liftoff. After heating to the VLS growth temperature (~700°C), Au–Si alloy dots are formed (Figure 5.3 (iv)). After patterning Au dots, the gaseous silicon (Si_2H_6 (disilane)) absorbed into the alloy dots. When the Si content in the Au–Si alloy dots supersaturates, the Si precipitates from the Au–Si alloy dot in the <111> direction at the interface between the dot and the Si substrate (Figure 5.3 (v)). For the substrate of the device, the parylene-C (5-μm-thick) was deposited and then the parylene around the needle is etched away by O_2 plasma (Figure 5.3 (vi)). After the device metallization with Au/Ti (Figure 5.3 (vii)), another parylene-C (5 μm) is deposited as the needle's insulator, while the parylene

around the needle is removed by O_2 plasma (Figure 5.3 (viii)). Parylene layers on both the needle's tip and the contact pad portions are simultaneously exposed (O_2 plasma). Finally, the device layer is released from the Si substrate by ethanol (Figure 5.3 (ix)).

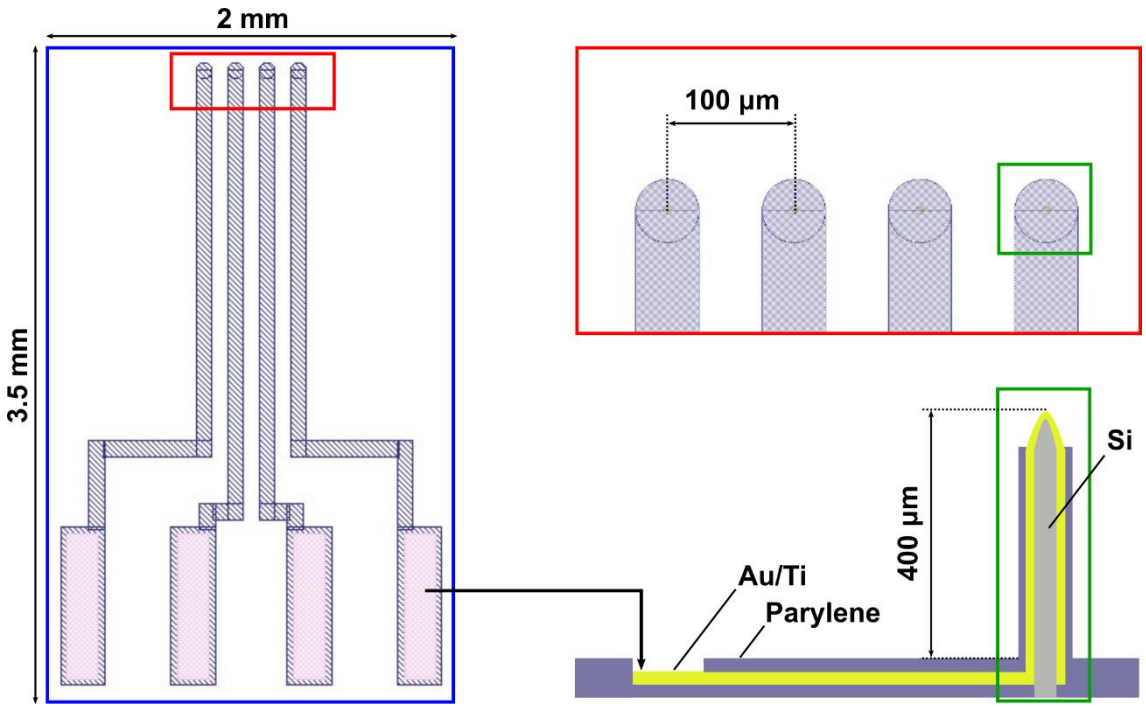

Figure 5.2 Layout of the microneedle-electrode-assembled flexible-film device.

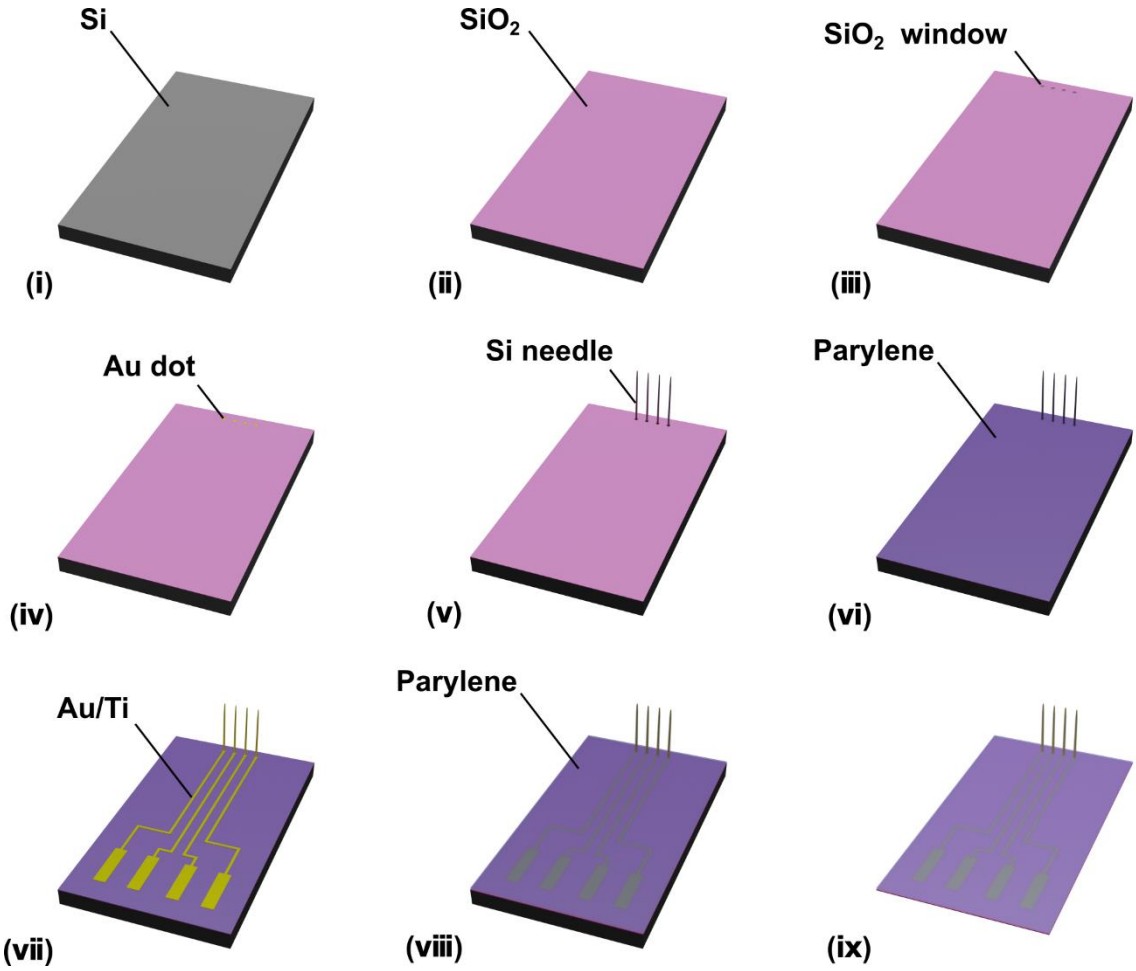

Figure 5.3 Fabrication of the microneedle-electrode-assembled flexible-film device. (i) Si (111) substrate. (ii) SiO_2 film formed on the Si substrate. (iii) SiO_2 window for forming the Si needle. (iv) Au dot formed on the Si substrate. (v) Si needle formed on the Si substrate with VLS growth method. (vi) Parylene-C for film substrate (bottom layer). (vii) Au/Ti patterned on the parylene film substrate. (viii) Parylene-C for insulating the needle portion and interconnections. (ix) The microneedle-electrode-assembled flexible-film device released from Si substrate using ethanol.

5.3 Device packaging and electrical characteristics

Figure 5.4 shows fabricated microneedle-electrode-assembled flexible-film device. The film device was cut 2 × 3.5 mm^2 by surgical scalpel and was released from Si substrate. The microneedle-electrode within film device showed 400 μm length and 5.7 μm diameter (blue and green square in Figure 5.4).

Figure 5.5 shows packaging of the microneedle-electrode-assembled flexible-film device. The film device was assembled to the polyimide-based flexible printed circuit

(FPC) via conductive paste for interconnection. For the insulation, the connection part between FPC and film device was covered with ultraviolet (UV)-curable resin.

The microneedle-electrodes impedance characteristics at 10 Hz – 10 kHz, measured in phosphate buffered saline (PBS) at room temperature, ranged from 26 ± 8 kΩ to 6.5 ± 1.7 MΩ [170 ± 50 kΩ (mean ± SD) at 1 kHz] (Figure 5.6). These values are sufficiently low for measuring the neuronal activity[4], [5], [9].

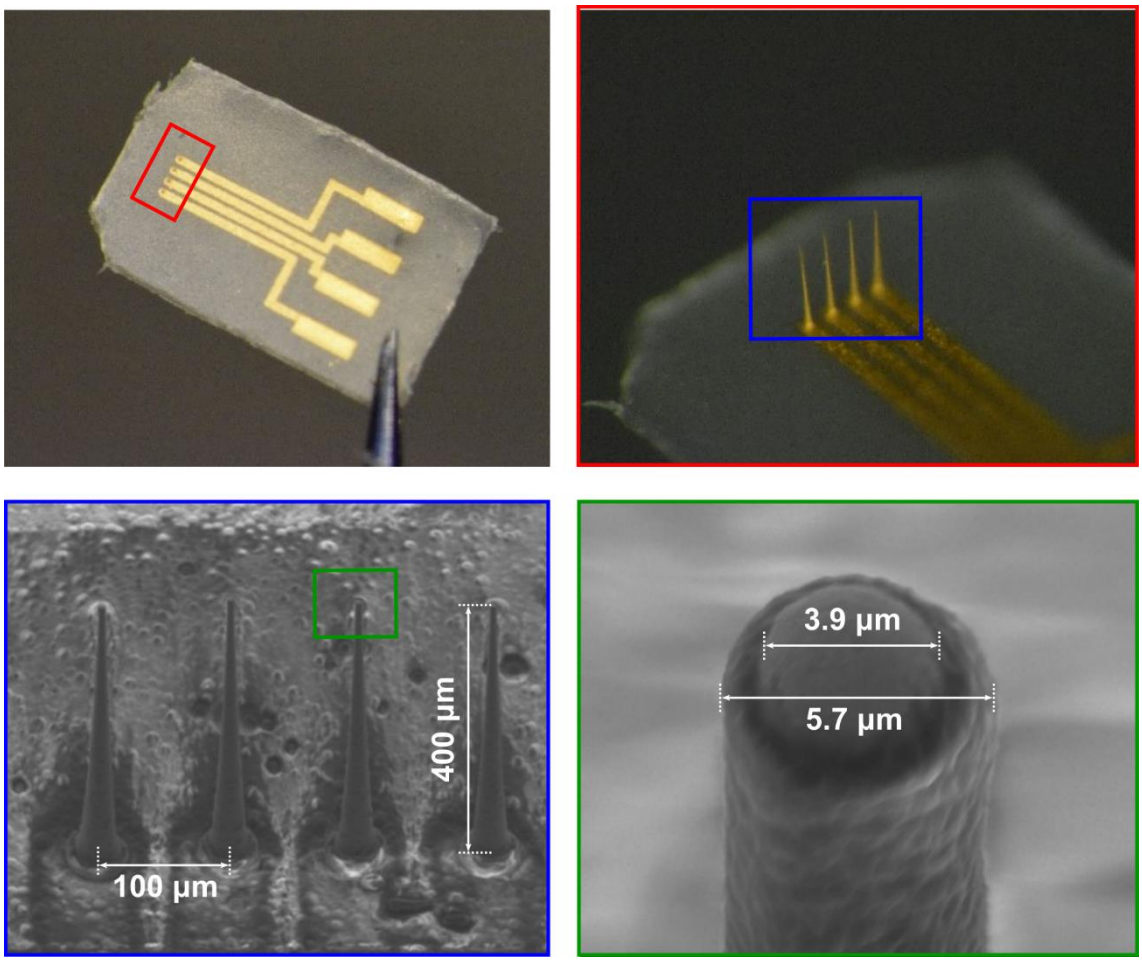

Figure 5.4 Fabricated microneedle-electrode-assembled flexible-film device.

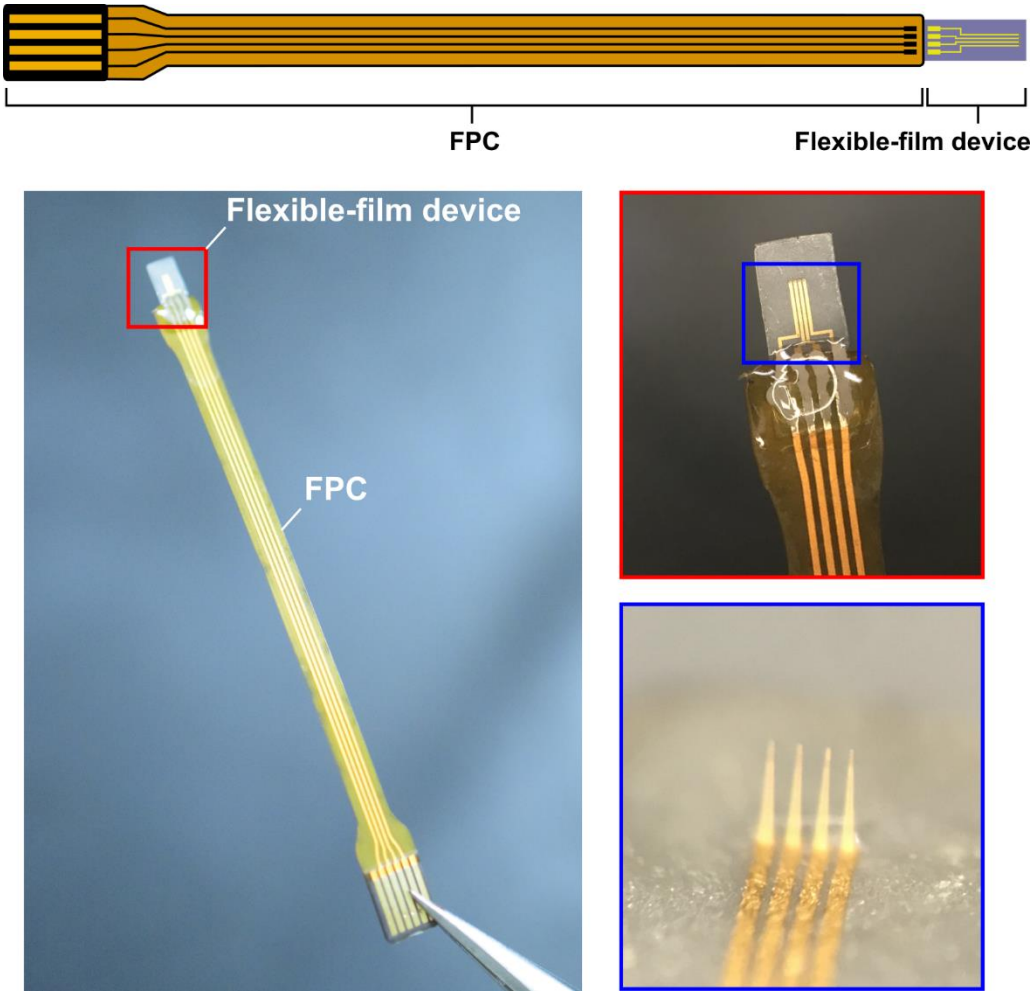

Figure 5.5 Schematic and photograph showing the packaging device.

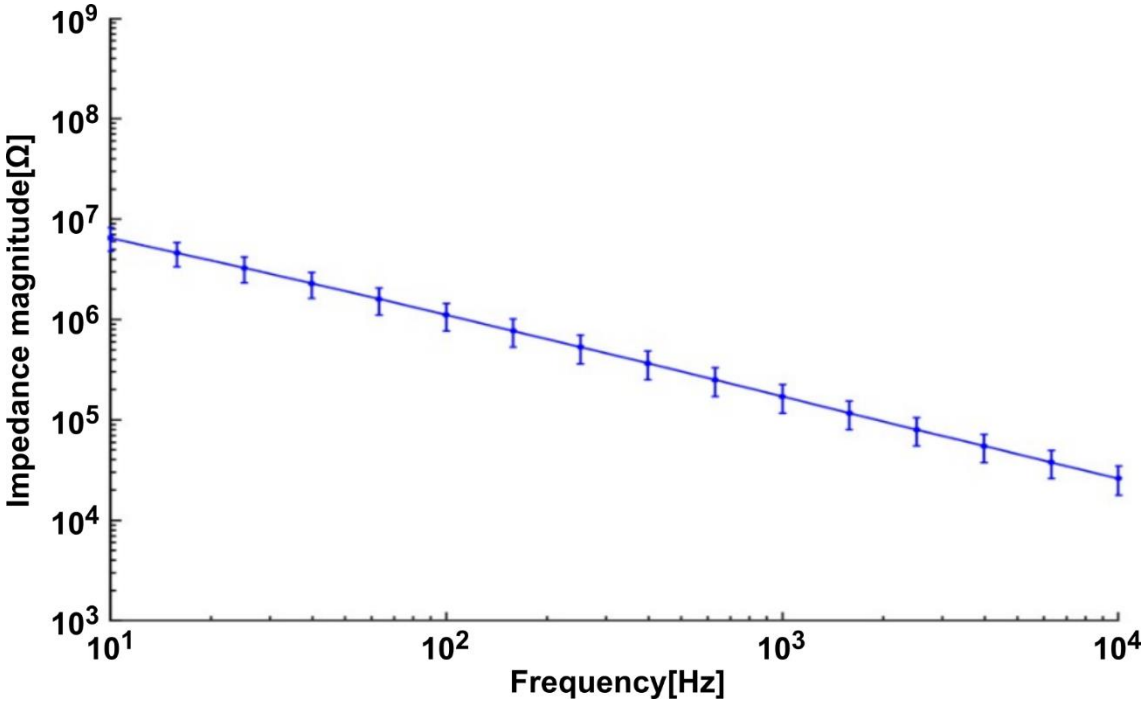

Figure 5.6 Impedance characteristics of microelectrodes measured at room temperature in PBS.

5.4 Acute in vivo neuronal recording

The ability to capture acute neuronal activity in vivo was demonstrated using the brain of a mouse (Figure 5.7). Intraperitoneal injections of urethane (50 µl of 10% solution per 10 g body weight) and chlorprothixene (100 µl of 0.5% solution per 10 g body weight) were used to anesthetize the mouse (male, 25–30 g). To record the visual response, after a cranial opening (3.2–3.5 mm on the lateral side and 4.0 mm on the caudal side from the bregma, with a diameter of 1–3 mm), the fabricated film device consisting of four microneedle-electrodes was inserted into the tissue and placed in the cortical layers of the primary visual cortex (V1) on the right hemisphere (~ 2.5 mm on the lateral side and 4.0 mm on the caudal side from the bregma) by manipulating the pin connector via PEG (Figure 4.5 in Chapter 4). A light-emitting diode (LED) array consisting of nine white LEDs on a 20-mm broad substrate was employed as a visual stimulus. While visual stimuli were delivered to the mouse's eye for 0.5 s, neuronal responses were recorded repeatedly using the four microneedle-electrodes implanted in the tissue (Figure 5.8). The second panel in Figure 5.8 displays waveforms recorded by each microneedle-electrode in the low-frequency band (filtering = 10–80 Hz), while the third panel shows waveforms recorded in the high-frequency band (filtering = 500–1,000 Hz). The bottom two panels

show raster plots and peri-stimulus time histograms (PSTHs) from each high-frequency band signal, respectively. The detection thresholds for each channel were set to be three times the standard deviation (σ) of the mean signal −0.5 to −1.0 s before the stimulus began. For microneedle-electrodes, the signals responding to visual stimuli occurred at roughly 50 ms, which was consistent with the latency of the mouse's visual response[10]. These findings imply that the recorded signals were susceptible to local field potentials and spikes elicited by visual stimuli.

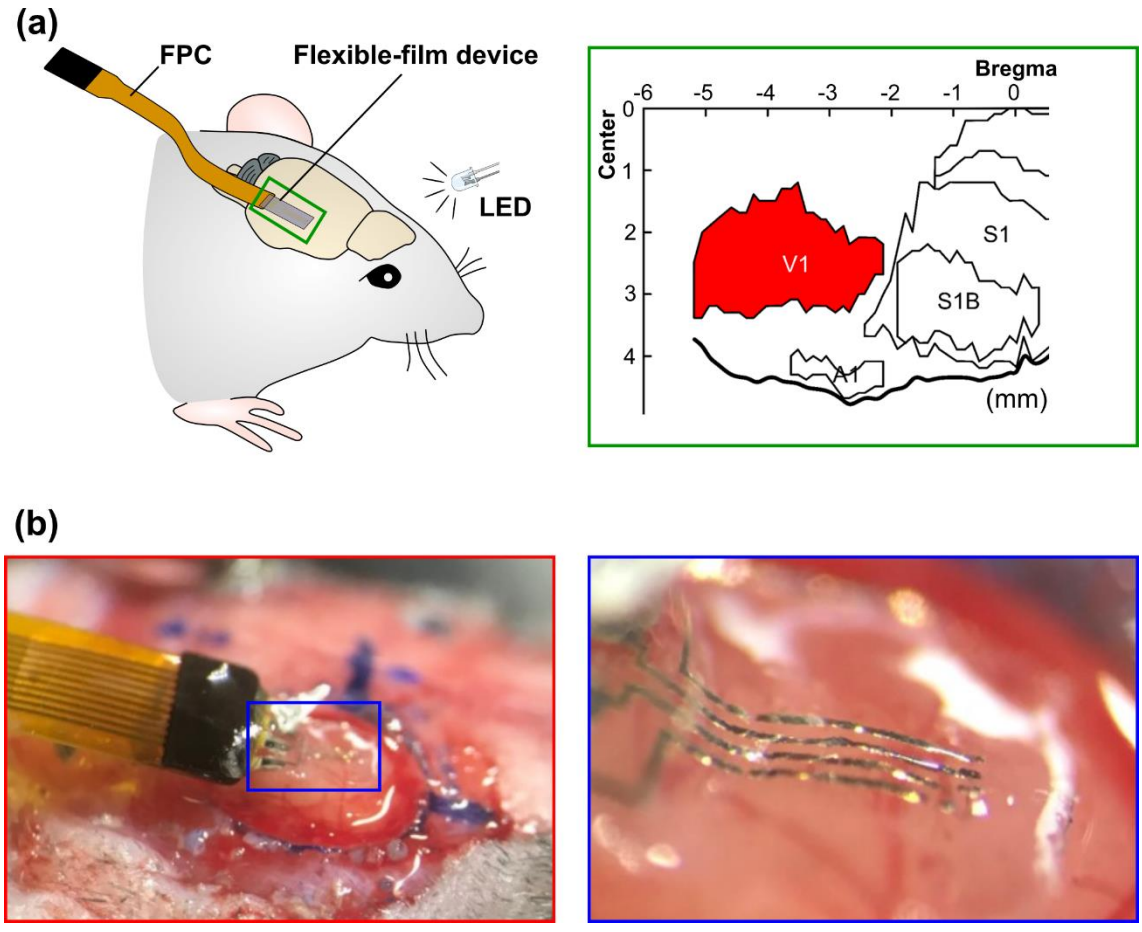

Figure 5.7 Acute in vivo neuronal recording using mouse brain. (a) Schematic of the recording setup. (b) Photograph of placed on brain tissue.

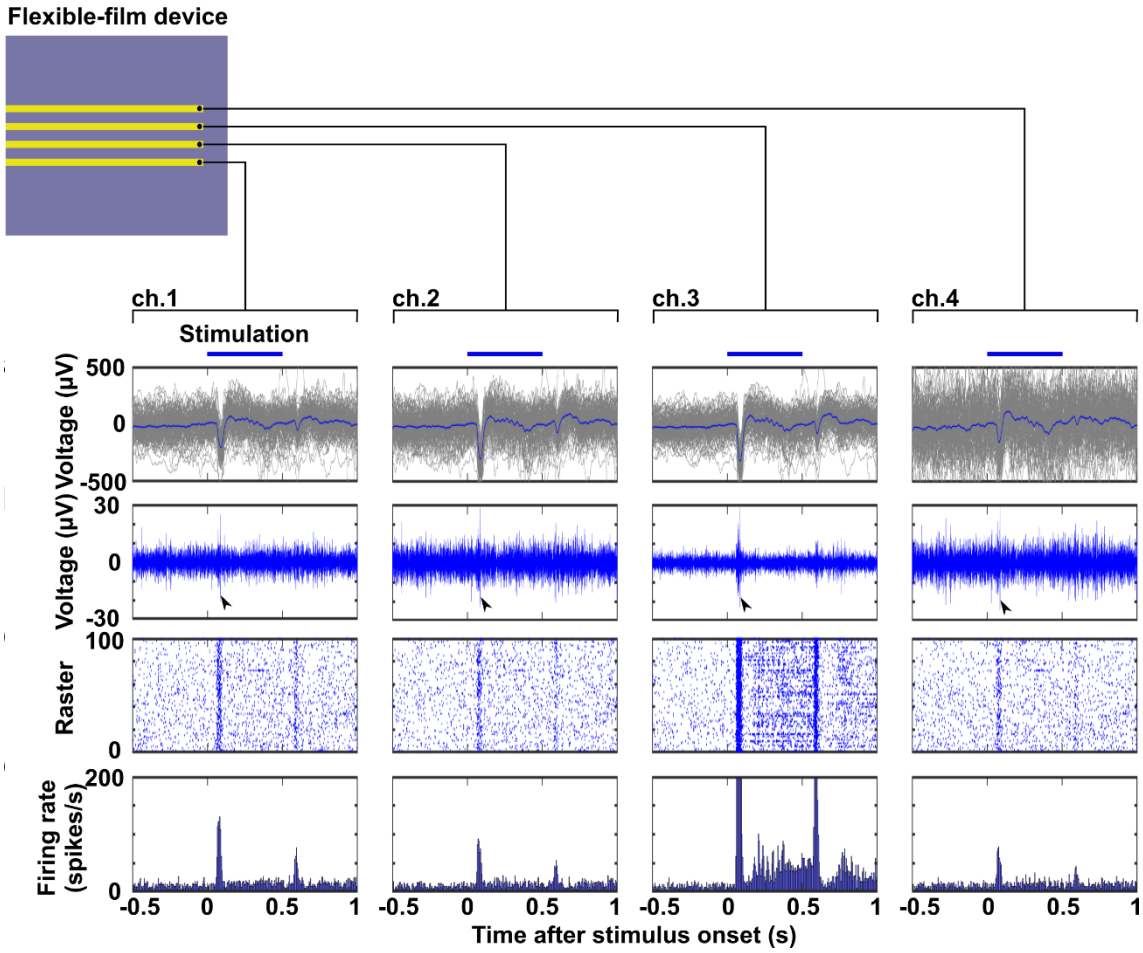

Figure 5.8 Signal waveforms recorded from the V1 via four embedded microneedle-electrodes in the tissue. Top panels represent timing of the optical stimulation. Second and third panels are low-frequency-band (filtering = 10–80 Hz, n = 100 trials) and high frequency-band (filtering = 500–1,000 Hz, single trial) signal waveforms, responsibility. Bottom two panels are raster plots and PSTHs, respectively, taken from the high frequency signals (n = 100 trials) The detection thresholds for each channel was 3 times the standard deviation (σ) of the mean signal − 0.5 to −1.0 s before the stimulus onset.

5.5 Chronic in vivo neuronal recording

The recording from mice implanted with a film device (wild-type C57 BL/6, 20–30 g prior to implantation) was evaluated. The film device contained microneedle-electrodes that were implanted into the cortical layers of the primary visual cortex on the right hemisphere. The film device was then coated with a gelatin sponge and dental cement after it had been penetrated. (Figure 5.9).

Figure 5.10a1 and a2 show low-frequency (filtering = 10–80 Hz) and high-

frequency (filtering = 500–1,000 Hz) band waveforms recorded 120 days after the device was implanted, respectively. Figure 5.10a3 and a4 show raster plot diagrams and PSTHs derived from high-frequency band signals with an amplitude threshold of three standard deviations (SDs, σ) of the mean signal −0.5 to −1.0 s before the stimulus began, respectively. For the microneedle-electrodes, the signals corresponding to visual stimuli occurred at roughly 50 ms, which was consistent with the latency of the mouse's visual response. [10] These results suggest that the recorded signals were subjected to the local field potentials and the spikes, which were evoked by the visual stimuli.

Additionally, I evaluated the chronic recording by the signal-to-noise ratio (SNR) of spikes (Figure 5.10b). The SNR was defined as the peak-to-peak amplitude of the mean waveform 0.005 to 0.1 s after the stimulus onset divided by the 3σ of the noise level. These SNRs are greater than 2.2 (mean) to 120 days without significant degradations.

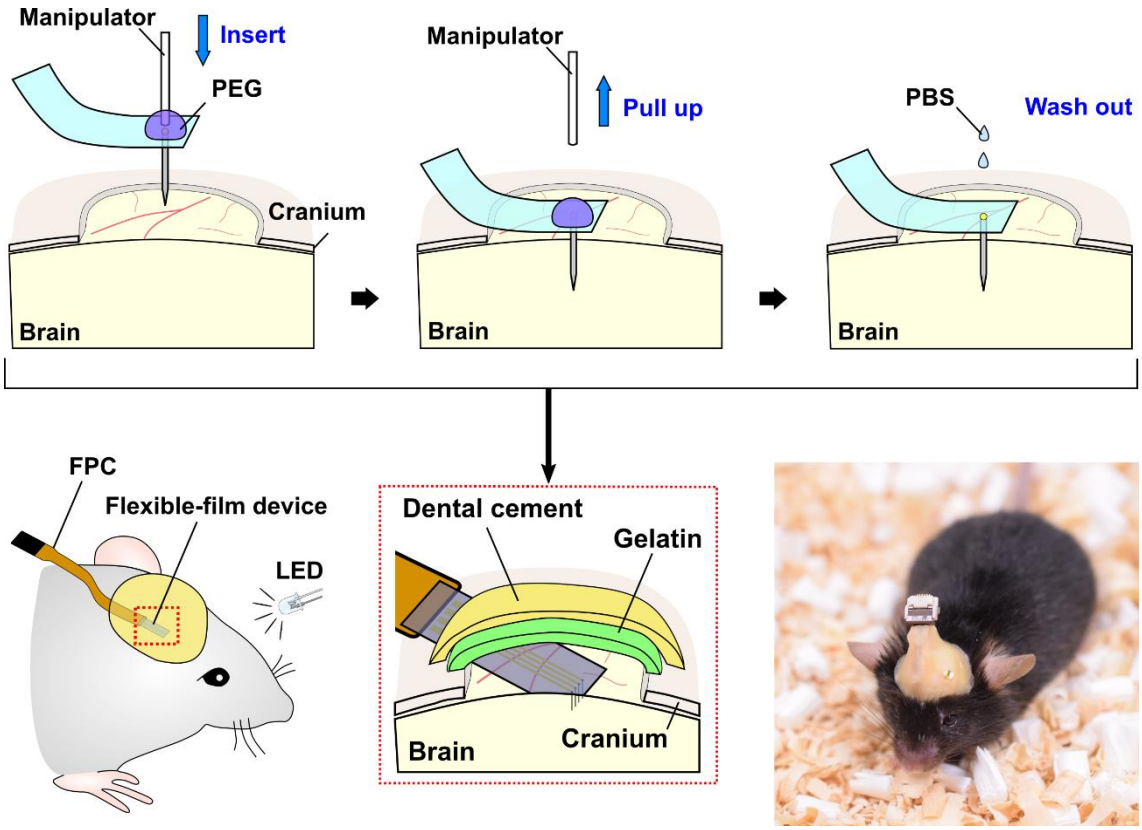

Figure 5.9 Schematic of the surgical procedure for the chronic recording and the photograph of the mouse that was implanted device.

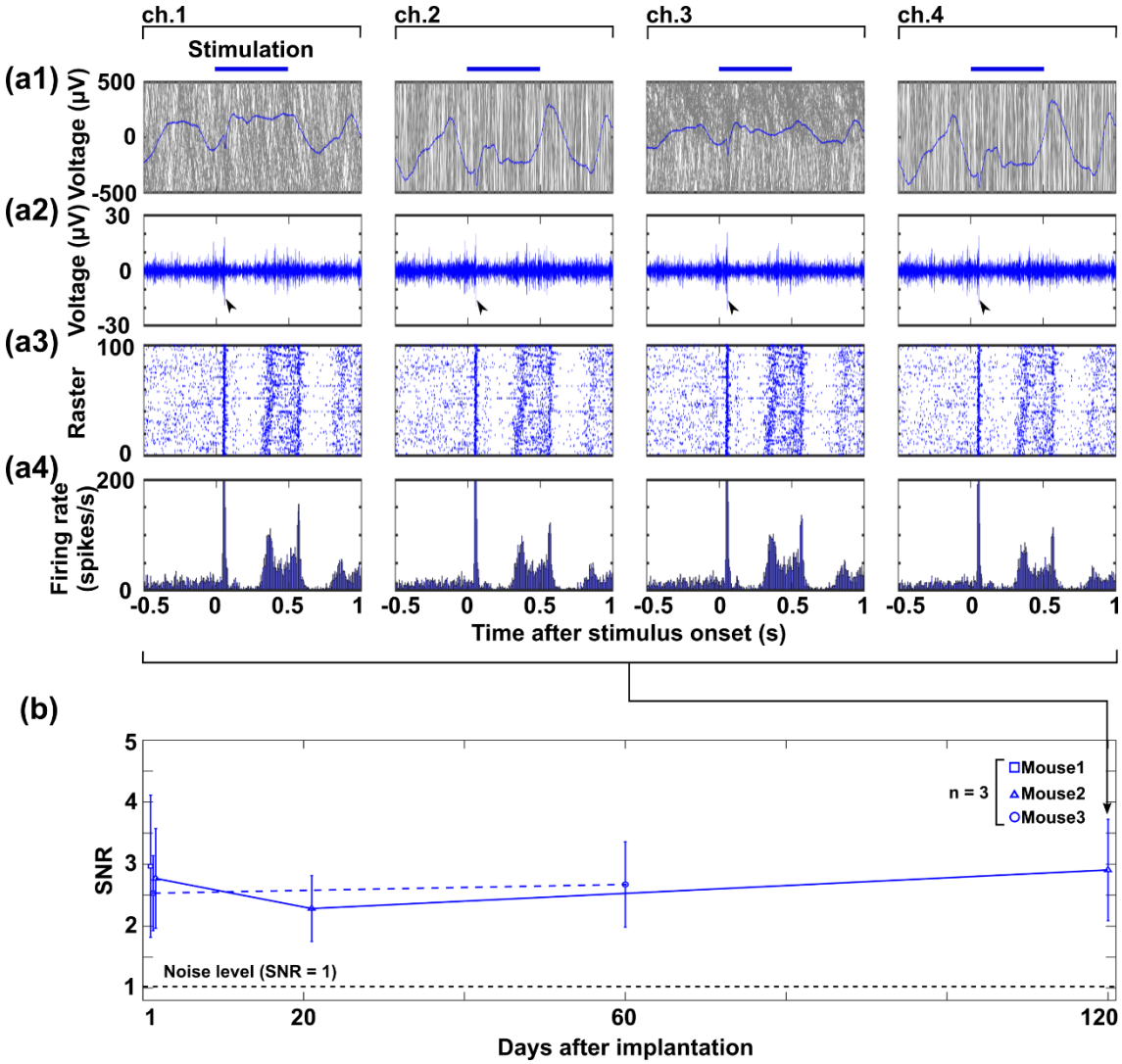

Figure 5.10 Chronic in vivo neuronal recording using mouse brain. (a) Signal waveforms recorded from the V1 via four microneedle-electrodes at 120 days after implantation. (b) SNR of spike detected on each mouse implanted device (mean ± SD, n = 100 trials for each device during the recording period).

5.6 Discussion

I proposed a microneedle-electrode-assembled flexible-film device for chronic in vivo recording with high spatiotemporal resolution multi-signal. In addition, I confirmed that the bottom of the microneedle-electrode array formed on the flexible film substrate enables to release from Si substrate without degradation of electrical characteristics. The result suggests it is possible to omit several device process steps in making needle electrode devices.

Furthermore, a surgical method for penetration of high-aspect-ratio electrode assembled on the flexible film substrate to brain tissue without physical vibration using PEG was also proposed. The PEG shows a "solid phase" at room temperature enables manipulation and penetration of the microneedle-electrode to the brain tissue without mechanical vibration. After device penetration, the PEG was dissolved by PBS and enabled to remove from the brain surface completely. In addition, the device substrate was based on flexible film and can be reduced tissue inflammation factor of pulsation of brain tissue for example breach of the blood-brain barrier and micromotion during device implantation. As an advanced way to use the dissolvable material, I can use a PEG-containing bioactive agent, which would reduce immune responses of the tissue[11].

I also analyzed the SNR during the microneedle-electrode-assembled flexible-film device implanted mouse for 4 months. The SNRs measured for 4 months showed no significant degradation. In addition, the microneedle-electrode array recorded the spike signals for 4 months without degradation the number of the recordable electrode. These results indicate that the proposed microneedle-electrode-assembled flexible-film device has the capability of high spatiotemporal recording for a long period.

5.7 Conclusions

This chapter proposed a microneedle-electrode-assembled flexible-film device for chronic in vivo recording with high spatiotemporal resolution multi-signal and minimally invasive implantation. I was able to record LFP and spike signals in an acute in vivo experiment using the constructed microneedle-electrode-assembled flexible-film technology. In addition, the constructed device was put on brain tissue using PEG, as described in Chapter 2, and the device was implanted for persistent in vivo recording. For four months, the implanted device displayed the LFP and spike signals. Furthermore, the SNR during the implantation was investigated. As a result, the SNRs for the first four months showed no significant difference.

Reference

[1] A. Hai, J. Shappir, and M. E. Spira, "In-cell recordings by extracellular microelectrodes," *Nature methods*, vol. 7, no. 3, pp. 200–202, 2010.

[2] L. Grob, H. Yamamoto, S. Zips, P. Rinklin, A. Hirano-Iwata, and B. Wolfrum, "Printed 3D electrode arrays with micrometer-scale lateral resolution for extracellular recording of action potentials," *Advanced Materials Technologies*, vol. 5, no. 3, p. 1900517, 2020.

[3] T. D. Y. Kozai *et al.*, "Ultrasmall implantable composite microelectrodes with bioactive surfaces for chronic neural interfaces," *Nature materials*, vol. 11, no. 12, pp. 1065–1073, 2012.

[4] H. Sawahata *et al.*, "Single 5 μm diameter needle electrode block modules for unit recordings in vivo," *Scientific Reports*, vol. 6, p. 35806, 2016.

[5] A. Fujishiro, H. Kaneko, T. Kawashima, M. Ishida, and T. Kawano, "In vivo neuronal action potential recordings via three-dimensional microscale needle-electrode arrays," *Scientific Reports*, vol. 4, pp. 1–9, 2014.

[6] Y. Kubota *et al.*, "Long nanoneedle-electrode devices for extracellular and intracellular recording in vivo," *Sensors and Actuators B: Chemical*, vol. 258, pp. 1287–1294, 2018.

[7] T. Saxena *et al.*, "The impact of chronic blood–brain barrier breach on intracortical electrode function," *Biomaterials*, vol. 34, no. 20, pp. 4703–4713, 2013.

[8] J. C. Barrese *et al.*, "Failure mode analysis of silicon-based intracortical microelectrode arrays in non-human primates," *Journal of neural engineering*, vol. 10, no. 6, p. 066014, 2013.

[9] T. Harimoto *et al.*, "Enlarged gold-tipped silicon microprobe arrays and signal compensation for multi-site electroretinogram recordings in the isolated carp retina," *Biosensors and Bioelectronics*, vol. 26, no. 5, pp. 2368–2375, 2011.

[10] K. Funayama, N. Hagura, H. Ban, and Y. Ikegaya, "Functional organization of flash-induced V1 offline reactivation," *Journal of Neuroscience*, vol. 36, no. 46, pp. 11727–11738, 2016.

[11] A. Lecomte *et al.*, "Silk and PEG as means to stiffen a parylene probe for insertion in the brain: Toward a double time-scale tool for local drug delivery," *Journal of Micromechanics and Microengineering*, vol. 25, no. 12, 2015.

Chapter 6

Summary

6.1 Summary

In this study, I provide numerous neuronal electrode and implant systems for chronic recording with excellent spatial and temporal resolution in mice. I developed surgical procedures using PEG dissolvable material in “solid phase” and “liquid phase.”” for low-invasive device implantation.

In Chapter 1, the method of detecting neural activity, including the advantages of the electrical measurement method and neural electrode, device implantation for chronic recording, and failure mechanism of the neural electrode, including mechanical and biological origins, were introduced. The objective of this research was also demonstrated.

In Chapter 2, the device penetration method for reducing tissue damage utilizing dissolvable materials, as well as the comparison of dissolvable materials and selection, are described.

In Chapter 3, the parylene-thread microelectrode was fabricated, and the tissue was penetrated using the sewing mechanism to guide the tungsten microneedle. I was able to obtain EMG signals from a mouse's MG muscle as well as neuronal signals of LFP and spike from its visual cortex in vivo using the thread-bioprobe. The proposed thread-bioprobe device, which has good device flexibility, electrodeposition

controllability, and implantation capabilities, will help with both acute and chronic in vivo electrophysiological recordings. To avoid physical stress on the tissue, a flexible thread device stitching method using a dissolvable PEG substance has been devised. These characteristics of both the flexible thread device and the surgical procedure were previously unattainable using traditional methods and technologies.

In Chapter 4, I proposed a chronic neuronal recording in mice in which a 5-μm-diameter microneedle electrode penetrates the brain tissue via dissolvable material-based detachment, and the device is put on it without being attached to the cranium, resulting in the floating electrode architecture. I presented a microelectrode penetration approach into brain tissue and device detachment with PEG dissolvable material for device implantation. The technology demonstrated the benefit of reducing physical stress to the tissue during device implantation as well as removal from the manipulator. For six months, the electrode displays steady recording with no substantial loss of signal-to-noise ratios, and minimal tissue damage is confirmed when compared to previous cranium-fixed electrodes with the same needle geometry. Although the electrode device requires future advancements such as downsizing and a wireless recording system, the proposed recording technology demonstrated substantial advantages in terms of high SNR during implantation and minimal tissue damage.

In Chapter 5, I proposed a microneedle-electrode-assembled flexible-film device for chronic in vivo recording with high spatiotemporal resolution multi-signal and less invasive implantation. I recorded LFP and spike signals in an acute in vivo experiment using the constructed microneedle-electrode-assembled flexible-film technology. In addition, the constructed device was put on brain tissue using PEG, as described in Chapter 2, and the device was implanted for persistent in vivo recording. For four months, the implanted device displayed the LFP and spike signals. Furthermore, the SNR during the implantation was investigated. As a result, the SNRs for four months showed no significant difference.

6.2 Future prospective

To elucidate brain function, it is important to detect neural activity in the brain with high spatial and temporal resolution over a lengthy period of time. Several key human disorders, including Parkinson's disease, Alzheimer's disease, and major depressive disorders, require an understanding of the basic neurological system from a

mammal model. In particular, in vivo chronic recording from a mouse with implanted low-invasive device is required.

In this study, I proposed high spatiotemporal neural recording system without tissue damage. The results of this research will provide detailed information about the nervous system. In particular, the recording system is useful in an application that requires massive signal information, such as Brain-Machine Interface (blue area in Figure 6.1). In addition, I demonstrated long period chronic recording in mice. The mice have been frequently used as a model organism for critical human disease. However, conventional experiments of behavioral tests provide complex data which is hard to analyze. Therefore, by combining the behavioral test and electrophysiology, quantitative output will be acquired from a model mouse with disease such as focal seizure (green area in Figure 6.1). This approach will contribute to drug screening. Furthermore, the proposed device enables recording from other nerve systems, including spinal cord and peripheral nerve. These targets relate to the sensation of pain, and chronical recording is needed to further study about it (red area in Figure 6.1).

I hope that the results of this research will be used as a powerful tool to accelerate elucidation of brain function in the future and hereby summarize this paper.

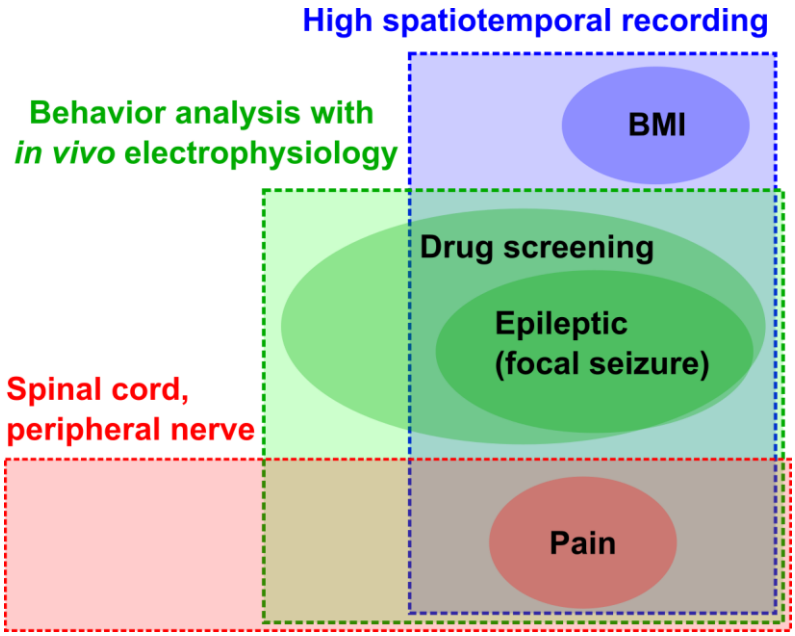

Figure 6.1 Applications of low invasive chronic recording system.

Acknowledgments

This thesis was written in the Department of Electrical and Electronic Information Engineering, Toyohashi University of Technology.

At first, I would like to express my sincere gratitude to my supervisor Professor Takeshi Kawano, Department of Electrical and Electronic Information Engineering, Toyohashi University of Technology. His support through balanced guidance, encouragement, and valuable suggestions has been invaluable for me to continue this research.

I would like to express my sincere gratitude to my supervisor of Professor Kazuaki Sawada, Department of Electrical and Electronic Information Engineering, Toyohashi University of Technology and Associate Professor Kowa Koida, Department of Computer Science and Engineering, Toyohashi University of Technology,

I would like to express my sincere thanks and gratitude to the Leading Program Assistant Professor Antal Berényi, Department of Physiology, University of Szeged, and Associate Professor Masahiro Ohsawa, Department of Neuropharmacology, Graduate School of Pharmaceutical Sciences, Nagoya City University, for their precise review.

I also would like to express my sincere thanks and gratitude to Professor Makoto Ishida, Associate Professor Kazuhiro Takahashi, Associate Professor, Toshihiko Noda, Assistant Professor Daisuke Akai, Assistant Professor, Choi Yong Joon for their valuable suggestions and discussions throughout my research work.

I would like to express my cordial thanks to Professor Rika Numano, Assistant Professor Hirohito Sawahata (currently Ibaraki National College of Technology), Assistant Professor, Shinnosuke Idogawa (currently National Institute of Technology, Kushiro College), Dr. Shota Yamagiwa (currently KIOXIA Corporation), Dr. Yoshihiro Kubota (currently KIOXIA Corporation), Dr. Yusuke Morikawa (currently KIOXIA Corporation) for their valuable suggestions and discussions on device fabrication and biological experiments throughout my research work.

I am grateful to Technical Engineer Dr. Takeshi Hizawa, Mr. Mitsuaki Ashiki, Mr. Hiroyuki Takase for their technical support and advice.

I am thankful to my group members, Mr. Ryohei Tonai, Mr. Tomoaki Banno, Mr. Akihiro Fuchigami, Mr. Khong Yi Nern, Mr. Tsubasa Nakamura, Mr. Hinata Sasaki, Mr.

Riki Hasegawa, Mr. Yuki Yagi, Mr. Chan Yi, Mr. Kensei Sakamoto, Mr. Sayaki Shimizu, Ms. Chen Yi, Ms. Miho Kontani for their assistance and co-operation during my research work.

I am grateful to the Professors at Integrated Electronics Corse for their valuable guidance and advice.

I am also thankful to Dr. Hajime Tsukada, Ms. Yuki Izawa, Ms. Yuri Tanaka, Ms. Chiharu Iwase and Mr. Yukiharu Ozaki for their help and activities in the Leading Program.

I would also like to thank Enago (www.enago.jp) for the English language review. Finally, I wish to offer thanks to my family for their love and support.

January 2022

Koji Yamashita